HARVARD UNIVERSITY
Graduate School of Arts and Sciences

DISSERTATION ACCEPTANCE CERTIFICATE

The undersigned, appointed by the

Department of Physics

have examined a dissertation entitled

Universal non-local observables at interacting quantum critical points

presented by Seth Paul Whitsitt

candidate for the degree of Doctor of Philosophy and hereby certify that it is worthy of acceptance.

Signature _____

Typed name: Professor Subir Sachdev, Chair

Signature _____

Typed name: Professor Eugene Demler

Signature _____

Typed name: Professor Daniel Jafferis

Date: April 17, 2018

Universal non-local observables at interacting quantum critical points

a dissertation presented
by
Seth Paul Whitsitt
to
The Department of Physics

in partial fulfillment of the requirements
for the degree of
Doctor of Philosophy
in the subject of
Physics

Harvard University
Cambridge, Massachusetts
April 2018

Thesis advisor: Subir Sachdev Seth Paul Whitsitt

Universal non-local observables at interacting quantum critical points

Abstract

This dissertation is devoted to the study of universal observables in quantum critical systems, most of which have a non-local character. The overarching goal of this work is to compute new universal observables of critical points to aid theoretical understanding of these systems.

We first consider the finite-size energy spectrum of quantum critical points on the torus. We compute the spectrum for the Wilson-Fisher conformal field theory in the $\epsilon = 3 - d$ expansion, where the energy spectrum maps onto a strongly-coupled problem in quantum mechanics. We also compute the energy spectrum to leading order in $1/N$, and we compare the two expansions. We then study the torus spectra associated with a class of confinement transitions in states with $\mathbb{Z}_2$ topological order. After introducing these universality classes, we show that the critical torus spectrum can be used to detect nontrivial effects like spontaneous symmetry breaking and emergent gauge degrees of freedom. We compare our analytic results with numerical simulations where available, demonstrating the utility of the torus spectrum as a useful characterization of the universality class of a quantum critical point.

We then present a computation of the von Neumann entanglement entropy of the Wilson-Fisher and Gross-Neveu conformal field theories in the large N limit. We obtain an exact mapping to the von Neumann entanglement entropy of a free quantum field theory, allowing an exact determination of the entanglement entropy in a number of cases.

We also study a critical point displaying impurity-driven critical behavior in a boson superfluid-insulator phase transition. The presence of an impurity drives the system to a new interacting universality class, which has critical exponents associated with the scaling dimensions of the impurity degree of freedom. We present the universal quantum field theory of this transition and compute the critical exponents and finite-temperature compressibility

at the critical point using the ϵ expansion.

Contents

Citations to previously published work

Much of the material in this thesis has been previously published in print. The relevant citations are given below.

Chapters 2-4

- Seth Whitsitt and Subir Sachdev, "*Transition from the $\mathbb{Z}_2$ spin liquid to antiferromagnetic order: spectrum on the torus*," Phys. Rev. B. **94** 085134 (2016).
- Michael Schuler, Seth Whitsitt, Louis-Paul Henry, Subir Sachdev, and Andreas M. Läuchli, "*Universal Signatures of Quantum Critical Points from Finite-Size Torus Spectra: A Window into the Operator Content of Higher-Dimensional Conformal Field Theories*," Phys. Rev. Lett. **117**, 210401 (2016).
- Seth Whitsitt, Michael Schuler, Louis-Paul Henry, Andreas M. Läuchli, and Subir Sachdev, "*Spectrum of the Wilson-Fisher conformal field theory on the torus*," Phys. rev. B **96**, 035142 (2017).

Chapter 5

- Seth Whitsitt, William Witczak-Krempa, and Subir Sachdev, "*Entanglement entropy of large-N Wilson-Fisher conformal field theory*," Phys. Rev. B **95**, 045148 (2017).

Chapter 6

- Seth Whitsitt and Subir Sachdev, "*Critical behavior of an impurity at the boson superfluid-Mott-insulator transition*," Phys. Rev. A **96**, 053620 (2017).

Acknowledgments

It is a great pleasure for me to thank the many collaborators and friends I had during my six years at Harvard. I would first like to express gratitude to my advisor, Subir Sachdev, for his mentorship and support. His unending enthusiasm and broad interests in physics made my time at Harvard an exciting and edifying experience.

In addition to Subir, I have been able to collaborate with and and learn from many other people. First I will thank my co-authors, William Witczak-Krempa, Michael Schuler, Andreas Läuchli, and Louis-Paul Henry. Chapter 6 of this thesis also involved important discussions with Kun Chen and Boris Svistunov regarding related work. I would like to thank Eugene Demler and Daniel Jafferis for agreeing to sit on my dissertation committee. I am also grateful to my physics mentors before I started at Harvard: my high school physics teacher Tom Williams, my undergraduate advisor Gregory Fiete, and my undergraduate TA/collaborator/friend Victor Chua.

I have especially benefitted from the many friends I made at Harvard, whether through physics discussions or for friendship and support. Just within Subir's group I would like to thank Richard Davison, Andreas Eberlein, Mathias Scheurer, Chong Wang, William Witczak-Krempa (again), Debanjan Chowdhury, Junhyun Lee, Andrew Lucas, Wenbo Fu, Aavishkar Patel, Julia Steinberg, and Rhine Samajdar. An extra special acknowledgement should be given to my perennial officemates Shubhayu Chatterjee and Alex Thomson, from whom I gained an enormous amount of support in both physics and life. Outside of the group I would like to thank Yulia Dovzhenko, Dan Kapec, Stephen Fleming, Kevin Thomp-

son, Leah Birch, Fionnuala Connolly, Anders Andreassen, and Jacob Baron.

My friends outside of Harvard have also been extremely supportive during these hectic years of doctoral research. I am especially grateful for the friendship of Adrian Haynes, Katherine Maddox, Shawn Stephens, and Cecilia Granger Acuff. Finally, I would like to thank my family. My mother and father, as well as my sisters Edith and Tara, have always been unconditional in their love and support. All four of them are a continual source of inspiration for me, and I always look to their example in pursuing my passions in life.

Dedicated to my father John,

my mother Elizabeth,

and my sisters Edith and Tara.

Chapter 1

Introduction

1.1 Phase transitions and universality

In statistical physics, the goal is to describe the macroscopic properties of a many-body system using only a few external parameters. For example, one may be interested in how the average density or magnetization varies as a function of temperature. These quantities will usually be analytic functions of the temperature, but occasionally there might be a phase transition where the dependence is non-analytic.

There are two possibilities for the nature of the phase transition. In the first case, the two phases on either side of the transition may coexist at the transition point, where the properties of the system change discontinuously as one moves from one phase to the other. These are termed discontinuous or first-order transitions. In contrast, at continuous or critical phase transitions, the two phases become identical as they reach the transition, and exist as a single homogeneous state at the critical point. The difference in certain thermodynamic quantities in the two phases (such as the magnetization) goes to zero smoothly, and the correlation length of the system diverges.

As an explicit example, consider the Ising model

$$H = -J \sum_{\langle ij \rangle} \sigma_i^z \sigma_j^z \tag{1.1}$$

Here, the Pauli matrices are defined on the sites of a lattice and can take the values $\sigma_i^z = \pm 1$. The Hamiltonian is invariant under taking all the $\sigma_i^z \to -\sigma_i^z$ simultaneously.

In two or more spatial dimensions, this system exhibits a continuous phase transition at some finite temperature T_c. For $T > T_c$, the system is a paramagnet with no net magnetization, while for $T < T_c$, the system acquires a net magnetization $M = \sum_i \langle \sigma_i^z \rangle$ which goes to zero smoothly as T increases to T_c.

It is interesting to note that the magnetization, along with other thermodynamic quantities, behave as power laws near the critical point. Defining $t = (T - T_c)/T_c$, one finds

$$M \sim (-t)^\beta \tag{1.2}$$

where $\beta \approx .33$ in three dimensions. As another example, the specific heat C behaves as

$$C \sim |t|^{-\alpha} \tag{1.3}$$

where $\alpha \approx .11$ in three dimensions. One may also define a characteristic length for correlations in the system by considering the length scale ξ over which the two-point correlation function decays exponentially in the $T > T_c$ phase, $\langle \sigma_i^z \sigma_j^z \rangle \sim \exp(-|i-j|/\xi)$, and one finds that this length scale diverges as

$$\xi \sim t^{-\nu} \tag{1.4}$$

for $\nu \approx .63$ in three dimensions.

The emergence of power laws at the critical point is a manifestation of scale invariance. As the correlation length diverges, the microscopic length scales of the system no longer determine the dependence of thermodynamic quantities on temperature. This leads to the

phenomenon of *universality*: if we alter the Ising Hamiltonian (1.1) to include more complicated interactions, it will not change the values of the critical exponents as long as the added interactions respect the same symmetries as the original model and are sufficiently short-ranged.

Universality is a powerful because the independence of the critical exponents on the microscopic details of the interactions means that these critical exponents should apply to real experimental systems, justifying the use of a simplified lattice model to describe the transition. Experiments many different systems, from uniaxial magnetics to the liquid-vapor transition in fluids such as water, display critical exponents consistent with the above values [1]. From these considerations, a theoretical framework was developed which explains the emergence of scale invariance and allows a computation of critical exponents.

1.2 Field theory and the renormalization group

In the field-theoretic Landau-Ginzburg-Wilson (LGW) approach to critical phenomena [2, 3], one describes the system of interest using a local coarse-grained order-parameter field $\phi(x)$ in the vicinity of the critical point. The order parameter is assumed to be zero in the disordered phase but non-zero in the ordered phase, so in the Ising model we would imagine the field $\phi(x)$ to be a scalar describing the local magnetization. We imagine we could obtain this by summing the spins around some local region:

$$\phi(x) \sim \sum_{x_i \in x} \sigma_i^z \tag{1.5}$$

We then write the partition function as

$$\mathcal{Z} = \int_a \mathcal{D}\phi(x) e^{-\beta \mathcal{H}[\phi(x)]} \tag{1.6}$$

where the Hamiltonian $\beta\mathcal{H}[\phi(x)]$ is determined by writing down the most general possible functional of the order parameter $\phi(x)$ which is consistent with the symmetries of the problem. For the Ising model, we would require that the Hamiltonian must be local and symmetric under $\phi(x) \to -\phi(x)$ and $x \to -x$, so

$$\beta\mathcal{H}[\phi(x)] = \int d^d x \left[\frac{1}{2} (\nabla\phi)^2 + \frac{s}{2}\phi^2 + \frac{u}{4!}\phi^4 + \frac{v}{6!}\phi^6 + \cdots \right] \tag{1.7}$$

We have chosen the units of $\phi(x)$ to set the coefficient of $\frac{1}{2}(\nabla\phi)^2$ to 1. The ellipses will also contain higher order gradients in the field. We have also represented the partition sum in the schematic notation $\int_a \mathcal{D}\phi(x)$, where a signifies some small length scale parametrizing the choice of regularization needed to make the continuum field theory finite.

At first sight, since the couplings and regularization of this theory are almost completely arbitrary, this theory appears to lack any quantifiable predictability. However, when we study the low-energy behavior of this theory under the renormalization group we find that if we consider the nonlinear terms to initially be small (so we are perturbing around the Gaussian theory), almost all of the interactions are irrelevant. In particular, if we apply a scale transformation $x \to x' = x/b$ to the theory (1.6-1.7), we find that the couplings renormalize as

$$\begin{aligned} u' &= b^{4-d} u \\ v' &= b^{6-2d} v \\ &\vdots \end{aligned} \tag{1.8}$$

to leading order, and the higher-order interactions decay with an even stronger b dependence for $d \leq 3$.

These results spell some difficulty for the field theoretic approach, as the quartic nonlinearity grows for any fixed spatial dimension less than 4, invalidating perturbation theory. However, if one works directly at $d = 4$, the first effect of interactions is to cause u to be

irrelevant, scaling to zero logarithmically:

$$u' = \frac{u}{1 + \alpha u \ln b} \qquad (d = 4) \tag{1.9}$$

where $\alpha > 0$. This led Wilson and Fisher [4] to consider a simultaneous expansion in both u and $\epsilon = 4 - d$, where a scale transformation becomes

$$u' = u \left[b^\epsilon + \frac{1}{1 + \alpha u \ln b} \right] \approx u \left(\epsilon \ln b - \alpha u \ln b \right) \tag{1.10}$$

One finds that there is an interacting fixed point at $u^* = \epsilon/\alpha$ which can be perturbatively controlled. This allows a computation of the scaling dimensions of operators, which are simply related to the critical exponents considered above. Extrapolating results for this theory to $\epsilon = 1$ gives good agreement with experiments and numerics on the three-dimensional Ising model [1]. The ϵ expansion forms the basis for many computations in this thesis, as it is one of the few interacting critical points which can be accessed perturbatively using field theory methods.

As an aside, we note that nearly every field theory with both scale invariance and rotational invariance possesses an even larger conformal symmetry, and are thus conformal field theories (CFTs). In two dimensions, conformal symmetry is powerful enough to exactly solve many CFTs [5]. Less is understood in higher dimensions, but recent work exploiting conformal symmetry has led to interesting new results in some interesting interacting CFTs such as the 3D Ising model [6, 7].

1.3 Quantum phase transitions

We now consider phase transitions where quantum physics plays a crucial role in the critical fluctuations. We note that while many phase transitions involve phases which require quantum mechanics for their description, the critical theory describing these transitions at

finite temperature is often described using classical statistical mechanics, as the length scale associated with thermal fluctuations dominates close enough to the critical point.

As the critical temperature decreases, however, quantum mechanics begins to be important in describing the critical fluctuations. One way to heuristically see the effect of quantum mechanics is to note that when $\hbar \neq 0$, we can define a new characteristic time scale

$$\tau = \frac{\hbar}{k_B T_c} \tag{1.11}$$

For time scales much longer than τ, we can ignore quantum effects and use the classical theory of dynamic critical phenomena [8]. However, as T_c goes to zero this new time scale diverges, and we enter the regime of quantum critical phenomena where dynamic and static fluctuations both diverge.

Many of the new properties inherent to quantum critical points derive from the interplay of dynamics and statics implied by the above argument. In particular, recall that the partition function of a many-body quantum system $\mathcal{Z} = \mathrm{Tr}\, e^{-\beta \hat{\mathcal{H}}}$ may be written in terms of an imaginary-time Feynman path integral

$$\mathcal{Z} = \int \mathcal{D}\phi(\tau, x) \exp\left\{ -\frac{1}{\hbar} \int_0^{\hbar\beta} d\tau d^d x \; \mathcal{L}[\phi(\tau, x)] \right\} \tag{1.12}$$

with $\mathcal{L}[\phi(\tau, x)]$ an appropriately chosen Lagrangian density. This takes the form of a classical Ginzburg-Landau theory in $d + 1$ spatial dimensions, showing again that quantum phase transitions have similar properties to classical phase transitions in one extra dimension due dynamic fluctuations. The relation between quantum phase transitions in d dimensions and classical phase transitions in $d + 1$ dimensions is quite general, and in many cases of interest one can directly use results from the higher-dimensional classical phase transition [9]. In particular, if a quantum phase transition is Lorentz invariant at low energies, its path integral will resemble a rotationally invariant classical system in one extra space dimension.

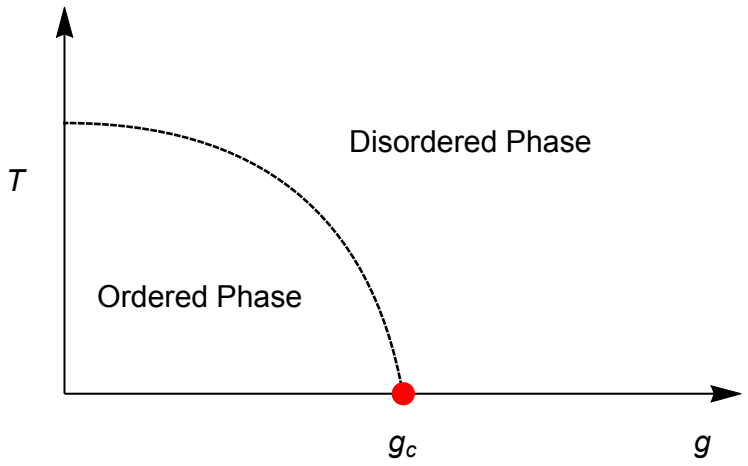

Figure 1.3.1: A possible phase diagram for a system with a quantum critical point. The parameter g drives quantum fluctuations while the temperature T drives thermal fluctuations. There is a crossover from quantum critical behavior to classical critical behavior as one approaches the dotted line at finite temperature.

The prototypical example of a quantum critical system is the transverse field Ising (TFI) model, given by the Hamiltonian

$$H = -J \sum_{\langle ij \rangle} \sigma_i^z \sigma_j^z - h \sum_i \sigma_i^x \tag{1.13}$$

The first term is identical to the classical Ising model of Eq. (1.1), while the second term is a transverse magnetic field which keeps the symmetry $\sigma^z \to -\sigma^z$, but acts to destroy the ferromagnetically polarized ground state. This drives a quantum phase transition at some critical h_c, and a renormalization group analysis of the resulting quantum field theory leads one to show that the critical exponents are in the same universality class as the classical Ising model in $d+1$ dimensions [9]. The phase diagram of this system in $d \geq 2$ takes the form shown in Figure 1.3.1.

1.4 Static observables unique to quantum critical points

Given the mapping from quantum to classical critical phenomena, many universal observables may be immediately obtained from the theory of classical critical phenomena. However, the special role of the time axis in the path integral leads to some new observables in the quantum theory which have no meaningful analogue in a classical context. Much of the new physics at quantum critical points is related to the real-time dynamics, especially at finite temperature, which requires an analytic continuation of the imaginary-time theory back to real time [9].

In this thesis we will only be studying static observables, and we will almost always work at $T = 0$. However, the splitting of spacetime into spatial and temporal pieces will still be important to us, as we will be studying the global properties of the low-lying states in the Hilbert space. Below we give a brief outline of the static observables of interest.

1.4.1 Finite-size energy spectrum

One of the most striking predictions of quantum mechanics is the quantization of energy levels in bound systems. When we place a quantum critical system in a finite volume, we similarly obtain a quantized energy spectrum, but the resulting spectrum will now take a universal form. For a Lorentz invariant quantum critical point,

$$E_n = \frac{\hbar c}{L} \xi_n \tag{1.14}$$

where c is the non-universal characteristic velocity scale, L is some length scale associated with the volume of the system, and the ξ_n are a set of universal numbers which depend on the critical theory and the shape of the finite volume of interest.

One case which has been studied previously is the finite-size spectrum of a conformal field theory on a sphere with radius R. Then Eq. (1.14) holds with $L = R$, and the numbers ξ_n

are in one-to-one correspondence with the scaling dimensions of the operators of the CFT [10].

We will be interested in the finite-size energy spectrum on the torus. Our interest is two-fold. First, the torus is by far the easiest translation-invariant geometry to work with in numerical simulations of lattice models, so computations on the torus are ideal for identifying critical behavior seen in numerics. Second, the nontrivial topology of the torus will allow the spectrum to probe the presence of exotic phases with topological order. Such phases are described by emergent gauge degrees of freedom, and configurations where a gauge flux winds around the cycles of the torus will dramatically alter the low-energy spectrum.

1.4.2 Ground state entanglement entropy

Two regions of a quantum system are said to be entangled if there are correlations between them, or equivalently if the wave function for both regions cannot be written as a product of independent wave functions. For the ground state of a many-body quantum system with local interactions, one generically expects that nearby points are entangled with each other, but regions which are far from each other compared to a microscopic scale are independent. However, in a critical system where the correlation length diverges, we may expect long-range entanglement.

We make this more quantitative by introducing the entanglement entropy. We consider dividing the total system into two regions A and B (see Figure 1.4.1), and then calculate the reduced density matrix associated with one of the regions,

$$\rho_A = \mathrm{Tr}_B\, \rho \tag{1.15}$$

where $\rho = |0\rangle\langle 0|$ is the density matrix for the ground state. Then the entanglement entropy

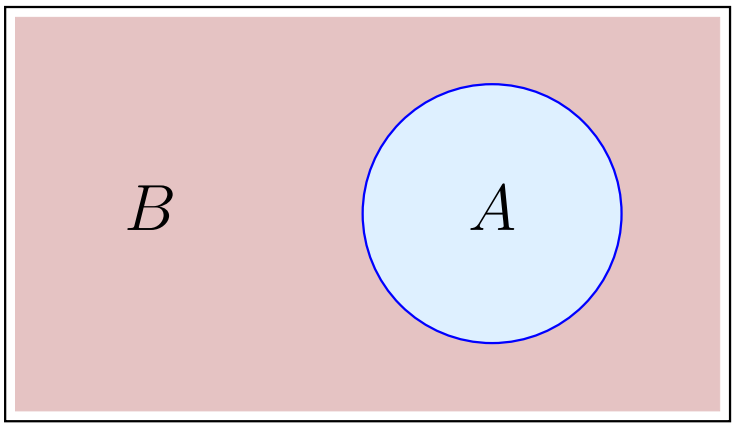

Figure 1.4.1: The division of a system into two parts for computing the entanglement entropy.

is the von Neumann entropy of the reduced density matrix,

$$S_A = -\operatorname{Tr} \rho_A \ln \rho_A \tag{1.16}$$

The local interactions across the boundary results in a term proportional to the perimeter of the boundary, $|\partial A|$, but in a CFT we generically find an extra term

$$S_A = \frac{|\partial A|}{a} - \gamma \tag{1.17}$$

The contribution γ depends on the CFT, and is only a function of the shape of the region. This universal term has applications in constraining renormalization group flows [11], and can also be computed in numerics on lattice models. However, few analytic results exist for interacting CFTs, so understanding more about CFT entanglement could lead to more interesting applications and results.

1.4.3 Impurities in quantum critical systems

A localized impurity interacting strongly with a quantum critical system will have nontrivial dynamic correlations controlled by its interactions with the bulk. In terms of the imaginary time path integral (1.12), the impurity exists on a 0+1 dimensional line interacting with the $d+1$ dimensional bulk. In this case, the system may also be interpreted classically in terms of a critical system interacting with a localized line defect. However, the quantum interpretation is more amenable to potential experimental applications, as the bulk critical theory is realized well-controlled cold-atom experiments which may be able to realize a local impurity potential [12]. We also calculate the universal finite-temperature compressibility of the system, which does not have a simple interpretation in terms of the corresponding classical theory.

1.5 Organization of thesis

The rest of this thesis details the explicit field-theoretic computation of many new universal quantities associated with quantum critical points. We summarize our findings here.

Chapters 2, 3, and 4 are all concerned with the computation of the finite-size spectrum of interacting quantum critical points on the torus. In Chapter 2 we detail the torus spectrum for the Wilson-Fisher conformal field theory (CFT) using the ϵ expansion. We show that this problem maps to finding the spectra of a series of *strongly-coupled* quantum mechanical Hamiltonians which must be solved numerically. Chapter 3 derives the Wilson-Fisher torus spectrum in the large N limit, which may be obtained more easily and thus allows some exact checks on certain behavior such the crossover of the spectrum into nearby phases.

Chapter 4 is concerned with the torus spectrum for a class of deconfined quantum critical points which describe confinement transitions in $\mathbb{Z}_2$ spin liquids. After reviewing these transitions, we give results using both the ϵ and large N expansions, and we give details on the case where the transition is between a $\mathbb{Z}_2$ spin liquid and antiferromagnetic order.

Particular focus is placed on the ability to detect nearby topological order and symmetry breaking from the structure of the low-energy spectrum. In all three chapters we discuss connections between our calculations and numerical simulations on lattice models, and in many cases we compare explicitly with results obtained with exact diagonalization.

In Chapter 5 we discuss the entanglement entropy of the Wilson-Fisher CFT in the large N limit. We obtain a general mapping between the Wilson-Fisher entropy and the entanglement entropy of free scalar fields with a mass gap determined by the properties of the interacting CFT. We use this mapping to give the Wisher-Fisher entanglement entropy for several cases of interest, showing in some cases that the entanglement entropy can undergo a large decrease under a renormalization group flow. Our results can also be used to map the entanglement entropy of the Gross-Neveu CFT to that of free Dirac fermions.

Chapter 6 studies the critical behavior of a localized impurity at the 2+1 dimensional superfluid-Mott insulator transition. Motivated by results seen in numerical simulations, we develop a critical quantum field theory describing the coupling between bulk critical modes and the impurity degree of freedom. We study this field theory using the ϵ expansion and find an interacting fixed point associated with the impurity. We calculate multiple critical exponents at this new universality class as well as the universal contribution to the compressibility at finite temperature. Comparison is made with numerics.

Chapter 2

Spectrum of the Wilson-Fisher conformal field theory on the torus: ϵ-expansion

2.1 Introduction

The identification of quantum critical behavior is an interesting problem in condensed matter and statistical mechanics. A major aspect of this is the emergence of universal low-energy behavior in the vicinity of a continuous quantum critical point, which is controlled by a conformal field theory (CFT) in the scaling limit.

In this chapter we explore the finite-size energy spectrum of the Wilson-Fisher CFT, also known as the critical O(N) model, in (d+1) spacetime dimensions. One case where the structure of the spectrum is well-understood is when the system is on the d-dimensional sphere S^d. In this case, conformal invariance implies the *state-operator correspondence*, which states that the energy spectrum takes the form $E_n = c\Delta_n/R$ where c is the model-dependent speed of light, R is the radius of the sphere, and the Δ_n are the scaling dimensions of the operators of the CFT in an infinite volume [10, 13]. These scaling dimensions are extremely con-

strained by conformal invariance, and the operator spectrum of many interesting CFTs has been mapped out using methods such as exact results available in two spacetime dimensions [5] and the conformal bootstrap [6, 7, 14–16].

The state-operator correspondence has proven to be very useful in studying $(1 + 1)$-dimensional critical points, where numerically computing the spectrum on the circle is routinely done to accurately identify critical points [17, 18]. However, in higher dimensions the curved geometry has proven to be difficult to implement accurately [19–23]. In light of these difficulties, it seems natural to instead study the universal energy spectrum on flat geometries such as the torus, where the energy spectrum still takes the form $E_n = c\xi_n/L$ for some universal set of constants ξ_n dependent on the shape of the torus. However, the structure of the torus spectrum is not simply related to the operator content, so one must use perturbative field theory.

In the present chapter we will use the ϵ-expansion, where $\epsilon = 3-d$, to compute the critical energy spectrum in quantum field theory. We will also compare with exact diagonalization (ED) of explicit lattice models with critical points in the O(1), O(2), and O(3) universality classes. We will show that the numerical computations show excellent agreement with the ϵ-expansion results. Beyond that, we will demonstrate that the critical low-energy torus spectra are intrinsically different among the distinct CFTs considered in this paper, characterizing the interpretation of the low-energy critical torus spectrum as a universal fingerprint of the underlying CFT and as a useful tool for investigating quantum critical points with diverse methods.

In Section 2.2 we will introduce our model and method, discussing how to treat fluctuations of the zero mode non-perturbatively using an effective Hamiltonian method. Section 2.3 details the structure of the effective Hamiltonians and how to compute them using perturbative quantum field theory, giving examples for several important special cases to demonstrate how the method works in general. In Section 2.4 we discuss how to numerically obtain the spectrum of the effective Hamiltonians in a few special cases, and give some explicit results

for the low-energy spectrum. In Section 2.5 we compare our analytic results to numerical results in several explicit lattice models, and we give conclusions in Section 2.6.

2.2 The method

The Wilson-Fisher CFT is described by the bare real-time Hamiltonian

$$H = \int d^d x \left(\frac{1}{2}\Pi_\alpha^2 + \frac{1}{2}\left(\nabla\phi_\alpha\right)^2 + \frac{s_0}{2}\phi_\alpha^2 + \frac{u}{4!}\phi_\alpha^4 + \Lambda \right) \tag{2.1}$$

where the index α ranges from $1, ..., N$. We are using the notation $\phi_\alpha^2 \equiv \phi_\alpha \cdot \phi_\alpha$ and $\phi_\alpha^4 \equiv \left(\phi_\alpha^2\right)^2$, so the model has full O(N) symmetry. We suppress time-dependence, set the speed of light to unity, and note that fields satisfy the equal-time commutator $[\phi_\alpha(x), \Pi_\beta(x')] = i\delta_{\alpha\beta}\delta^d(x - x')$. We have included a bare ground state energy density Λ, which is needed to renormalize the ground state energy. The critical point is obtained by tuning $s_0 = s_c$, while u approaches a fixed value u^*. This is a strongly-coupled theory for any finite $d < 3$ and N, but its universal properties can be computed as a power series in either $\epsilon = 3 - d$ or $1/N$.

We are interested in the finite-size spectrum of the above model on a spatial torus in $d = 2$, which is parametrized by complex coordinates $x = x_1 + ix_2$. We use the standard parametrization of the torus in terms of two complex periods, ω_1 and ω_2, and define the complex modular parameter $\tau \equiv \omega_2/\omega_1$ with real and imaginary parts denoted by $\tau = \tau_1 + i\tau_2$. Below, we will often give results in terms of the length scale $L \equiv |\omega_1|$. The area of the torus is given by $\mathcal{A} = \mathrm{Im}\left(\omega_2\omega_1^*\right) = \tau_2 L^2$. This geometry is pictured in Fig. 2.2.1.

In the following we calculate the spectrum in the ϵ-expansion, which forces us to introduce extra dimensions [4]. To this end, we consider $d/2$ copies of the desired two-dimensional spatial geometry, which retains the point-group and modular symmetries of the system while avoiding the introduction of any additional unphysical parameters. We then expand in ϵ, and set $\epsilon = 1$ to obtain predictions for the $d = 2$ system.

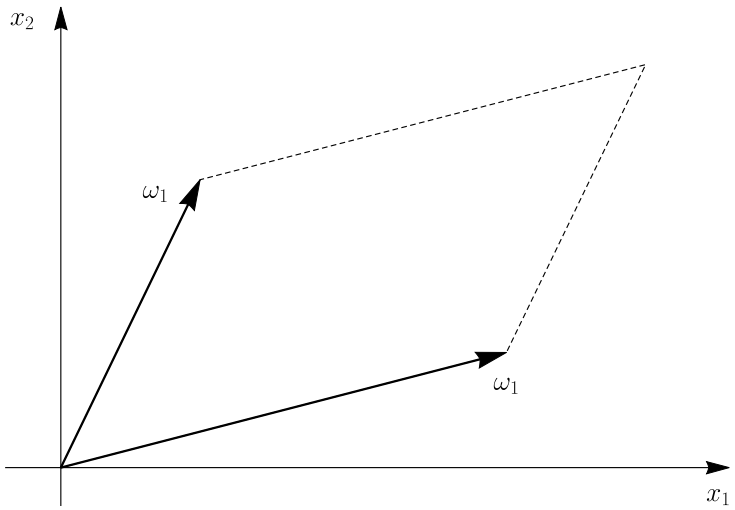

Figure 2.2.1: The geometry of the torus on which our theory is defined. Here we have defined complex coordinates $x = x_1 + ix_2$, and we define the two complex periods ω_1 and ω_2. Then our geometry is the one pictured where the point x and the point $x + n\omega_1 + m\omega_2$ are associated with each other for any $n, m \in \mathbb{Z}$.

As usual, we will need to eliminate the bare couplings in favor of finite renormalized couplings. Because renormalization is entirely due to short-distance divergences, the finite-volume theory on a manifold with no curvature must have identical renormalization constants to the infinite volume theory, since the only new length scale is large compared to the cutoff. Here we use a modified minimal subtraction scheme [24], where divergent poles in ϵ are subtracted with extra factors of

$$S_{d+1} = \frac{2}{\Gamma(d/2)\,(4\pi)^{d/2}} \tag{2.2}$$

attached. We introduce the renormalized coupling g by

$$u = Z_4 \frac{\mu^\epsilon g}{S_{d+1}} \tag{2.3}$$

In our calculations, we will always set g to its fixed point value immediately after poles in ϵ

have been subtracted. We also write

$$s_0 = s_c + Z_2 s \tag{2.4}$$

where s is a renormalized tuning parameter describing relevant perturbations across the critical point at $s = 0$.

We are also interested in the dependence of the ground state energy as a function of the geometry of the torus and the tuning s. This requires introducing the counterterm

$$\Lambda = Z_\Lambda \frac{s^2 Z_2^2 S_{d+1}}{\mu^\epsilon} \tag{2.5}$$

which renders the energy density finite. In the above expressions, the Z factors contain poles in ϵ, and μ is an arbitrary energy scale. In principle one also needs to renormalize the fields ϕ_α, but these will not contribute to the leading order expressions so we ignore this here. For a review of these definitions and their relation to $L = \infty$ observables, see Appendix A.1.

The main technical feature of the ϵ-expansion in a finite volume is the importance of the zero-momentum mode. Since the fields are gapless at the fixed point for $\epsilon \to 0$, the zero mode generates incurable infrared divergences in perturbation theory. These can be related to the failure of expanding around mean field theory, where the zero mode can have arbitrarily large fluctuations in the absence of interactions. This results in a continuum of zero mode excitations for the free field theory, whereas the interacting theory must have a gap and a discrete set of states, since the quartic term in the Hamiltonian will suppress fluctuations of the zero mode. Therefore, the free field theory with a zero mode is not the correct starting point in perturbation theory.

As was first realized by Lüscher [25], and further developed by others studying finite size effects in classical critical phenomena [26, 27], the solution is to separate the zero mode and treat it non-perturbatively. Since the finite momentum modes have an effective gap, they can be safely integrated out in a path integral approach, leading to an effective action for

the zero momentum modes which must be treated exactly. Here we pursue a Hamiltonian approach rather than a path integral approach, but our method is the same in principle. We note that a similar real-time approach was used to study low-energy spectrum of Yang-Mills theory on the torus in Ref. [28].

We expand the fields and their conjugate momenta as

$$\begin{aligned}
\phi_\alpha(x) &= \mathcal{A}^{\frac{1-d}{4}}\varphi_\alpha + \frac{1}{\mathcal{A}^{d/4}}\sum_{k\neq 0}\frac{e^{ik\cdot x}}{\sqrt{2\omega_k}}\left(b_\alpha(k) + b_\alpha^\dagger(-k)\right) \\
\Pi_\alpha(x) &= \mathcal{A}^{-\frac{d+1}{4}}\pi_\alpha - \frac{i}{\mathcal{A}^{d/4}}\sum_{k\neq 0}\sqrt{\frac{\omega_k}{2}}e^{ik\cdot x}\left(b_\alpha(k) - b_\alpha^\dagger(-k)\right)
\end{aligned} \tag{2.6}$$

where $\omega_k = \sqrt{|k|^2 + s_0}$ and $k \cdot x = \mathrm{Re}(kx^*)$. The values of momentum summed over are determined by the shape of the torus, see Appendix A.3. Our expansion has been chosen such that the operators φ_α, π_α, and $b_\alpha(k)$ are dimensionless and have the commutation relations

$$[\varphi_\alpha, \pi_\beta] = i\delta_{\alpha\beta}, \qquad [b_\alpha(k), b_\beta^\dagger(k')] = \delta_{\alpha\beta}\delta_{kk'} \tag{2.7}$$

We now insert this expression into (2.1) and separate the Hamiltonian into a "free" and "interaction" part, where we insist that all zero-mode contributions are included in the interaction part:

$$\begin{aligned}
H &= H_0 + V, \\
H_0 &= \mathcal{E}_0 + \sum_{k\neq 0}\omega_k b_\alpha^\dagger(k) b_\alpha(k),
\end{aligned} \tag{2.8}$$

We are defining the bare ground state energy

$$\mathcal{E}_0 = \mathcal{A}^{d/2}\Lambda + \frac{N}{2}\sum_{k\neq 0}\omega_k, \tag{2.9}$$

and an interaction Hamiltonian,

$$\begin{aligned} V &= \frac{1}{\sqrt{\mathcal{A}}}\left\{\frac{\pi^2}{2}+\frac{1}{2}\mathcal{A}s_0\varphi^2+\frac{u\mathcal{A}^{\epsilon/2}}{4!}\varphi^4\right\} \\ &+ \frac{1}{\sqrt{\mathcal{A}}}u\mathcal{A}^{\epsilon/2}\left(\frac{\delta_{\alpha\beta}}{12}\varphi^2+\frac{1}{6}\varphi_\alpha\varphi_\beta\right)\sum_{k\neq 0}\frac{\chi_\alpha(-k)\chi_\beta(k)}{2\mathcal{A}^{1/2}\omega_k} \\ &+ \frac{1}{\sqrt{\mathcal{A}}}\frac{u\mathcal{A}^{\epsilon/2}}{6}\varphi_\alpha\sum_{k,k'\neq 0}\frac{\chi_\alpha(k)\chi_\beta(k')\chi_\beta(-k-k')}{(8\mathcal{A}^{3/2}\omega_k\omega_{k'}\omega_{k+k'})^{1/2}} \\ &+ \frac{1}{\sqrt{\mathcal{A}}}\frac{u\mathcal{A}^{\epsilon/2}}{4!}\sum_{k,k',k''\neq 0}\frac{\chi_\alpha(k)\chi_\alpha(k')\chi_\beta(k'')\chi_\beta(-k-k'-k'')}{4(\mathcal{A}^2\omega_k\omega_{k'}\omega_{k''}\omega_{k+k'+k''})^{1/2}} \end{aligned} \tag{2.10}$$

where $\chi_\alpha \equiv b_\alpha(k)+b_\alpha^\dagger(-k)$, and repeated latin indices are summed. We can now develop perturbation theory in V. The ground state energy (2.9) will be renormalized along with interactions in our final expressions and expanded to the appropriate order in ϵ.

Since the zero mode does not appear in the unperturbed Hamiltonian, the unperturbed eigenstates are given by

$$H_0\Psi[\varphi_\alpha]|k,\alpha;k',\beta;\cdots\rangle = (\mathcal{E}_0+\omega_k+\omega_{k'}+\cdots)\,\Psi[\varphi_\alpha]|k,\alpha;k',\beta;\cdots\rangle \tag{2.11}$$

Here, the energies are determined by the Fock states created by the $b_\alpha^\dagger$ operators, but states can be multiplied by *arbitrary* normalizable functionals of the zero mode $\Psi[\varphi_\alpha]$. So the unperturbed states are infinitely degenerate, but this degeneracy is broken in perturbation theory.

We use a perturbation expansion developed by Bloch [29] which is well-suited to dealing with degeneracy. The method involves deriving an effective Hamiltonian within each degenerate subspace whose spectrum gives the splitting of that subspace. So we find an operator H_{eff} such that

$$H_{\text{eff}}|\alpha_0\rangle = E_\alpha|\alpha_0\rangle \tag{2.12}$$

where $|\alpha_0\rangle$ are the set of unperturbed degenerate states, and

$$E_\alpha = \epsilon_0 + \mathcal{O}(V) \tag{2.13}$$

are the exact energies under the full interacting Hamiltonian, where ϵ_0 is the unperturbed energy of the states $|\alpha_0\rangle$.

We review the derivation of Bloch's effective Hamiltonian in Appendix A.2. The main result needed is that the effective Hamiltonian at leading order is given by

$$H_{\text{eff}} = \epsilon_0 P_0 + P_0 V P_0 + P_0 V \frac{1 - P_0}{\epsilon_0 - H_0} V P_0 + \mathcal{O}(V^3) \tag{2.14}$$

where P_0 is the projection operator onto the degenerate subspace $|\alpha_0\rangle$. The calculation of the effective Hamiltonian will result in UV divergences due to summations over infinitely large momenta implicitly contained in Eq. (2.14), so this is the step where the theory is renormalized.

From Eq. (2.11), we can infer the action of H_{eff} on our degenerate subspaces. An arbitrary state in a given degenerate manifold takes the form

$$\sum_{a=1}^{M} \Psi_a[\varphi] \, |\{k_i\}\rangle_a \tag{2.15}$$

where M is the number of Fock states with the same energy. This degeneracy between inequivalent Fock states will be due to O(N) symmetry or discrete rotation symmetry. The effective Hamiltonian will take the form of an $M \times M$ matrix which acts as

$$\sum_{b=1}^{M} H_{\text{eff},ab} \; \Psi_b[\varphi]|\{k_i\}\rangle_b = E \; \Psi_a[\varphi]|\{k_i\}\rangle_a \tag{2.16}$$

This effective Hamiltonian will be a function of π and φ. Due to the commutation relations, the action of π on $\Psi_a[\varphi]$ is $\pi_\alpha = -i\frac{\partial}{\partial \varphi_\alpha}$, so this will be a set of M coupled differential

equations. In practice, symmetries of the interaction will allow us to consider smaller block-diagonal subspaces separately. For our model, the interaction conserves momentum and O(N) rotations, which further constrains the form of H_{eff} and its eigenvectors.

2.3 Calculation of the effective Hamiltonians

2.3.1 Structure of the effective Hamiltonians

Before proceeding with explicit calculations, we first describe the general structure of the effective Hamiltonian and its dependence on ϵ, and discuss the perturbative spectrum of the Hamiltonian for small ϵ. We give this discussion prior to explicit calculations because we will see that the perturbation theory is reordered in the scaling limit, leading to a modified expansion in fractional powers of ϵ. We will find that the terms in V do not contribute to the ϵ-dependence of the spectrum that would be naïvely inferred by Eq. (2.10), so our analysis will aid us in correctly finding the leading contributions when we turn to explicit calculations. We will also highlight how the behavior of the spectrum changes depending on the magnitude of the tuning parameter s.

Here we will consider the effective Hamiltonian when the Fock state is non-degenerate ($M = 1$ in Eq. (2.16)), since the analysis is similar in the general case. From Eq. (2.14), the effective Hamiltonian at leading order takes the form

$$\begin{aligned} H_{\text{eff}} &= \mathcal{E}_0 + \frac{1}{\sqrt{\mathcal{A}}}\left[K\frac{\pi^2}{2} + \frac{1}{2}R\varphi^2 + \frac{U}{4!}\varphi^4\right] + \cdots \\ K &= 1 + \mathcal{O}(\epsilon^2) \\ R &= \mathcal{A}s + r_1\epsilon + \mathcal{O}(\epsilon^2) \\ U &= \frac{48\pi^2\epsilon}{N+8} + \mathcal{O}(\epsilon^2) \end{aligned} \tag{2.17}$$

where the ellipses will include additional operators which will not appear until $\mathcal{O}(\epsilon^2)$. The coefficient of each term will be a regular series in ϵ. Here we write r_1 as the $\mathcal{O}(\epsilon)$ coefficient

of the operator φ_α^2. We have used the relations in Appendix A.1 to set the quartic coupling to its fixed point.

Since we are interested in the critical regime, we first consider the theory for $s = 0$. In this case, the coefficients of the quadratic and quartic terms are both $\mathcal{O}(\epsilon)$, but the structure of the spectrum can be made more clear by making the canonical transformation

$$\varphi \to \epsilon^{-1/6}\varphi, \qquad \pi \to \epsilon^{1/6}\pi \tag{2.18}$$

after which the Hamiltonian is given by

$$H_{\text{eff}} = \mathcal{E}_0 + \frac{\epsilon^{1/3}}{\sqrt{\mathcal{A}}}\left[K\frac{\pi^2}{2} + \frac{1}{2}R\epsilon^{-2/3}\varphi^2 + \frac{U/\epsilon}{4!}\varphi^4\right] + \cdots \tag{2.19}$$

We see that when $s = 0$, the Hamiltonian takes the form

$$H_{\text{eff}} = \mathcal{E}_0 + \frac{\epsilon^{1/3}}{\sqrt{\mathcal{A}}}h(\epsilon) \tag{2.20}$$

where

$$\begin{aligned} h(\epsilon) &= k\frac{\pi^2}{2} + \frac{1}{2}r\varphi^2 + u\varphi^4 \\ k &= 1 + \mathcal{O}(\epsilon^2) \\ r &= \epsilon^{1/3}\left(r_1 + \mathcal{O}(\epsilon)\right) \\ u &= \frac{48\pi^2}{N+8} + \mathcal{O}(\epsilon) \end{aligned} \tag{2.21}$$

We see that $h(0)$ is a pure quartic anharmonic oscillator whose spectrum gives the spectrum of H_{eff} to order $\epsilon^{1/3}$. Furthermore, the leading corrections are given by obtaining the spectrum of $h(\epsilon)$ in a perturbation series in $\epsilon^{1/3}$. Thus, the spectrum of the Wilson-Fisher fixed point at small ϵ has mapped to the spectrum of a quartic anharmonic oscillator in a strong-coupling expansion.

If we repeat the above analysis for $s \neq 0$, we find that the quadratic coefficient of the reduced Hamiltonian $h(\epsilon)$ is modified to

$$r = \frac{\mathcal{A}s}{\epsilon^{2/3}} + \epsilon^{1/3}\left(r_1 + \mathcal{O}(\epsilon)\right) \tag{2.22}$$

For $\mathcal{A}s \gtrsim \epsilon^{2/3}$, our previous analysis no longer holds. The spectrum will be given by a weak-coupling expansion around a simple harmonic oscillator Hamiltonian provided $\mathcal{A}s \gg \epsilon$. This is sensible because our entire approach has been based on the gaplessness of the zero mode, whereas a nonzero s contributes a gap. For large enough values of $\mathcal{A}s$, we do not need to separate the zero mode, and we could have done a normal expansion around Gaussian field theory, which is equivalent to the weak coupling expansion in the current effective Hamiltonian approach. The crossover from a weakly-coupled oscillator with a particle-like spectrum to a strongly-coupled oscillator signals the breakdown of particle-like excitations at the quantum critical point. It is interesting that this occurs already for arbitrarily small values of ϵ, reflecting the importance of interactions in confining the zero mode.

In the following we will always assume

$$\mathcal{A}s = \mathcal{O}(\epsilon) \tag{2.23}$$

or smaller, so that we may use the same strong-coupling expansion of $h(\varepsilon)$ at $s = 0$ and $s \neq 0$.

The reordering of the perturbative expansion requires a modified analysis of our perturbation theory. This can be most easily visualized by representing terms in the effective Hamiltonian diagrammatically, associating extra factors of $\epsilon^{-1/6}$ with factors of φ anticipating the utility of the transformation in Eq. (2.18). With this in mind, we can schematically rewrite the interaction Hamiltonian Eq. (2.10) after the canonical transformation to identify

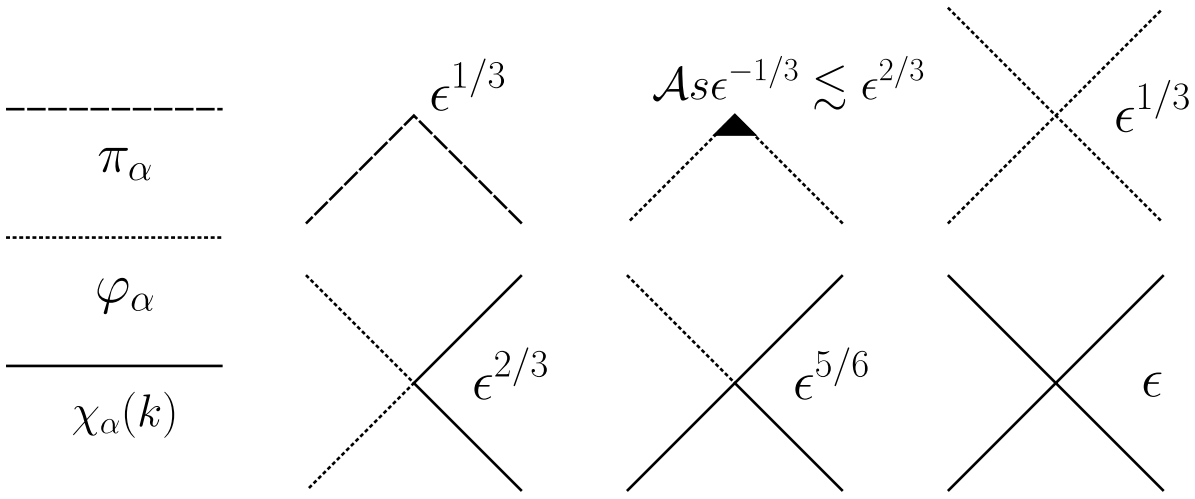

Figure 2.3.1: (Left) Lines representing the insertion of the operators π_α, φ_α, and $\chi_\alpha(k) \equiv b_\alpha(k) + b^\dagger_\alpha(-k)$. (Right) The vertices of the interaction Hamiltonian coupling the zero modes to the finite momentum modes. The top three vertices represent the three terms on the first line of Eq. (2.10), and appear in every effective Hamiltonian. The bottom three vertices represent the last three lines of Eq. (2.10) respectively. As argued in Section 2.3.1, the labelled powers of ϵ refer to the order at which each vertex contributes to the spectrum.

the individual terms with the correct powers of ϵ:

$$\begin{aligned} V &= \frac{\epsilon^{1/3}}{\sqrt{\mathcal{A}}}\left\{\frac{\pi^2}{2} + \frac{1}{2}\frac{\mathcal{A}s_0}{\epsilon^{2/3}}\varphi^2 + \frac{u\mathcal{A}^{\epsilon/2}}{\epsilon^{1/3}4!}\varphi^4\right\} + \frac{\epsilon^{2/3}}{\sqrt{\mathcal{A}}}\left(\frac{\delta_{\alpha\beta}}{12}\varphi^2 + \frac{1}{6}\varphi_\alpha\varphi_\beta\right)M^{(2)}_{\alpha\beta} \\ &+ \frac{\epsilon^{5/6}}{\sqrt{\mathcal{A}}}\varphi_\alpha M^{(1)}_\alpha + \epsilon M^{(0)} \end{aligned} \tag{2.24}$$

Here, the $M^{(n)}$ coefficients involve n factors of finite-momentum modes. With this form of the interaction, we write down the vertices associated with V in Fig. 2.3.1. Then in calculating the effective Hamiltonian from Eq. (2.14) we organize the ϵ-expansion diagrammatically using these vertices. In practice it is easier to work directly with Eq. (2.10) to compute the effective Hamiltonian, but the correct order of each term's contribution to the energy spectrum will be given by the ϵ coefficient pictured in Fig. 2.3.1.

2.3.2 Effective Hamiltonians for low-lying states

In this section we will give the explicit derivation of the effective Hamiltonians for the lowest-lying states in the Fock spectrum. We will perform the calculation for increasingly complex cases, with each example having an added subtlety compared to the previous case, after which the general structure for the effective Hamiltonian splitting an arbitrary Fock state should follow.

Fock vacuum

We begin by considering the splitting of the Fock vacuum. This will give us the lowest-lying zero-momentum states, including the energy gap. The unperturbed eigenstate is

$$\Psi[\varphi]|0\rangle. \tag{2.25}$$

Since $P_0 = |0\rangle\langle 0|$, the effective Hamiltonian will be of the form

$$\mathcal{H}_{\text{eff},k=0} = h_{k=0}|0\rangle\langle 0|. \tag{2.26}$$

From Eq. (2.16), the Schrödinger equation acting on the unperturbed subspace reduces to

$$h_{k=0}\Psi[\varphi] = E\Psi[\varphi] \tag{2.27}$$

where, using Eq. (2.14), the reduced Hamiltonian $h_{k=0}$ at one-loop is given by

$$h_{k=0} = \mathcal{E}_0 + \langle 0|V|0\rangle - \langle 0|V\left(\frac{1-|0\rangle\langle 0|}{H_0-\mathcal{E}_0}\right)V|0\rangle. \tag{2.28}$$

At this point we note that every term appearing in $h_{k=0}$ can be associated with a diagram. The three terms in this equation correspond to diagrams with zero, one, and two vertices respectively. Because the interaction V conserves momentum, each vertex must also enforce

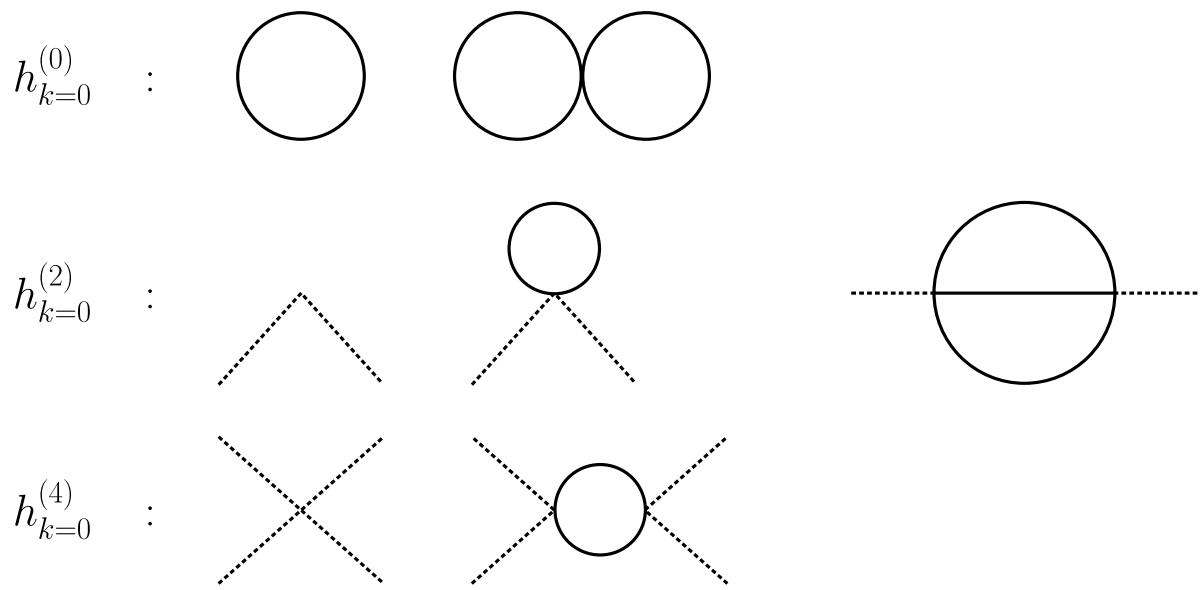

Figure 2.3.2: (Left) The diagrams which contribute to the effective Hamiltonian at leading order. Each row is associated with a term written in Eq. (2.29). (Right) The leading two-loop contribution to the effective Hamiltonian, which we do not calculate.

momentum conservation. The expectation values and sums over k implies one must contract all $\chi(k)$ propagators. Finally, the presence of the projector in the last term means we must contract the two vertices, preventing any disconnected diagrams from appearing.

Writing the effective Hamiltonian as

$$h_{k=0} = \frac{1}{\sqrt{\mathcal{A}}}\frac{\pi_\alpha^2}{2} + h^{(0)}_{k=0} + h^{(2)}_{k=0}\varphi_\alpha^2 + h^{(4)}_{k=0}\varphi_\alpha^4, \tag{2.29}$$

we collect the one-loop terms which contribute to the effective Hamiltonian in Fig. 2.3.2. At $\mathcal{O}(\epsilon^{5/3})$ we encounter a nontrivial two-loop diagram, also pictured in Fig. 2.3.2, so we truncate the spectrum to order $\epsilon^{4/3}$.

Using Eq. (2.10), we obtain

$$\begin{aligned}
h^{(0)}_{k=0} &= \mathcal{A}^{(3-\epsilon)/2}\Lambda + \frac{N}{2}\sum_{k\neq 0}\sqrt{|k|^2+s_0} + \frac{u\mathcal{A}^{\epsilon/2}}{\mathcal{A}^{3/2}}\frac{N(N+2)}{4(4!)}\left[\sum_{k\neq 0}\frac{1}{\sqrt{|k|^2+s_0}}\right]^2 \\
h^{(2)}_{k=0} &= \frac{\varphi^2}{2}\tau_2^{1/2}LsZ_2 + \frac{u\mathcal{A}^{\epsilon/2}}{2\tau_2 L^2}\left(\frac{\delta_{\alpha\beta}}{12}\varphi^2 + \frac{1}{6}\varphi_\alpha\varphi_\beta\right)\sum_{k\neq 0}\frac{\delta_{\alpha\beta}}{\sqrt{|k|^2+s}} \qquad (2.30) \\
h^{(4)}_{k=0} &= \frac{u\mathcal{A}^{\epsilon/2}}{\sqrt{\tau_2}L}\frac{\varphi^4}{4!} - \frac{\left(u\mathcal{A}^{\epsilon/2}\right)^2}{8\tau_2^2L^4}\left(\frac{\delta_{\alpha\beta}}{12}\varphi^2 + \frac{1}{6}\varphi_\alpha\varphi_\beta\right)\left(\frac{\delta_{\gamma\delta}}{12}\varphi^2 + \frac{1}{6}\varphi_\gamma\varphi_\delta\right)\sum_{k\neq 0}\frac{\delta_{\alpha\gamma}\delta_{\beta\delta}+\delta_{\alpha\delta}\delta_{\beta\gamma}}{\left(|k|^2+s\right)^{3/2}}
\end{aligned}$$

At this point, we need to evaluate these infinite sums in $3-\epsilon$ dimensions, and we need to renormalize the theory. These technical details are treated at length in the Appendices. In Appendix A.3 it is shown how to evaluate infinite sums in arbitrary dimension, and in Appendix A.4 these three expressions are explicitly evaluated, and the cancellation of all divergences is demonstrated. We obtain the following effective Hamiltonian:

$$\begin{aligned}
h_{k=0} &= \mathcal{E}_{k=0} + \frac{1}{\sqrt{\tau_2}L}\left(\frac{\pi_\alpha^2}{2} + \frac{R}{2}\varphi_\alpha^2 + \frac{U}{4!}\varphi_\alpha^4\right) \\
\mathcal{E}_{k=0} &\equiv \frac{\pi N}{\tau_2 L}f^{(3-\epsilon)}_{-1/2}(\tau,s,\mu) + \frac{1}{\sqrt{\tau_2}L}\frac{N(N+2)}{N+8}\frac{\epsilon}{8}\tau_2 f^{(3)}_{1/2}(\tau,s,\mu)^2 \\
R &\equiv \tau_2 L^2 s + 2\pi\epsilon\left(\frac{N+2}{N+8}\right)\tau_2^{1/2}f^{(3)}_{1/2}(\tau,s,\mu) \\
U &\equiv \frac{48\pi^2\epsilon}{N+8}\left\{1 - \frac{\tau_2^{3/2}\epsilon}{4\pi}f^{(3)}_{3/2}(\tau,s) + \frac{3\,(3N+14)}{(N+8)^2}\epsilon\right\} \qquad (2.31)
\end{aligned}$$

Thus, the lowest states in the spectrum of the O(N) Wilson-Fisher fixed point are given by solving the quantum mechanics problem of an isotropic, N-dimensional anharmonic oscillator. Here, the special functions $f^{(d)}_\nu(\tau,s,\mu)$ are given explicitly in Eqns. (A.54-A.56), and the function $f^{(3-\epsilon)}_{-1/2}(\tau,s,\mu)$ should be expanded to first order in ϵ.

The functions $f^{(d)}_{-1/2}$ and $f^{(d)}_{1/2}$ depend on the renormalization scale μ, which can be eliminated by applying renormalization conditions on the $s \neq 0$ ground state energy and the energy gap. In this paper we will not eliminate μ, since the infinite volume quantities are non-analytic around the critical point. However, our assumption that $s \sim \mathcal{O}(\epsilon)$ allows us to

set s to zero in many of the terms. We furthermore note that at the critical point, $s = 0$, the μ-dependence drops out and the spectrum is a universal function of τ, N, and ϵ. The coefficients of the Hamiltonian are modular invariant at $s = 0$, which follows from Eq. (A.44) and the modular invariance of $\mathcal{A} = \tau_2 L^2$.

After performing a canonical transformation similar to Eq. (2.18), this Hamiltonian takes the form

$$h_{k=0} = \mathcal{E}_{k=0} + \frac{1}{\sqrt{\tau_2} L} \left(\frac{U}{4!}\right)^{1/3} \left(\frac{\pi_\alpha^2}{2} + \frac{R U^{-2/3}}{2} \varphi_\alpha^2 + \varphi_\alpha^4\right) \tag{2.32}$$

We will primarily work with this form of the Hamiltonian in Section 2.4.

Single particle Fock states

We now consider the splitting of the single particle state

$$\Psi_\alpha[\varphi]|k, \alpha\rangle \tag{2.33}$$

where we assume there are no multi-particle Fock states with the same momentum and energy, so we only need to consider an N-fold degenerate manifold. This assumption should hold for the smallest values of $|k|$. The effective Hamiltonian can be written as a matrix equation acting on the vector of functions Ψ_α:

$$\sum_{\beta=1}^{N} h_{k,\alpha\beta} \Psi_\beta[\varphi] = E \Psi_\alpha[\varphi] \tag{2.34}$$

where the effective Hamiltonian $h_{k,\alpha\beta}$ can be represented by an $N \times N$ matrix whose components are

$$h_{k,\alpha\beta} = \left(\sqrt{k^2 + s_0^2} + \mathcal{E}_0\right) \delta_{\alpha\beta} + \langle k, \alpha | V | k, \beta \rangle - \langle k, \alpha | V \left(\frac{1 - \sum_\alpha |k, \alpha\rangle\langle k, \alpha|}{H_0 - \sqrt{|k|^2 + s} - \mathcal{E}_0}\right) V | k, \beta \rangle \tag{2.35}$$

and $|k, \alpha\rangle = b_\alpha^\dagger |0\rangle$.

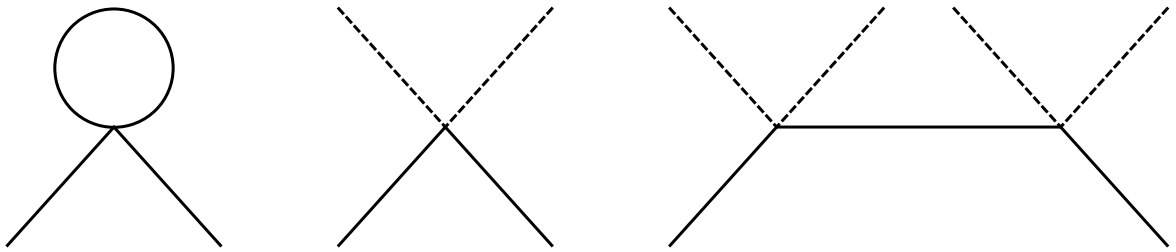

Figure 2.3.3: Diagrams which contribute new terms to the effective Hamiltonian for the splitting of a single Fock state.

The terms in this equation can also be given a diagrammatic representation: one can consider all diagrams with two external finite-momentum lines carrying momentum k. However, the external momenta do not need to be contracted with the vertices in any of the terms. As a consequence, we obtain a term

$$h_{k,\alpha\beta} \supset h_{k=0}\delta_{\alpha\beta} \tag{2.36}$$

simply by taking the diagrams in Fig. 2.3.2 and drawing a disconnected solid line in them. In addition to these, we will get new contributions due to the extra diagrams pictured in Figure 2.3.3. Only one of these diagrams contains a loop, so there will only be a single new divergence which is cancelled by the mass renormalization of s_0 in the first term of Eq. (2.35).

An explicit calculation similar to the one done for the Fock vacuum results in

$$\begin{aligned} h_{k,\alpha\beta} &= \left(\mathcal{E}_k + h_{k=0}\right)\delta_{\alpha\beta} + \frac{1}{\sqrt{\tau_2}L}\left(\frac{R_k}{2}\left(\varphi_\eta^2\delta_{\alpha\beta} + 2\varphi_\alpha\varphi_\beta\right) + \frac{U_k}{4!}\left(\delta_{\alpha\beta}\varphi_\eta^4 + \varphi_\eta^2\varphi_\alpha\varphi_\beta\right)\right) \\ \mathcal{E}_k &\equiv \sqrt{|k|^2+s} + \frac{1}{L}\left(\frac{N+2}{N+8}\right)\frac{\pi\epsilon}{\sqrt{|k|^2+s}} f^{(3)}_{1/2}(s,\tau,\mu) \\ R_k &\equiv \frac{1}{\tau_2 L^2}\frac{8\pi^2\epsilon}{(N+8)}\frac{1}{\sqrt{|k|^2+s}} \\ U_k &\equiv -\frac{1}{\tau_2^2 L^4}\frac{192\pi^4\epsilon^2}{(N+8)^2}\frac{1}{\left(|k|^2+s\right)^{3/2}} \end{aligned} \tag{2.37}$$

For $N > 1$, this is an anisotropic anharmonic oscillator.

Two-particle Fock states

We now consider mixing between states of the form

$$\Psi_{\alpha\beta}[\varphi]|k_1,\alpha;k_2,\beta\rangle \tag{2.38}$$

We have $|k_1,\alpha;k_2,\beta\rangle = S_{12}b^\dagger_\alpha(k_1)b^\dagger_\beta(k_2)|0\rangle$ where we require a Bose symmetry factor: $S_{12} = \frac{1}{\sqrt{2}}$ if $k_1 = k_2$ and $\alpha = \beta$, and $S_{12} = 1$ otherwise. We will assume that there are no one-particle or $\geq$ 3-particle states with overlap with this state. However, we will consider the case where there exists inequivalent states $|k_1,\alpha;k_2,\beta\rangle$, $|k_3,\alpha;k_4,\beta\rangle$, such that

$$\sqrt{|k_1|^2+s}+\sqrt{|k_2|^2+s} = \sqrt{|k_3|^2+s}+\sqrt{|k_4|^2+s} \tag{2.39}$$

Because the interaction V conserves momentum, these states will only mix if

$$k_1+k_2 = k_3+k_4. \tag{2.40}$$

Such states can contribute to the low-energy spectrum on the torus. For example, on the square ($\tau = i$) torus the states $|2\pi/L,\alpha;-2\pi/L,\beta\rangle$ and $|2\pi i/L,\alpha;-2\pi i/L,\beta\rangle$ are inequivalent but can mix.

The effective Hamiltonian is now calculated in a similar manner to the previous two cases, and there is an obvious diagrammatic generalization of the previous rules. We now draw diagrams with four external lines with momenta k_i, $i = 1,...,4$. We then consider all possible contractions with either zero, one, or two vertices. We once again find a piece proportional to $h_{k=0}$, which involves the diagrams in Fig. 2.3.2 but with the four external lines contracted and disconnected to the vertices. In addition, we get contributions which are simply the diagrams in Fig. 2.3.3 but with a single additional finite-momentum line disconnected from the rest. Finally, we obtain the additional diagram pictured in Fig. 2.3.4, which can connect

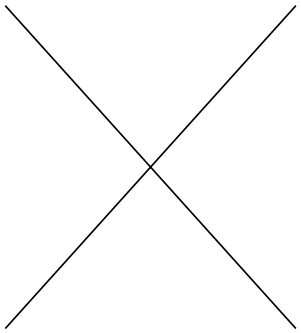

Figure 2.3.4: The additional diagram which contributes to the splitting of the two-particle Fock states.

the inequivalent states considered above. This does not contain a loop, so it is finite.

An explicit calculation gives

$$\begin{aligned} h_{2k,\alpha\beta;\mu\nu} &= \left[\frac{\delta_{\alpha\mu}\delta_{\beta\nu}\delta_{k_1k_3}\delta_{k_2k_4}+\delta_{\alpha\nu}\delta_{\beta\mu}\delta_{k_1k_4}\delta_{k_2k_3}}{1+\delta_{\mu\nu}\delta_{k_3k_4}}\right] h_{k=0} \\ &+ \frac{\delta_{\alpha\mu}\delta_{k_1k_3}\delta_{k_2k_4}}{1+\delta_{\mu\nu}\delta_{k_3k_4}}\left[h_{k_3,\beta\nu}-\delta_{\beta\nu}h_{k=0}\right]+\frac{\delta_{\alpha\nu}\delta_{k_1k_4}\delta_{k_2k_3}}{1+\delta_{\mu\nu}\delta_{k_3k_4}}\left[h_{k_4,\beta\mu}-\delta_{\beta\mu}h_{k=0}\right] \\ &+ \frac{1}{\tau_2^{3/2}L^3}\frac{4\pi^2\epsilon}{(N+8)}\frac{(\delta_{\alpha\beta}\delta_{\mu\nu}+\delta_{\alpha\mu}\delta_{\beta\nu}+\delta_{\alpha\nu}\delta_{\beta\mu})}{\left[(|k_1|^2+s)(|k_2|^2+s)(|k_3|^2+s)(|k_4|^2+s)\right]^{1/2}}\frac{\delta_{k_1+k_2,k_3+k_4}}{(1+\delta_{k_1k_2}\delta_{k_3k_4}\delta_{\alpha\beta}\delta_{\mu\nu})} \end{aligned} \tag{2.41}$$

The first two lines of Eq. (2.42) can be given in terms of the the zero-particle and single-particle Hamiltonians, while the last term is new and contributes a constant shift in the energy. It is the last term which can mix two states unrelated by O(N) symmetry, leading to a multidimensional Hamiltonian even when $N = 1$.

Mixing between one- and two-particle Fock states

We now consider the effective Hamiltonian which couples the states $|k,\alpha\rangle$ and $|k_1,\gamma;k_2,\delta\rangle$. In order for these states to mix, we need

$$\begin{aligned} \sqrt{|k_1|^2+s}+\sqrt{|k_2|^2+s} &= \sqrt{|k|^2+s} \quad , \\ k_1+k_2 &= k_3. \end{aligned} \tag{2.42}$$

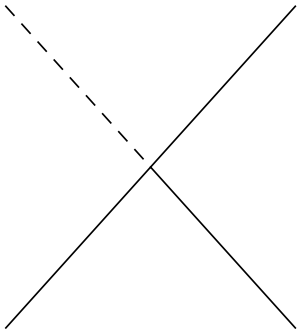

Figure 2.3.5: The diagram which contributes to the effective Hamiltonian mixing single-particle and two-particle Fock states.

While this set of equations is very restrictive, when $s = 0$ it can be satisfied by choosing k_1 and k_2 to be collinear, so in our expressions where $\mathcal{A}s \lesssim \epsilon$, we always have $s \ll |k|^2$ and these states will mix. We will assume here that the only other mixing is due to O(N) symmetry.

We can write the Hamiltonian mixing these two states as

$$\begin{pmatrix} h_{k,\alpha\beta} & h_{\alpha;\gamma\delta} \\ (h_{\beta;\mu\nu})^\dagger & h_{2k,\mu\nu;\gamma\delta} \end{pmatrix} \begin{pmatrix} |k,\beta\rangle \\ |k_1,\gamma;k_2,\delta\rangle \end{pmatrix} = E_n \begin{pmatrix} |k,\alpha\rangle \\ |k_1,\mu;k_2,\nu\rangle \end{pmatrix} \tag{2.43}$$

where the diagonal Hamiltonians are given by the one-particle and two-particle cases above, and the off-diagonal elements are

$$h_{\alpha;\gamma\delta} = \langle k,\alpha|V|k_1,\gamma,k_2,\delta\rangle - \langle k,\alpha|V\left(\frac{1-P_k}{H_0 - \sqrt{|k|^2+s} - \mathcal{E}_0}\right)V|k_1,\gamma,k_2,\delta\rangle \tag{2.44}$$

where P_k is the projector onto the degenerate subspace. We want all diagrams with three external lines with momenta k, k_1, and k_3. This leads to the diagram in Figure 2.3.5, which is finite, giving

$$h_{\alpha;\gamma\delta} = \frac{1}{\sqrt{\tau_2}L}\frac{4\sqrt{2}\pi^2\epsilon}{(N+8)}\frac{(\delta_{\alpha\gamma}\varphi_\delta + \delta_{\alpha\delta}\varphi_\gamma + \delta_{\delta\gamma}\varphi_\alpha)}{((|k|^2+s)(|k_1|^2+s)(|k_2|^2+s))^{1/4}} \tag{2.45}$$

This coupling between Fock states with different particle number is another manifestation of the breakdown of well-defined quasiparticles at a quantum critical point.

At this point we hope it is clear how to generalize these results to more complicated cases. As one moves higher in the spectrum, more degeneracies between Fock states are possible and more complicated effective Hamiltonians will be needed.

2.4 Numerical solution of the effective Hamiltonians

It remains to find the spectrum of the effective Hamiltonians perturbatively in ϵ. This must be done numerically, since the quartic anharmonic oscillator has no analytic solution. Given that there are many effective Hamiltonians, and each needs to be solved to at least third order in perturbation theory to obtain the $\epsilon^{4/3}$ contribution, this is one of the biggest barriers to obtaining the spectrum.

Here we show how to obtain the spectrum for most of the low-lying effective Hamiltonians in the $N = 1$ case, where the Hamiltonians are often one-dimensional quartic oscillators. For $N > 1$, we will confine ourselves to solving the effective Hamiltonian which splits the Fock vacuum, where rotational invariance allows us to map it to a one-dimensional differential equation in "radial" coordinates.

In Appendix A.7 we discuss of the $N = \infty$ limit of the ϵ expansion, where we can solve the spectrum of the Fock vacuum effective Hamiltonian exactly. We show agreement with the results of the large-N expansion of Chapter 3 wherever possible.

2.4.1 $N = 1$

We exploit the fact that most of the effective Hamiltonians for the low-lying states can be written in the form (see e.g. Eq. (2.32))

$$H_{\text{eff}} = \mathcal{E} + uh[r] \tag{2.46}$$

where

$$h[r] = -\frac{1}{2}\frac{d^2}{d\varphi^2} + \frac{r}{2}\varphi^2 + \varphi^4 \tag{2.47}$$

Here, $\mathcal{E}$ is a known function of ϵ, and

$$\begin{aligned} u &= u_1\epsilon^{1/3} + u_2\epsilon^{4/3} + \mathcal{O}(\epsilon^{7/3}) \\ r &= r_1\epsilon^{1/3} + \mathcal{O}(\epsilon^{4/3}) \end{aligned} \tag{2.48}$$

for some constants r_1, $u_{1,2}$ which depend on the specific effective Hamiltonian in question. Then we need the spectrum of $h[r]$ in a power series in r. After writing

$$h[r]\Psi[\varphi] = \lambda_n(r)\Psi[\varphi], \tag{2.49}$$

expansion of the spectrum in ϵ can be written

$$\lambda_n(r) = \sum_{m=0}^{\infty} c_{n,m} r^m \tag{2.50}$$

Assuming we know the coefficients $c_{n,m}$ which appear in this expansion, we can simply write down the spectrum to the desired order:

$$E_n(\epsilon) = \mathcal{E} + u_1 c_{n,0}\epsilon^{1/3} + u_1 r_1 c_{n,1}\epsilon^{2/3} + u_1 r_1^2 c_{n,2}\epsilon + \left(u_1 r_1^3 c_{n,3} + u_2 c_{n,0}\right)\epsilon^{4/3} + \mathcal{O}\left(\epsilon^{5/3}\right) \tag{2.51}$$

$\tau = i$	$\kappa = 0$	$\kappa = 1$	$\kappa = \sqrt{2}$	$\kappa = 2$
	-0.12			
	1.70			
	5.04			
		6.28		
		8.76		
LE			8.90	
	8.90			
			11.23	
		12.29		
				12.55

Table 2.4.1: Low-lying spectrum of the critical Ising model on the square torus from ϵ-expansion, including the ground state energy. The states shaded gray are odd under the global $\mathbb{Z}_2$ symmetry, while the unshaded states are $\mathbb{Z}_2$ even. Here we parametrize the momentum by $\kappa = L|k|/(2\pi)$.

Fortunately, the numerical calculation of the coefficients $c_{n,m}$ has been extensively studied in the literature. In Ref. [30], Tables 7 and 10, the coefficients $c_{n,m}$ for $m = 1, .., 10$, $n = 1, ..., 10$ are given with at least five digit accuracy. Thus, for one-dimensional effective Hamiltonians, the spectrum can be obtained.

However, there can still be multi-dimensional effective Hamiltonians for $N = 1$ due to mixing between different Fock states. Fortunately, the form of the mixing is often very simple. In computing the low-lying spectrum, the first mixing one comes across is between two inequivalent two-particle states, as described in Section 2.3.2. There, the effective Hamiltonian acting on these two states takes the form

$$h_{2k} = h_{2k,1}\mathbb{I} + h_{2k,2}\sigma^x \tag{2.52}$$

where $h_{2k,2}$ is of order ϵ and is independent of the zero mode. In this case, we can diagonalize the Hamiltonian by inspection, obtaining the energy splitting

$$\begin{aligned} E_{2k,-} &= E_{2k,1} - h_{2k,2} \\ E_{2k,+} &= E_{2k,1} + h_{2k,2} \end{aligned} \tag{2.53}$$

where $E_{2k,1}$ are the energies of $h_{2k,1}$.

Finally, we do encounter the states described in Section 2.3.2 which mix the single-particle and two-particle Fock states. In this case, we must numerically calculate the contribution. However, this is made easier by the fact that the order $\epsilon^{5/6}$ term arises in first-order perturbation theory, so we only need the zeroth order wave functions. That is, we first numerically calculate the zeroth order wave functions which diagonalize h_k and h_{2k}, and then we compute the overlap

$$\int_{-\infty}^{\infty} d\varphi \Psi_k[\varphi]\Psi_{2k}[\varphi]h_{1k2} \tag{2.54}$$

We calculate the unperturbed wave function numerically using the same shooting method described in Appendix A.5 for the $N > 1$ case.

The low-lying spectrum of the critical Ising model on the square torus is given in Table 2.4.1.

2.4.2 $N > 1$

Here we will focus on the splitting of the Fock vacuum, where the Hamiltonian is an isotropic N-dimensional oscillator. We begin with Eq. (2.32):

$$h_{k=0} = \mathcal{E}_{k=0} + \frac{1}{\sqrt{\tau_2}L}\left(\frac{U}{4!}\right)^{1/3}\left(\frac{\pi_\alpha^2}{2} + \frac{RU^{-2/3}}{2}\varphi_\alpha^2 + \varphi_\alpha^4\right) \tag{2.55}$$

Then defining

$$h_N[s] = -\frac{1}{2}\nabla_\varphi^2 + \frac{s}{2}\varphi_\alpha^2 + \varphi_\alpha^4 \tag{2.56}$$

and the reduced couplings

$$\begin{aligned} \frac{1}{\sqrt{\tau_2}L}\left(\frac{U}{4!}\right)^{1/3} &= u_1\epsilon^{1/3} + u_2\epsilon^{4/3} + \mathcal{O}(\epsilon^{7/3}) \\ RU^{-2/3} &= r_1\epsilon^{1/3} + \mathcal{O}(\epsilon^{4/3}), \end{aligned} \tag{2.57}$$

we obtain Eq. (2.51) except the coefficients $c_{n,m}$ will depend on N.

To make further progress, we take advantage of the fact that $h_N[r]$ can be written in spherical coordinates, after which it separates into a known angular equation and a one-dimensional radial equation. We go to hyperspherical coordinates

$$\begin{aligned}
\varphi_1 &= \rho \cos \\
\varphi_1 &= \rho \sin\theta_1 \cos\theta_2 \\
\varphi_1 &= \rho \sin\theta_1 \sin\theta_2 \cos\theta_3 \\
&\vdots \\
\varphi_{N-1} &= \rho \sin\theta_1 \cdots \sin\theta_{N-2} \cos\theta_{N-1} \\
\varphi_N &= \rho \sin\theta_1 \cdots \sin\theta_{N-2} \sin\theta_{N-1}
\end{aligned} \tag{2.58}$$

Then the Laplacian can be written in the separable form

$$\nabla^2_\varphi = \sum_{i=1}^{N} \frac{\partial^2}{\partial^2 \varphi_i} = \frac{1}{\rho^{N-1}} \frac{\partial}{\partial \rho} \rho^{N-1} \frac{\partial}{\partial \rho} + \frac{1}{\rho^{N-1}} \nabla^2_{S^{N-1}} \tag{2.59}$$

where $\nabla^2_{S^{N-1}}$ is the Laplacian on the $(N-1)$-sphere. We will not use the coordinate representation of this operator, but instead use what is known of its spectrum [31]. The eigenvectors and eigenvalues are given by

$$-\nabla^2_{S^{N-1}} Y_{\ell,\ell_1,\ell_2,\ldots,\ell_{N-2}}(\theta_i) = \ell\,(\ell + N - 2)\, Y_{\ell,\ell_1,\ell_2,\ldots,\ell_{N-2}}(\theta_i) \tag{2.60}$$

where the eigenfunctions can be given in terms of Gegenbauer polynomials of the $\cos\theta_i$, and

the indices can range from

$$\begin{aligned} \ell &= 0, 1, 2, ... \\ \ell_1 &= -\ell_2, -\ell_2 + 1, -\ell_2 + 2, ..., \ell_2 \\ \ell_2 &= 0, 1, 2, ..., \ell_3 \\ \ell_3 &= 0, 1, 2, ..., \ell_4 \\ &\vdots \\ \ell_{N-2} &= 0, 1, 2, ..., \ell \end{aligned} \tag{2.61}$$

The spectrum does not depend on the the ℓ_i. This gives a degeneracy for a given eigenvalue ℓ of

$$\mathcal{N}(\ell, N) = \frac{(2\ell + N - 2)(\ell + N - 3)!}{\ell!(N-2)!} \tag{2.62}$$

for $N \geq 3$. For $N = 2$, there is only one eigenfunction for each ℓ, but the states Y_ℓ and $Y_{-\ell}$ are degenerate (these are simply the states $e^{i\ell\theta}$ and $e^{-i\ell\theta}$), so the degeneracy is

$$\mathcal{N}(\ell, 2) = \begin{cases} 1 & \ell = 0 \\ 2 & \ell > 0 \end{cases} \tag{2.63}$$

Finally, we note that the eigenfunctions are in the symmetric traceless tensor representation of O(N), and we can label these representations using the eigenvalue ℓ.

With these eigenfunctions, we can express our functionals as

$$\Psi[\varphi] = R_{n,\ell}(\rho) Y_{\ell,\ell_1,\ell_2,...,\ell_{N-2}}(\theta_i) \tag{2.64}$$

and the eigenvalue equation becomes

$$\frac{1}{2}\left(-\frac{1}{\rho^{N-1}} \frac{\partial}{\partial r} \rho^{N-1} \frac{\partial}{\partial \rho} - \frac{\ell\,(\ell + N - 2)}{\rho^{N-1}} + r\rho^2 + 2\rho^4 \right) R_{n,\ell}(\rho) = E_{n,\ell} R_{n,\ell}(\rho) \tag{2.65}$$

$\tau = i$	$\ell = 0$	$\ell = 1$	$\ell = 2$	$\ell = 3$	$\ell = 4$
	-0.986				
		0.96			
			3.66		
	4.74				
				6.79	
LE		8.31			
					10.32
			12.12		
				16.19	
					20.52

Table 2.4.2: Low-lying spectrum of the critical O(2) model on the square torus from ε-expansion, including the ground state energy. These states are obtained from the effective Hamiltonian which gives the splitting of the $k = 0$ Fock vacuum. The $\ell = 0$ states are non-degenerate while the $\ell > 0$ states are two-fold degenerate.

Here we have introduced a radial quantum number n, which corresponds to the number of zeros in R. We have reduced our problem to a one-dimensional eigenvalue equation, and we wish to find the spectrum perturbatively in r. In analogy with the $N = 1$ case, we write this expansion as

$$E_{n,\ell} = \sum_{m=0}^{\infty} c_{n,\ell,m} r^m \tag{2.66}$$

We have obtained the coefficients of the perturbative expansion in r for $N = 2, 3, 4$, $\ell = 0, ..., 4$ and $n = 0, 1$ numerically. We obtained these by first solving the $r = 0$ equation numerically for the wave function and energy. We then used logarithmic perturbation theory [32, 33], which is well-suited to this problem because it allows one to find the coefficients of the expansion directly from the unperturbed energy and wave function without needing excited states. We detail this approach and give the relevant numerical results in Appendix A.5. Using these results, the energy to leading order is

$$E_{n,\ell}(\epsilon) = \mathcal{E} + u_1 c_{n,\ell,0} \epsilon^{1/3} + u_1 r_1 c_{n,\ell,1} \epsilon^{2/3} + u_1 r_1^2 c_{n,\ell,2} \epsilon + \left(u_1 r_1^3 c_{n,\ell,3} + u_2 c_{n,\ell,0}\right) \epsilon^{4/3} + \mathcal{O}\left(\epsilon^{5/3}\right) \tag{2.67}$$

We give the lowest-lying states for $N = 2$ and $N = 3$ at the critical point in Tables 2.4.2

$\tau = i$	$\ell = 0$	$\ell = 1$	$\ell = 2$	$\ell = 3$	$\ell = 4$
	-2.28				
		-0.66			
			1.74		
	2.95				
				4.59	
LE		6.20			
					7.81
			9.69		
				13.45	
					17.47

Table 2.4.3: Low-lying spectrum of the critical O(3) model on the square torus from ε-expansion, including the ground state energy. These states are obtained from the effective Hamiltonian which gives the splitting of the $k = 0$ Fock vacuum. The states have degeneracy $2\ell + 1$.

and 2.4.3.

2.5 Comparison with numerical calculation of critical torus spectra from lattice models

In this section we compare our analytic results with the numerical spectra obtained using exact diagonalization (ED) on explicit lattice models.

2.5.1 $N = 1$

We first consider the $O(1) = \mathbb{Z}_2$ critical point, also known as the critical Ising model. These results were presented in Reference [34], which contains further technical details about the numerical computation. Numerical computations were performed for the ferromagnetic two-dimensional transverse field Ising (TFI) model,

$$H_{\text{TFI}} = -J \sum_{\langle i,j \rangle} \sigma_i^z \sigma_j^z - h \sum_i \sigma_i^x \tag{2.68}$$

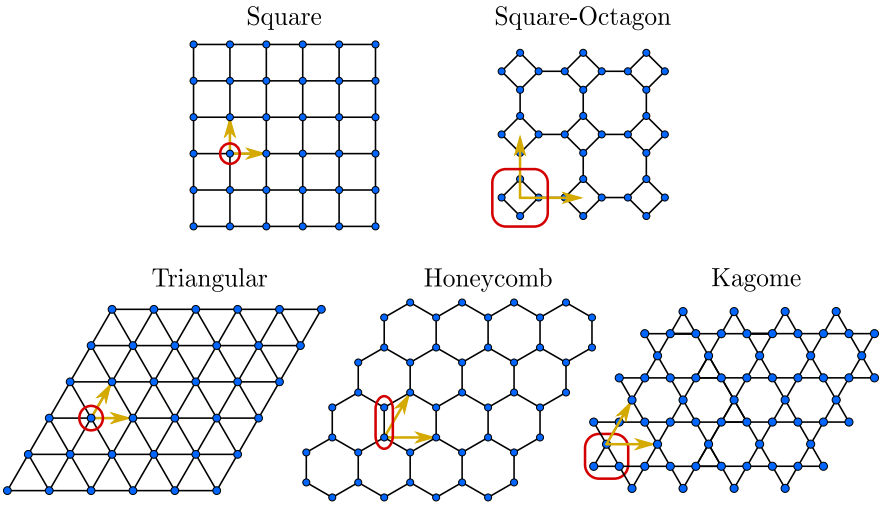

Figure 2.5.1: The different lattice geometries used for the TFI model. The red boxes indicate the lattice basis cells and the arrows mark the Bravais-vectors. The square and square-octagon lattices obey a C_4 rotational symmetry; the triangular, honeycomb and kagome lattices a C_6 rotational symmetry.

For large h/J, the spins are polarized along with the field h in the x direction, and the system has a unique paramagnetic ground state. In the small h/J limit, the system spontaneously breaks the $\mathbb{Z}_2$ symmetry $\sigma_i^z \to -\sigma_i^z$, and the system is in a ferromagnetic state with a two-fold degenerate ground state in an infinite volume. At some intermediate non-universal value $(h/J)_c$, there is a quantum phase transition between these two states which is described by the $N = 1$ Wilson-Fisher CFT [9].

This model was simulated on five different lattices, see Figure 2.5.1. The lattices considered have either square (C_4) or hexagonal (C_6) discrete rotational symmetry microscopically, but in the vicinity of the critical point we expect these to flow to the same rotationally-invariant CFT in the IR. The lattices are then studied with periodic (toroidal) boundary conditions, where for simplicity they are given boundary conditions with the same point-group symmetries as the microscopic lattices. In particular, the lattices with square symmetry are placed on a torus with modular parameter $\tau = i$, which the lattices with hexagonal symmetry are on a torus with modular parameter $\tau = 2\pi i/3$.

In comparing ED with analytic results, we must also take into account that the dispersion

depends on the non-universal value of the speed of light,

$$E_n = \frac{c}{L}\xi_n(\tau) \tag{2.69}$$

In the previous sections of this paper we have used units where $c = 1$, but in explicit lattice models the speed of light will depend on the microscopic details. For the TFI model, quantum Monte Carlo (QMC) computations were performed for each of the lattices to extrapolate the speed of light. In particular, the energy splitting for the lowest $\mathbb{Z}_2$ odd states for a range of momenta $[k_{\min}, k_{\max}]$ were computed and extrapolated to the thermodynamic limit, and fitting these to a linear spectrum $E(k) = E_0 + ck$ allowed a computation of c. More details, including explicit values for c/J in the critical TFI model on these five lattices, are given in Reference [34].

The rest of the low-energy spectrum is computed using ED on lattices of increasing size, up to a total of 40 sites. The energy levels are extrapolated to the thermodynamic limit by finding the asymptotic value of LE as a function of $1/L$. The numerical and analytic results are explicitly compared in Figure 2.5.2.

2.5.2 $N = 2$

We now consider the O(2) critical point, also known as the quantum XY model. Two different lattice models will be utilized to study the critical spectrum of this universality class numerically. The first is a spin-1 model, $S = 1$, with single-ion anisotropy [35, 36]

$$H_1^{\mathrm{O}(2)} = -J\sum_{\langle i,j\rangle}\left(S_i^x S_j^x + S_i^y S_j^y\right) - J_z\sum_{\langle i,j\rangle} S_i^z S_j^z + D\sum_i (S_i^z)^2 \tag{2.70}$$

We set the energy scale by choosing $J = 1$. For small D the system orders ferromagnetically in the x-y spin plane, while for large D the system approaches a product state of single spins with $S^z = 0$. The phase transition is found to be in the XY/O(2) universality class. The

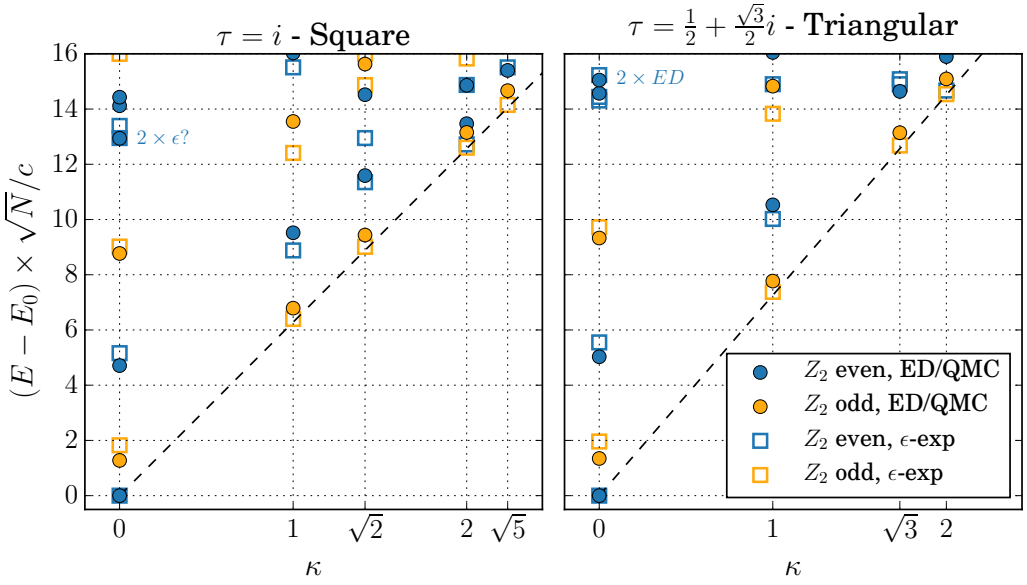

Figure 2.5.2: Universal torus spectra for the Ising CFT for the modular parameters $\tau = i$ (left panel) and $\tau = 1/2 + \sqrt{3}/2i$ (right panel). Full symbols denote numerical results obtained by ED or QMC, while empty symbols denote the ϵ-expansion results. The dashed line shows a dispersion according to the speed of light. In this figure, N is the total number of lattice sites.

parameter J_z can be tuned within a range around zero to check the stability of our results.

The second model we consider is the spin-1/2 XY-bilayer model [36, 37]. It consists of two usual ferromagnetic XY layers with additional XY couplings between them. We denote a spin located on site i in the first (second) layer as $S_{i,1(2)}$, the model is then described by

$$H_2^{\mathrm{O}(2)} = -J \sum_{n=1}^{2} \sum_{\langle i,j \rangle} \left(S_{i,n}^x S_{j,n}^x + S_{i,n}^y S_{j,n}^y \right) + J_\perp \sum_i \left(S_{i,1}^x S_{i,2}^x + S_{i,1}^y S_{i,2}^y \right) \tag{2.71}$$

We only consider positive couplings $J, J_\perp > 0$ here and set our energy scale $J = 1$. For large $J_\perp$ the system is described by a product state of singlets on each interlayer bond, whereas a XY-ferromagnet is formed in each plane for small $J_\perp$. The two phases are separated by a XY quantum critical point at $J_\perp = J_\perp^c = 5.460(1)J$ [37][1]

To calculate the critical torus energy spectrum, we compute the spectrum of the Hamilto-

[1]The energy spectrum of this model is conserved under changing the sign of $J \to -J$ when the momenta for odd S^z levels are shifted as $\mathbf{k} \to \mathbf{k} + (\pi, \pi)$. Therefore, the critical coupling $J_\perp^c$ is identical for both, ferromagnetic and antiferromagnetic $J = \pm 1$.

nians at criticality on finite-size toric clusters numerically. We multiply the finite-size spectra with the linear system size L to get rid of the dominant scaling and then extrapolate these spectra in $1/N$ to the thermodynamic limit. Further details about the numerical approach can be found in Reference [38].

In Fig. 2.5.3 we present the numerically obtained critical O(2) torus energy spectrum in the $\kappa = 0$ and $\kappa = 1$ sectors. Here and in the following we only show the lowest energy levels for $\ell \leq 4$ which are in the fully symmetric representation regarding the lattice point-group symmetry. We also restrict our discussion to square lattices, $\tau = i$. Results for triangular geometry $\tau = \frac{1}{2} + \frac{\sqrt{3}}{2}i$ are given in Reference [38]. The spectrum is normalized such that the lowest gap in the $\ell = 0$ sector is set to $\Delta_{\varepsilon_T} \equiv \Delta_{\ell=0} = 1$. To demonstrate the stability of the numerical results and the universality of the spectrum, the different models and parameters considered for O(2) universality are shown with different symbols and colors in the plot. For $\kappa = 0$ we also plot the ϵ-expansion results with empty diamonds to compare them with the numerics. We find that they agree reasonably well and show a qualitatively identical structure.

Here we also note that the four relevant fields in the O(2) CFT [1] correspond to the lowest $\ell = 1$, $\ell = 2$ and $\ell = 3$ levels as well as the first excited $\ell = 0$ level in the critical torus spectrum (all $\kappa = 0$). Interestingly, these are the four lowest states in the spectrum. A similar matching occurs in the Ising CFT, where the two relevant fields correspond to the two lowest levels in the critical spectrum [34]. It may be a general feature that relevant fields of the CFT have light analogues in the critical torus spectrum.

2.5.3 $N = 3$

In this section, we study the critical torus spectrum of the O(3) CFT numerically. To do so, we again consider two different lattice models with a critical point known to be described by the O(3) universality class. The first model is the prototypical Heisenberg bilayer model

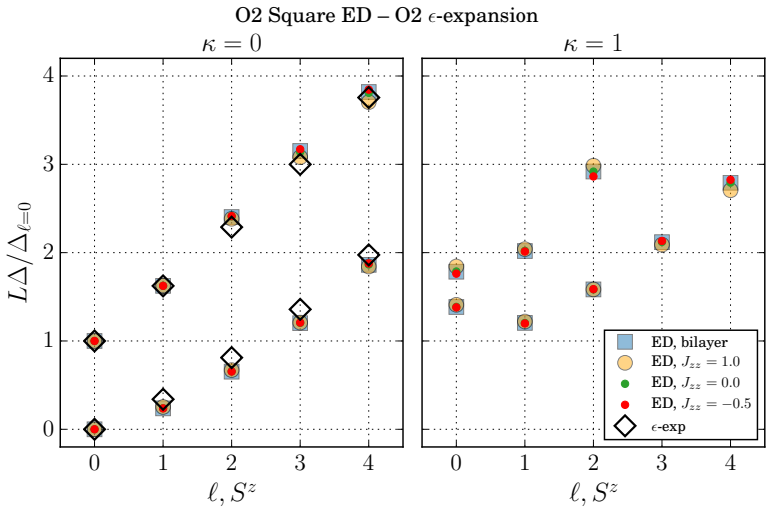

Figure 2.5.3: Critical torus energy spectrum for the O(2) CFT on a square geometry $\tau = i$ in the $\kappa = 0$ (left) and the $\kappa = 1$ (right) sectors. The results are normalized such that $\Delta_{\ell=0} = 1$. Full symbols denote ED results for different models/parameters, empty black diamonds show the ϵ-expansion results for the critical O(2) CFT ($\kappa = 0$ only). $\ell = 0$ levels are non-degenerate, while $\ell > 0$ levels are two-fold degenerate (times the geometrical multiplicity of $\kappa > 0$ levels). Note that the ED results only show levels in the fully symmetric representation regarding the lattice point-group symmetry. Levels in other point-group representations start to appear above $\Delta/\Delta_{l=0} \gtrsim 2$ for $\kappa = 0$.

[39–42]. It consists of spin-1/2 on two layers with nearest-neighbour Heisenberg intraplane couplings and Heisenberg interplane couplings on the rungs:

$$H_1^{O(3)} = J \sum_{n=1}^{2} \sum_{\langle i,j \rangle} (\mathbf{S}_{i,n} \cdot \mathbf{S}_{j,n}) + J_2 \sum_i \mathbf{S}_{i,1} \cdot \mathbf{S}_{i,2} \tag{2.72}$$

$S_{i,n}$ denotes a spin on site i in layer n. We set ferromagnetic intraplane couplings $J = -1$ and antiferromagnetic rung couplings $J_2 > 0$. For large J_2 the groundstate is a product state of singlets on each rung, whereas the groundstate for small J_2 is the direct product of Heisenberg ferromagnets within each plane. The phases are separated by an O(3) critical point.

The second model we want to investigate here is a Heisenberg model on a 2D square lattice

with columnar dimerization of bonds [43, 44]. The Hamiltonian for this ladder model is

$$H = J \sum_{\langle i,j \rangle} \mathbf{S}_i \cdot \mathbf{S}_j + J_2 \sum_{\langle i,j \rangle'} \mathbf{S}_i \cdot \mathbf{S}_j \tag{2.73}$$

Every second horizontal bond on the lattice is chosen to be in the family $\langle i,j \rangle'$, such that these dimerized bonds form ladders and every spin is part of exactly one dimerized bond. We set all couplings antiferromagnetic and set the energy scale $J = 1$. For $J_2/J = 1$ a Néel AFM is stabilized on a square lattice and for large J_2/J a product state of singlets on the bonds $\langle i,j \rangle'$ is formed as a groundstate. These phases are separated by an O(3) transition at the critical coupling $(J_2/J)_c = 1.9096(2)$ [43].

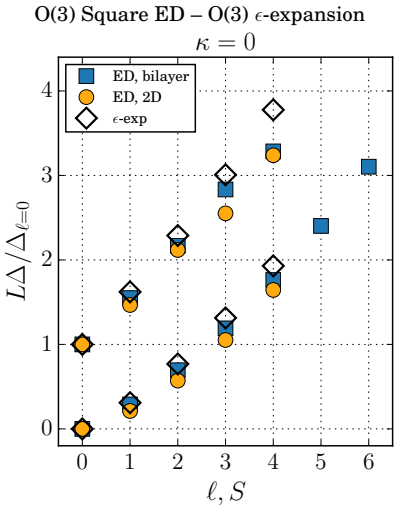

Figure 2.5.4: Critical torus energy spectrum for the O(3) CFT on a square lattice in the $\kappa = 0$ sector obtained from the models Eq. (2.72) (blue squares) and Eq. (2.73) (yellow circles). The results are normalized such that $\Delta_{l=0} = 1$. Empty black diamonds show the ϵ-expansion results for the O(3) CFT. The levels are $2l + 1$-fold degenerate. Note that the ED results only show levels in the fully symmetric representation regarding the lattice point-group symmetry. Levels in other point-group representations start to appear above $\Delta/\Delta_{l=0} \gtrsim 2$ for $\kappa = 0$.

We proceed similar to the case of $N = 2$ to compute the critical torus energy spectrum for the O(3) CFT numerically. The critical spectrum is shown in Fig. 2.5.4 together with the ϵ-expansion results. We again observe a decent agreement between the two methods and qualitatively identical critical torus spectra. Larger deviations for the second level in

$\ell = 4$ are probably related to difficulties in the extrapolation to the thermodynamic limit, as the available system sizes are strongly limited for these models. Although the critical torus spectra in the $\kappa = 0$ sector seems to look very similar for the O(2) and O(3) CFTs, their degeneracy structure is inherently different. For O(3) the levels are $(2\ell+1)$-fold degenerate, whereas they are 2-fold (1-fold) degenerate for $\ell > 0$ ($\ell = 0$) in the O(2) CFT. Further numerical results can be found in Reference [38].

2.6 Conclusions

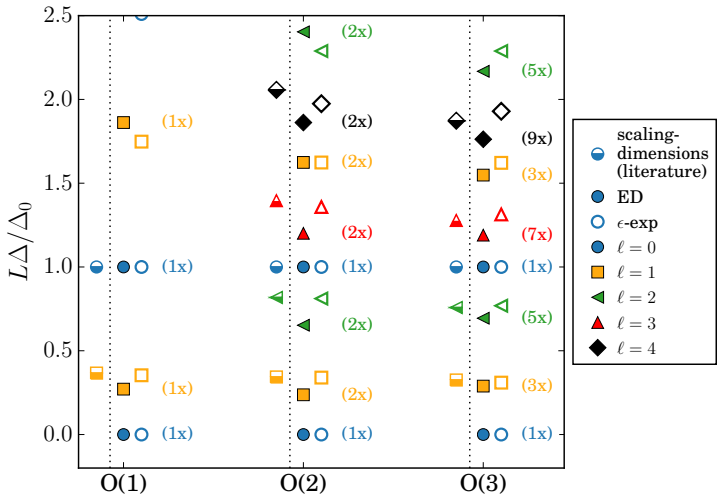

Figure 2.6.1: Critical low-energy torus spectra for the discussed O(N) CFTs for $\kappa = 0$ and $\ell \leq 4$ compared to the operator scaling dimensions of the CFTs from Refs. [6, 45]. The spectra and scaling dimensions are normalized by the gap Δ_0 to the first excited state with $\ell = 0$. Full symbols denote results from numerics (ED), open symbols show ϵ-expansion results. Half-filled symbols show the operator scaling dimensions of the corresponding CFTs as a comparison. The different symbols represent the different values of ℓ. The numbers in parentheses give the degeneracy of the levels. The level structure including degeneracies is qualitatively different between the distinct CFTs and can be considered as a universal fingerprint of the CFT. The operator scaling dimensions correspond to the critical energy spectrum of the Hamiltonians on a sphere. Interestingly, the structure of the operator dimensions and the torus spectrum are very similar for the low levels with an additional low $\ell = 1$ level in the torus spectrum.

In this chapter, we have demonstrated how to compute the torus energy spectrum of the Wilson-Fisher CFT from quantum field theory in the ϵ-expansion, showing the expected

emergence of a spectrum determined entirely by the universality class of the CFT and the spatial geometry of the torus. We compared this to the spectrum of several explicit lattice models at their respective quantum critical points using ED, and have shown that the analytic and numerical calculations agree well with each other, highlighting that the finite-size spectrum is a useful universal fingerprint for identifying quantum criticality. In Fig. 2.6.1 we show a comparison of the critical torus low-energy spectra for $N = 1, 2, 3$ in the $\kappa = 0$ sector which substantiates this interesting aspect of a universal fingerprint. Additionally, we compare the critical torus spectra with operator scaling dimensions of the corresponding CFTs from literature [6, 45]. We note a quantitative match between the low-energy critical torus spectrum at $\kappa = 0$ and the (rescaled) operator dimensions. This match may be a coincidence, as there is no known mapping between the torus spectrum and the operator dimension. It is not known what constitutes the complete data for a three-dimensional CFT, and whether the torus spectrum is new data or whether is can be related to the set of operator scaling dimensions.

We hope that our work has shed light on the nature of the finite-size spectrum in CFTs where conformal invariance does not lead to simple and exact results, and that our calculations aid in identifying critical behavior in numerical studies of quantum lattice models by investigation of the critical energy spectrum. The methods used in this work should also be applicable to computing the finite-size spectra of other CFTs, such as an ϵ-expansion approach to the Gross-Neveu-Yukawa CFT.

Chapter 3

Spectrum of the Wilson-Fisher conformal field theory on the torus: large-N expansion

3.1 Introduction

In this chapter, we will develop the finite-size spectrum of the Wilson-Fisher conformal field theory on the torus using an expansion in $1/N$, where N is the number of fields. The structure of this expansion is dramatically different from the ϵ expansion considered in Chapter 2, as the zero momentum mode does not play a special role. The $1/N$ perturbation expansion proceeds in the standard fashion [24, 46], with the only difference being that the diagrams are over discrete momenta. The spectrum is then obtained by finding poles in the correlation functions. We will see that the simplified form of the expansion at leading order will allow an easy computation of the complete spectrum in the whole critical regime, including for $s \neq s_c$, allowing us to track how the spectrum evolves between the two phases on either side of the transition.

Section 3.2 will set up the large N expansion, while Section 3.3 will detail how to obtain

the torus spectrum, with details on how the spectrum evolves as one tunes between the two phases. We conclude in Section 3.4, where we also discuss the relative utility of the large N and ϵ expansions in describing the Wilson-Fisher CFT spectrum.

3.2 General formalism

In this section, we develop our formalism for the large-N expansion of the critical O($2N$) model. For a review of the large-N expansion, see Ref. [46]. We take the Euclidean action

$$\mathcal{S} = \int d\tau d^2x \left(|\partial_\mu z_\alpha|^2 + us|z_\alpha|^2 + \frac{u}{2N} \left(|z_\alpha|^2 \right)^2 \right). \tag{3.1}$$

where z_α are complex fields with $\alpha = 1, 2, ..., N$. Our choice of complex rather than real fields is motivated by applications in Chapter 4; all of the results in this chapter which depend on N are also valid for odd $2N$. We will perform the large N expansion at fixed u, and tune the quadratic coupling to its critical value $s = s_c$. Subsequently we will take the $u \to \infty$ limit in each term to obtain the scaling limit. We will also consider deviations from the critical coupling $s - s_c$.

The field theory is defined on a spatial torus parametrized by complex coordinates as in Chapter 2 and Appendix A.3, see Figure 2.2.1. The torus is defined by two complex periods ω_1 and ω_2, an area $\mathcal{A} = \mathrm{Im}(\omega_2 \omega_1^*)$, and we define the dimensionless modular parameter $\tau = \omega_2/\omega_1$ with real and imaginary parts denoted $\tau = \tau_1 + i\tau_2$. We will also define the length scale $L \equiv |\omega_1|$.

We can rewrite the path integral (up to an unimportant constant) as

$$Z = \int \mathcal{D} z_\alpha \exp \left(- \int d^2x d\tau \left[|\partial_\mu z_\alpha|^2 + \frac{u}{2N} \left(|z_\alpha|^2 + \frac{Ns}{2} \right)^2 \right] \right). \tag{3.2}$$

We decouple the quartic term by introducing an auxiliary field $\tilde{\lambda}$:

$$Z = \int \mathcal{D}z_\alpha \mathcal{D}\tilde{\lambda} \exp\left(- \int d^2x d\tau \left[|\partial_\mu z_\alpha|^2 + i\tilde{\lambda}\left(|z_\alpha|^2 + \frac{Ns}{2} \right) + \frac{N\tilde{\lambda}^2}{2u} \right] \right). \tag{3.3}$$

The z_α can be integrated out, obtaining an action for $\tilde{\lambda}$,

$$Z = \int \mathcal{D}\tilde{\lambda} \exp\left[-N \ \mathrm{Tr} \ln\left(-\partial_\tau^2 - \nabla^2 + i\tilde{\lambda} \right) - N \int d\tau d^2x \left(\frac{\tilde{\lambda}^2}{2u} + \frac{s}{2} i\tilde{\lambda} \right) \right]. \tag{3.4}$$

At $N = \infty$, we should expand around the saddle point value, which we call $i\tilde{\lambda} = \Delta^2$, and is given by

$$\frac{\Delta^2}{u} = \frac{s}{2} + \frac{1}{\mathcal{A}} \sum_k \int \frac{d\omega}{2\pi} \frac{1}{\omega^2 + |k|^2 + \Delta^2}. \tag{3.5}$$

At this point we tune $s \to s_c$ such that the correlation length diverges when $\mathcal{A} \to \infty$. From Eq. (3.3), it is clear that the correlation length at $N = \infty$ is just the inverse of Δ, so s_c is

$$s_c = -2 \int \frac{d\omega}{2\pi} \frac{d^2k}{4\pi^2} \frac{1}{(\omega^2 + |k|^2)} = -2 \int \frac{d^2k}{4\pi^2} \frac{1}{2k}. \tag{3.6}$$

We can add and subtract s_c from Eq. (3.5) while taking the limit $u \to \infty$, and we find

$$s - s_c = \int \frac{d^2k}{4\pi^2} \frac{1}{k} - \frac{1}{\mathcal{A}} \sum_k \frac{1}{\sqrt{|k|^2 + \Delta^2}}. \tag{3.7}$$

This equation is to be solved for Δ, yielding an answer of the form $\Delta = \#/L$, where $\#$ is a universal function of $L(s - s_c)$ independent of the regularization scheme at large momenta. From the general theory of finite-size scaling [26], the energy levels should take the form

$$E_n = \frac{1}{L} X_n \left[L^{1/\nu} (s - s_c) \right], \tag{3.8}$$

for some universal set of functions X_n, so our expressions are appropriate for $\nu = 1$ at $N = \infty$ in $(2 + 1)$-dimensions.

Divergent sums are computed using dimensional regularization, which sets $s_c = 0$. The sums are performed in a similar way to the computations for the ϵ expansion in Appendix A.3, except we never need to separate out the zero momentum mode. Dimensional regularization will also renormalize the theory automatically, so we will not need to introduce any counter terms. In terms of the special functions defined in Appendix A.3.1, we write the gap equation as

$$g^{(2)}_{1/2}(\Delta, \tau) = -2\pi L(s - s_c), \tag{3.9}$$

which is solved numerically. At the critical point, $s = s_c$, the gap Δ depends only on the geometry of the torus. We note that Δ is a monotonically increasing function of $(s - s_c)$.

We also find the ground-state energy. This is computed from the path integral by temporarily taking a finite length in the time-direction, $0 < t < T$, and then taking the limit

$$E_0 = -\lim_{T\to\infty} \frac{1}{T} \ln Z. \tag{3.10}$$

Directly taking $i\tilde{\lambda} = \Delta^2$ and $u = \infty$, this is given by

$$\begin{aligned} E_0 &= N \sum_k \int \frac{d\omega}{2\pi} \ln\left(\omega^2 + |k|^2 + \Delta^2\right) + \frac{Ns}{2} \mathcal{A}\Delta^2 \\ &= N \sum_k \int \frac{d\omega}{2\pi} \ln\left(\omega^2\right) + N \sum_k \sqrt{|k|^2 + \Delta^2} + \frac{Ns}{2} \mathcal{A}\Delta^2. \end{aligned} \tag{3.11}$$

We subtract the first term, which is independent of the system size and boundary conditions. The remaining sum is evaluated using dimensional regularization,

$$E_0 = \frac{2\pi N}{\tau_2 L} g^{(2)}_{-1/2}(\Delta, \tau) + \frac{N(s - s_c)}{2} \tau_2 L^2 \Delta^2, \tag{3.12}$$

where the special function $g^{(2)}_{-1/2}(\Delta, \tau)$ is defined in Eq. (A.46). Our choice of renormalization has set $E_0 = 0$ at $s = s_c$ and $L = \infty$, where the theory has full conformal invariance.

Now that we have the saddle point value of $\tilde{\lambda}$ at $N = \infty$, we can read off the Euclidean-time

propagator of z_α

$$G_0(k,i\omega) \equiv \int d^2x d\tau e^{-ixk-i\omega\tau}\langle z_\alpha(x,\tau) z_\beta^\dagger(0,0)\rangle = \frac{\delta_{\alpha\beta}}{\omega^2+k^2+\Delta^2}. \tag{3.13}$$

We also expand in the fluctuations of $\tilde{\lambda}$. Writing $i\tilde{\lambda} = \Delta^2 + i\lambda/\sqrt{N}$, the effective action is

$$\begin{aligned} Z &= \int \mathcal{D}\lambda \exp\left(-\mathcal{S}_0 - \mathcal{S}_1\right), \\ \mathcal{S}_0 &= \frac{1}{2\mathcal{A}}\sum_k \int \frac{d\omega}{2\pi}\left(\Pi(k,\omega)+\frac{1}{u}\right)\lambda^2 \end{aligned} \tag{3.14}$$

with

$$\begin{aligned} \Pi(k,i\omega) &= \frac{1}{\mathcal{A}}\sum_q \int \frac{d\Omega}{2\pi} \frac{1}{(\Omega^2+|q|^2+\Delta^2)((\omega+\Omega)^2+|k+q|^2+\Delta^2)} \\ &= \frac{1}{\mathcal{A}}\sum_q \frac{\sqrt{|q|^2+\Delta^2}+\sqrt{|k+q|^2+\Delta^2}}{2\sqrt{(|q|^2+\Delta^2)(|k+q|^2+\Delta^2)}((\sqrt{|q|^2+\Delta^2}+\sqrt{|k+q|^2+\Delta^2})^2+\omega^2)} \end{aligned} \tag{3.15}$$

and $\mathcal{S}_1$ contains nonlinear terms. We discuss $\mathcal{S}_1$ and $1/N$ corrections in Appendix A.6. We see that the λ propagator at $N=\infty$ is

$$D_0(k,i\omega) \equiv \int d^2x d\tau e^{ixk+i\omega\tau}\langle \lambda_\alpha(x,\tau)\lambda_\beta^\dagger(0,0)\rangle = \frac{1}{\Pi(k,i\omega)+1/u}. \tag{3.16}$$

This is related to the propagator of $|z_\alpha|^2$. This is most easily seen directly from the action (3.3), where λ is not a dynamical field. Integrating out the field $i\lambda$ is equivalent to replacing it by its equation of motion,

$$i\lambda = \frac{u}{\sqrt{N}}|z_\alpha|^2 + \sqrt{N}\left(\frac{us}{2}-\Delta^2\right). \tag{3.17}$$

So the propagator of λ is related to the propagator of $|z_\alpha|^2$ by

$$\langle |z_\alpha|^2(x,\tau)|z_\alpha|^2(0)\rangle_c = -\frac{N}{u^2}\langle\lambda(x,\tau)\lambda(0)\rangle. \tag{3.18}$$

This can also be verified by coupling a source J to $|z_\alpha|^2$ and taking functional derivatives [47].

3.3 Spectrum

We describe the spectrum in terms of "n-particle states," which are created by n fields:

$$\underbrace{b_\alpha^\dagger b_\beta^\dagger \cdots b_\gamma^\dagger}_{n} |0\rangle. \tag{3.19}$$

We define $b_\alpha^\dagger$ with indices running from $\alpha = 1, ..., 2N$. The single-particle states are created by a single z field, so by the form of the z propagator, their energy is given by the Hamiltonian

$$H_0 = E_0 + \sum_{k\alpha} \sqrt{|k|^2 + \Delta^2} b_\alpha^\dagger(k) b_\alpha(k), \tag{3.20}$$

where $\alpha = 1, ..., 2N$. The energy of the state $b_\alpha^\dagger(k)|0\rangle$ is given by

$$E_1(k) = E_0 + \sqrt{|k|^2 + \Delta^2}. \tag{3.21}$$

This state is in the fundamental representation of $\mathrm{O}(2N)$, so it is $2N$-fold degenerate in addition to any degeneracies between values of k.

Two particle states with momentum k take the form

$$b_\alpha^\dagger(q) b_\beta^\dagger(k-q)|0\rangle \tag{3.22}$$

for all choices of momentum q. We decompose this into irreducible representations of $\mathrm{O}(2N)$, which must separately have definite energy:

$$b_\alpha^\dagger b_\beta^\dagger = \delta_{\alpha\beta}\left(\frac{1}{2N} b_\gamma^\dagger b_\gamma^\dagger\right) + \left(b_{[\alpha}^\dagger b_{\beta]}^\dagger\right) + \left(b_{(\alpha}^\dagger b_{\beta)}^\dagger - \frac{\delta_{\alpha\beta}}{2N} b_\gamma^\dagger b_\gamma^\dagger\right) \equiv \delta_{\alpha\beta} S + A_{\alpha\beta} + T_{\alpha\beta}. \tag{3.23}$$

These are the singlet, antisymmetric tensor, and symmetric traceless tensor representations respectively. Simple counting shows that S creates one state, $A_{\alpha\beta}$ creates $N(2N-1)$ states, and $T_{\alpha\beta}$ creates $(2N-1)(2N+2)/2$ states. Note that if $q = k - q$, the antisymmetric representation will not be present.

At this point we can use the analysis above. At $N = \infty$, the z propagator takes the form of a free boson with dispersion $\sqrt{|k|^2 + \Delta^2}$, so one would naïvely expect all states to have energy given by the Hamiltonian (3.20). However, this is not the case for the singlet state, since

$$\langle |z_\alpha|^2(x,\tau)|z_\beta|^2(0,0)\rangle \propto \langle \lambda(x,\tau)\lambda(0,0)\rangle. \tag{3.24}$$

So the fact that that the propagator of λ takes a nontrivial form at $N = \infty$ has the effect of shifting the energy of singlet states. The energies of the singlet states are given by the poles in $D(k, i\omega)$, or equivalently the zeros of $\Pi(k, i\omega)$. From Eq. (3.15) we see that Π is always convergent in $d = 2$, so we can sum the series numerically to find the singlet energies, which are given by

$$\Pi(k, E_2^{(S)}(k)) = 0. \tag{3.25}$$

In contrast the antisymmetric tensor and symmetric traceless tensor remain degenerate at $N = \infty$, giving $4N^2 - 1$ degenerate states with energy

$$E_2(k) = E_1(q) + E_1(k - q) \tag{3.26}$$

for all choices of the momentum q, where $E_1(q)$ is the single particle energy, Eq. (3.21). The choice of q can also induce additional degeneracies for any given total momentum k. In addition, we saw that if $q = k - q$ there will be no antisymmetric part, so there will only be a degeneracy of $(2N-1)(2N+2)/2$ from $\mathrm{O}(2N)$ symmetry.

Going beyond the two-particle states, we expect that a general state will be given by an application of

$$b_\alpha^\dagger(k_1) b_\beta^\dagger(k_2) b_\gamma^\dagger(k_3) b_\sigma^\dagger(k_4) \cdots |0\rangle. \tag{3.27}$$

degeneracy	$\kappa = 0$	$\kappa = 1$	$\kappa = \sqrt{2}$
1	0		
$2N$	1.512		
$(2N+2)(2N-1)/2$	3.024		
$\binom{2N+2}{3} - 2N$	4.536		
$2\binom{1+2N}{2N-2} - \binom{3+2N}{4}$	6.048		
$8N$		6.463	
$2\binom{2+2N}{2N-2} - \binom{4+2N}{5}$	7.560		
$4(4N^2-1)$		7.975	
1	8.126		
$8N$			9.013
$2\binom{3+2N}{2N-2} - \binom{5+2N}{6}$	9.072		

Table 3.3.1: Lowest energy splittingss $L(E - E_0)$ and their degeneracy at $s = s_c$ for large-N on the square torus. The ground state energy is given by $E_0 = -.329N$. Here, $\kappa = L|k|/2\pi$.

Past the two-particle states, the decomposition into irreducible representations becomes more involved. Generally, the states will decompose into singlets with energies given by the zeros of $\Pi(k, E(k))$, and states described by $\mathrm{O}(2N)$ traceless tensors with energies given by by Fock spectrum of Eq. (3.20). Extra degeneracies can occur due to discrete point group symmetries of the torus, and sometimes degeneracies are reduced if some of the $b^\dagger$s are indistinguishable.

3.3.1 Evolution of the spectrum of a function of $s - s_c$

In this section, we discuss the general structure of the finite-size spectrum as a function of $s - s_c$, which can be worked out on general principles in the limits $s = s_c$, $s \gg s_c$, and $s \ll s_c$. We show that our model takes the correct form in these limits before giving explicit results on the evolution of the as $s - s_c$ is varied.

Critical point

At criticality, $s = s_c$, the system at an infinite volume has full conformal invariance, and there is no scale in the theory. The excitation spectrum forms a gapless continuum, $E = k$. As a result, when the system is placed on a torus, the only possible dependence that the energy can have on the size of the system is $1/L$. Therefore, the quantities LE will be universal functions of τ only. This dependence is automatic from our finite-size calculations, where the solution to the gap equation will give a pure number for $L\Delta$, and all energies manifestly have $1/L$ dependence.

Disordered phase

In the disordered phase, $s > s_c$, the system develops a gap m even at $L = \infty$, and the low-energy excitations will take the form $E = \sqrt{|k|^2 + m^2}$. In the scaling limit, m is of order $(s - s_c)^\nu$ and $\nu = 1$ at $N = \infty$. This energy gap implies that all correlations decay exponentially over a length scale $1/m \sim 1/(s - s_c)$, resulting in a very weak dependence on finite-size effects when the system is placed on a torus of size L, provided $Lm \sim L(s-s_c) \gg 1$. Therefore, we expect the finite-size spectrum of the disordered phase to evolve to the form $E = \sqrt{|k|^2 + \Delta^2}$ at increasing $(s - s_c)$, where $\Delta = m + \mathcal{O}(e^{-Lm})$ takes the same value as it does in an infinite volume up to exponentially small corrections in $L(s - s_c)$, and the momenta k are quantized according to the required boundary conditions. We also note that the threshold for singlet excitations in an infinite volume is $2m$, so the absence of large finite-size corrections suggests that the two-particle singlet spectrum will merge with the other two-particle states.

The properties of the disordered phase can be verified explicitly. By taking the $L \to \infty$ limit of Eq. (3.9), we find the exact gap in an infinite volume,

$$m = 2\pi(s - s_c). \tag{3.28}$$

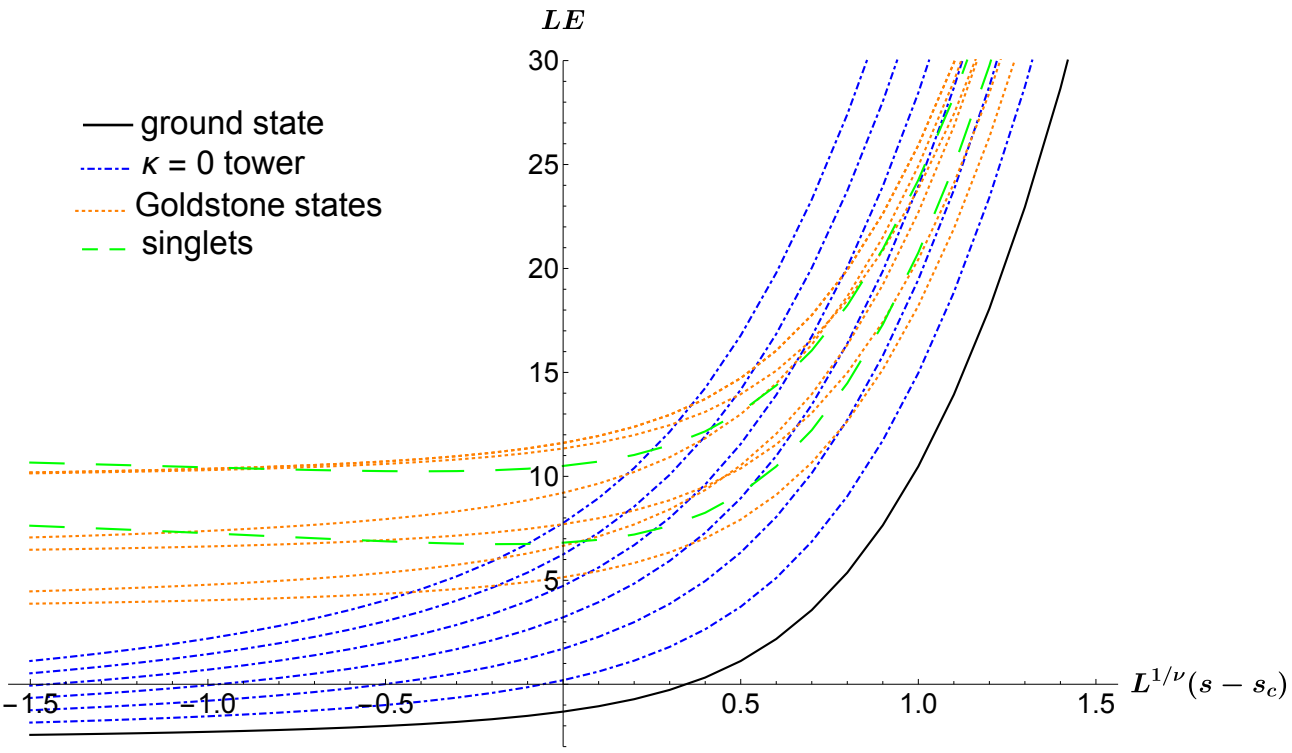

Figure 3.3.1: The evolution of the spectrum LE for the large N O(N) model as a function of the tuning parameter $L^{1/\nu}(s - s_c)$ on the square torus, $\tau = i$. Note that $\nu = 1$ at leading order in $1/N$. The energy levels are defined so that $E = 0$ at $s = s_c$ and $L = \infty$, and the current plot shows the energy levels for $N = 4$. We label the states by their behavior in the ordered region, distinguishing between the tower, the Goldstone modes, and the singlet states. Our choice of states is not not exhaustive, but they highlight the main features of each region.

This can be compared with the gap in a finite volume when $s \gg s_c$. In this limit, $L\Delta$ is large and we can expand $g^{(2)}_{1/2}(\Delta, \tau)$, obtaining

$$\Delta = 2\pi(s - s_c) + \mathcal{O}\left(\frac{1}{L^2(s - s_c)^2} e^{-L^2(s-s_c)^2}\right), \qquad s \gg s_c \tag{3.29}$$

The energies of the two-particle singlet states can be numerically verified to merge with the other two-particle states in this limit.

Ordered phase

In the ordered phase, $s < s_c$, the finite-size spectrum differs considerably from the infinite volume case. In an infinite volume, there is a degenerate ground-state manifold of states at

zero momentum which are related by the O($2N$) symmetry, and a properly prepared system will pick a single one of these states, spontaneously breaking the symmetry. The stable excitations above the ground state consist of $2N-1$ Goldstone modes with a linear dispersion, $E = c|k|$, corresponding to transverse fluctuations of the order parameter about its ground state value. In addition, there will be an unstable continuum of excitations associated with transverse fluctuations of the order parameter and fluctuations of its amplitude ϕ_α^2, which will be mixed by interactions [47].

In contrast, in a finite volume the ground state must be a non-degenerate O($2N$) singlet, and spontaneous symmetry breaking is impossible. Instead of a ground state manifold, there will be a "tower of states" above the ground state at $k = 0$ with energies scaling as $E \sim 1/\mathcal{A}$ with the system size [48–53]. In the thermodynamic limit, this tower "collapses" into the ground state, and a symmetry-broken state can be formed as an extensive superposition of states in the tower.

One can analyze the general properties of the tower of states by forming an effective Hamiltonian for their spectrum. This can be derived by integrating out the finite-momentum modes and finding an effective Hamiltonian for the zero-momentum component of the field [26]. For a system with O($2N$) symmetry, the effective Hamiltonian for the tower takes the form

$$H_{tower} = E_0 + \frac{\mathbf{L}^2}{\kappa \mathcal{A} N \left(s_c - s\right)} \tag{3.30}$$

up to corrections induced by fluctuations of the finite momentum modes. Here, $\mathbf{L}_i$, $i = 1, 2, .., N(2N-1)$ are the generators of rotations in O($2N$), and κ is a constant which will be non-universal away from the scaling limit. The effective Hamiltonian for the tower is simply an O($2N$) rigid rotator, and the energy levels are given by

$$E_{\text{tower}} = E_0 + \frac{\ell(\ell + 2N - 2)}{\kappa N (s_c - s) \mathcal{A}}, \qquad \ell = 0, 1, 2, ... \tag{3.31}$$

This constrains the level spacing between states in the tower. In our present calculation,

we take the $N = \infty$ limit, and obtain equally-spaced energy levels. The eigenfunctions of Eq. (3.30) in the angular basis are the hyperspherical harmonics on S^{2N-1}, which are the higher-dimensional generalization of the familiar spherical harmonics on the two-sphere. These eigenfunctions are in the symmetric traceless tensor representations of O($2N$), and their degeneracy is given by

$$\text{Deg.} = 2\binom{\ell + 2N - 3}{2N - 2} + \binom{\ell + 2N - 3}{\ell}. \tag{3.32}$$

We can verify the above structure in our model by taking the limit $s \ll s_c$ in the gap equation (3.9). We find that the gap takes the form

$$\Delta = \frac{1}{\mathcal{A}(s_c - s)} + \mathcal{O}\left((\mathcal{A}(s_c - s))^{-2}\right), \qquad s \ll s_c. \tag{3.33}$$

The states created purely by $|k| = 0$ will form an equally spaced spectrum above the ground state with this $1/\mathcal{A}$ dependence on the system size, and by the analysis in Section 3.3 they will be in the symmetric traceless tensor representations of O($2N$), in agreement with the above analysis.

The states created by finite-momentum operators will have an energy given by $E = |k| + \mathcal{O}(\Delta^2/|k|)$, and transform in either traceless tensor or singlet representations. These correspond to the Goldstone modes in the infinite-volume system, but there will be no distinction between the longitudinal and transverse fluctuations since symmetry is unbroken. We note that even the zero-momentum states created by the singlet operator approach the expected spectrum for multi-particle Goldstone states.

3.3.2 Results

For an explicit example, we consider the square torus, $\tau = i$, where both spatial directions have length L. Precisely at $s = s_c$, the energy levels are a set of universal numbers times $1/L$; in Table 3.3.1 we have given the lowest-lying energy levels at the critical point and their

total degeneracy. We show the evolution of the spectrum LE as a function of $L(s - s_c)$ in Figure 3.3.1, choosing states which highlight important features of the spectrum.

3.4 Conclusions and comparison with ϵ-expansion

In the large N limit, we can in principle obtain the entire spectrum at criticality, and even track how specific states evolve between their expected behavior in the disordered and ordered regimes. The tower of states is known to be a useful tool for determining spontaneous symmetry breaking in numerical simulations [50, 51], so a study of the change in its structure as the system is tuned to a critical point could be a benefit to identifying the critical theories strongly correlated systems (e.g. frustrated spin systems). For a specific application along these lines, we will investigate a phase transition into a phase with topological order in Chapter 4 and see that the presence of proximate topological order alters the torus spectrum at criticality and even in the non-topological phase.

The ease in obtaining the entire spectrum is a definite benefit of the large N calculation over the ϵ expansion detailed in Chapter 2. In the ϵ expansion, obtaining the spectrum requires numerically solving coupled differential equations which become increasingly complex for increasing values of k and N. The perturbative structure of the ϵ expansion also changes drastically as one tunes away from the critical point, as the relative magnitudes of $L(s - s_c)$ and ϵ will alter the relative importance of interactions (see Section 2.3.1). In contrast, there is no trouble with tuning away from criticality in the large N expansion.

However, the simple leading order results of the large N expansion appear to be less consistent quantitatively with critical spectra obtained numerically for physically relevant values of N. The spectrum at large N takes the simple form of free relativistic particles with a dispersion $\sqrt{k^2 + \Delta^2}$, and there are large degeneracies between different irreducible representations of O(N). These features are artifacts of the expansion, and corrections in $1/N$ should split these degeneracies and result in a spectrum which is not particle-like.

In contrast, the energy spectrum at leading order in the ϵ expansion already took the form of a strongly-coupled quartic oscillator, resulting in a set of energy levels which are not equally spaced. The energies of finite momentum states cannot be obtained by simply boosting zero momentum states, $\Delta \to \sqrt{k^2 + \Delta^2}$, showing a breakdown of Lorentz invariance. These properties are closer to the qualitative picture of a quantum critical fluid being far from the free particle limit, and appear to show good agreement with numerics on critical lattice systems (see Section 2.5). As such, we expect the ϵ expansion to be better for obtaining quantitative predictions about critical spectra due to its capturing non-perturbative aspects of the underlying conformal field theory, while the large N expansion is beneficial in obtaining qualitative predictions such as the evolution of particular states between phases.

Chapter 4

Confinement transitions in $\mathbb{Z}_2$ spin liquids: spectrum on the torus

4.1 Introduction

In this chapter we will discuss a class of phase transitions which occur proximate to $\mathbb{Z}_2$ topological order, and study the finite-size torus spectrum of these transitions. This is a particularly interesting application of the results derived in Chapters 2 and 3, because the nearby topologically ordered phase alters the nature of the spectrum due to the nontrivial topology of the torus. We show that the torus spectrum is a useful diagnostic for both the topologically ordered phase and for quantum critical points outside of the standard symmetry-breaking paradigm.

By definition, a phase with gapped topological order is described by a topological quantum field theory [54, 55]. This leads to a ground state degeneracy which is sensitive to the topology of the underlying manifold that the theory is defined on, and the existence of gapped excitations carrying fractional quantum numbers and fractional statistics. Crucially, topological order cannot be characterized by any local order parameter, so the critical points we consider below are necessarily outside of the standard symmetry breaking paradigm. In

particular, the phase transitions are described as *deconfined quantum critical points*, meaning their explicit description requires degrees of freedom carrying charges under deconfined gauge fields [56, 57].

This chapter is organized as follows. Section 4.2 gives a review of $\mathbb{Z}_2$ topological order and defines the critical $\mathrm{O}(N)^*$ class of confinement transitions. Section 4.3 will give the prescription for computing the spectrum of the critical $\mathrm{O}(N)^*$ model on the torus, and we give explicit results for a confinement transition between two phases without symmetry breaking, comparing with numerical simulations. Section 4.4 discusses an explicit realization of the critical $\mathrm{O}(4)^*$ model as a model for a phase transition between the $\mathbb{Z}_2$ spin liquid and non-collinear antiferromagnetic order. The spectrum of the critical $\mathrm{O}(4)^*$ model is computed in the large N expansion, and a discussion of the evolution of the spectrum across different phases is given in detail. We conclude in Section 4.5.

4.2 $\mathbb{Z}_2$ topological order and the $\mathrm{O}(N)^*$ models

General considerations from quantum field theory allow for a rich enumeration of possible topological orders [54, 55], but in this chapter we will focus on the simple case of $\mathbb{Z}_2$ topological order which arises in many models of frustrated spin systems [58–60]. Phases with $\mathbb{Z}_2$ topological order can equivalently be described as deconfined phases of a $\mathbb{Z}_2$ gauge theory [61]. Such theories can contain two kinds of charged excitations: a particle which is electrically charged under the gauge field called the e particle, and a particle which is a magnetic monopole of the gauge field called the m particle.

Interestingly, the e and m particles are *mutual semions*. This means that as one adiabatically transports the e particle around the m particle (or vice-versa), the wave function picks up an overall minus sign, see Figure 4.2.1. In a phase where these excitations are deconfined, this implies a ground state degeneracy on the torus. In particular, one can create a pair of e particles and a pair of m particles, and by winding them along different cycles of the torus

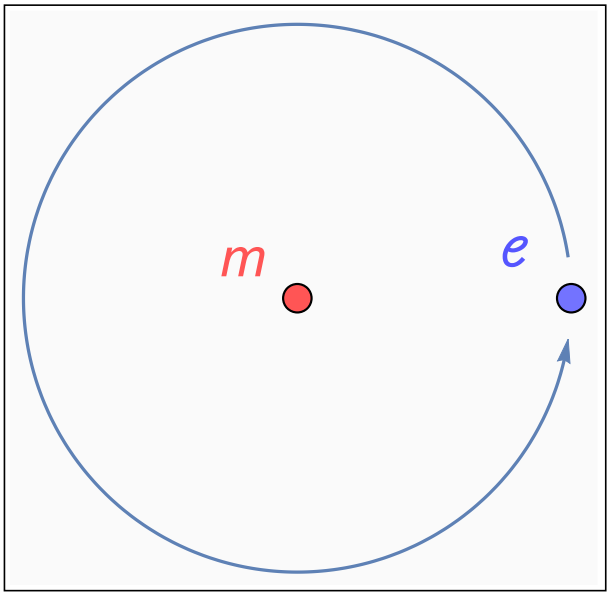

Figure 4.2.1: Transport of

and then annihilating both pairs, one can reach an orthogonal state with the same energy (in the large torus limit). By choosing either one or both of the cycles of the torus to wind one of the particles around, one can reach three other distinct ground states, leading to a four-fold ground state degeneracy on the torus. The properties of this ground state can be encoded by a topological field theory [61].

We now consider the condensation of one of the particles. We choose the condense the e particle, but the same considerations apply for the m. The nontrivial statistics between the two particles implies that the m particles will confine due to the e condensate. As one creates two m particles and attempts to separate them by a length L, there will be a linear energy cost due to the magnetic flux tube separating them (Figure 4.2.2). This is simply the $\mathbb{Z}_2$ analogue of the energy cost of an Abrikosov flux tube in a superconductor, which scales as the linear size of the flux tube.

We now develop the critical field theory for confinement in a $\mathbb{Z}_2$ spin liquid by considering

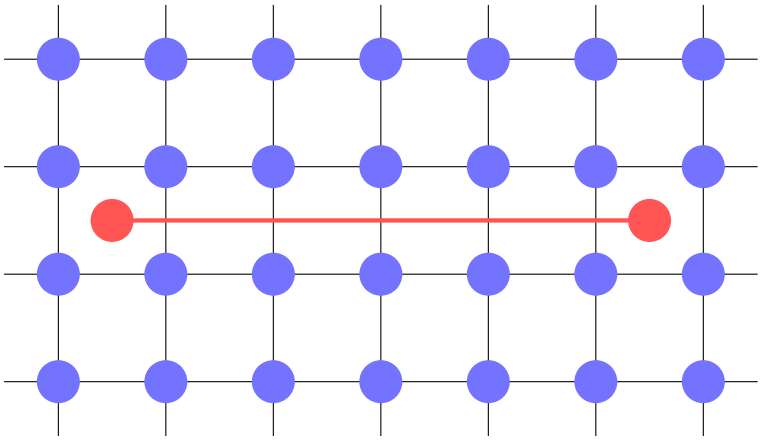

Figure 4.2.2: Visual representation of a pair of m particles being separated in an e condensate.

the condensation of a field $\phi(x) \sim e$. For now we assume that there are no global symmetries in our system. Since the m particle remains gapped through the phase transition, we can take its mass to infinity in the scaling limit. The only remaining principle we can use to write down a field theory is $\mathbb{Z}_2$ gauge invariance: $\phi \sim -\phi$. This leads to the same critical field theory as the 2+1D Ising model:

$$\mathcal{S} = \int d^3x \left[\frac{1}{2} (\partial_\mu \phi)^2 + \frac{s}{2}\phi^2 + \frac{u}{4!}\phi^4 \right] \tag{4.1}$$

However, because $\phi \to -\phi$ is a gauge transformation rather than a symmetry, there is no notion of symmetry breaking for the $s < 0$ phase. This is a continuous phase transition between two distinct phases without any local order parameter, so it lies outside of the LGW paradigm. This is called the Ising* universality class. We note that although we have only sketched a derivation here, the correspondence between this critical point and the Ising model can be established by precise duality between an explicit $\mathbb{Z}_2$ lattice gauge theory and the Ising model [62], and that this critical point is stable under perturbations away from where the exact duality holds [63].

We now generalize this theory to allow the field ϕ to transform as a vector under a global $\mathrm{O}(N)$ symmetry, ϕ_α. Because of the gauge equivalence, the physical symmetry of this theory is $\mathrm{O}(N)/\mathbb{Z}_2$. The natural generalization of the above action is then just the Wilson-Fisher

CFT,

$$\mathcal{S} = \int d^3x \left[\frac{1}{2} \left(\partial_\mu \phi_\alpha \right)^2 + \frac{s}{2} \phi_\alpha^2 + \frac{u}{4!} \left(\phi_\alpha^2 \right)^2 \right] \tag{4.2}$$

where $\phi_\alpha^2 = \sum_{\alpha=1}^{N} \phi_\alpha \phi_\alpha$. Since ϕ_α carries a $\mathbb{Z}_2$ gauge charge, this is termed the O(N)* model [64], and it describes a continuous phase transition between a state with $\mathbb{Z}_2$ topological order and a state with spontaneous symmetry breaking.

The original realizations of $\mathbb{Z}_2$ topological order appeared as disordered spin liquid phases in frustrated magnets [59, 60, 65], where the e and m particles are conventionally labeled a 'spinon' and a 'vison' respectively. In these systems, the spinon transforms as an SU(2) spinor under rotations, while the vison transforms under a discrete space group of the underlying lattice. A theory of a confinement transition of the $\mathbb{Z}_2$ spin liquid driven by the condensation of visons was initially presented in Refs. [66, 67], in terms of a frustrated Ising model obtained from an 'odd' dimer model; the same theory appeared later in other models [64, 68, 69], and in recent work [70–72]. The confined state leads to lattice symmetry breaking, and at the critical point the discrete symmetry usually enlarges and one obtains O(2)* (also called XY*) criticality. In Section 4.4 we will discuss a theory [73, 74] for the condensation of spinons in detail.

For many purposes, the critical behavior of the O(N)* model resembles that of the O(N) model. Gauge invariant operators such as ϕ^2 have the same scaling dimensions as their O(N) counterparts, so certain critical exponents will be identical to those for the Wilson-Fisher fixed point. However, the scaling dimension of any gauge invariant operator cannot be given by ϕ_α, so any local order parameter for a symmetry-broken phase in these models must be composite in the field ϕ_α [75]. The O(N)* models have also been shown to have extra contributions to their entanglement entropy relative to the O(N) models [76]. Finally, the finite size spectra for these models is distinct from the conventional Wilson-Fisher case, as we discuss in detail for the rest of this chapter.

4.3 Spectrum of the critical O(N)* model on the torus

We first consider the O(N)* theory on a finite simply-connected space, such as the sphere. Then the $\mathbb{Z}_2$ gauge constraint simply means that we must only include states with the correct global $\mathbb{Z}_2$ charge. That is, we arrange all of the energy eigenstates of the O(N) model into states which are even and odd under the $\mathbb{Z}_2$ transformation $\phi_\alpha \to -\phi_\alpha$,

$$\Psi_{n,\pm}[-\phi_\alpha(x)] = \pm\Psi_{n,\pm}[\phi_\alpha(x)] \tag{4.3}$$

where the $\Psi_{n,\pm}$ are wavefunctionals of the field. Then we have two choices, we either only keep the states $\Psi_{n,+}$ or we only keep the states $\Psi_{n,-}$. In the two cases, we either say that we are in the 'even' or 'odd' sector of the $\mathbb{Z}_2$ gauge theory. Our choice for which sector we need to describe a given microscopic system will depend on the precise relation between the microscopic Hamiltonian and the emergent $\mathbb{Z}_2$ gauge theory. For example, in the systems considered in Section 4.4 below, the system is in the even (odd) sector of the gauge theory if the total number of half-odd-integer spins in the system is even (odd).

We now consider the spectrum on the torus. Because of the gauge equivalence $\phi_\alpha \sim -\phi_\alpha$, we must now allow the boundary conditions

$$\phi_\alpha(x + n\omega_1 + m\omega_2) = \pm\phi_\alpha(x) \tag{4.4}$$

where n and m are integers and $\omega_{1,2}$ are the two cycles of the torus (see Figure 2.2.1). We are allowing a $\mathbb{Z}_2$ flux to thread through the holes of the torus; such fluxes do not appear in the simply connected case because they must wind around visons, which we are assuming have a large gap.

Thus, the full spectrum of the O(N)* model on the torus is obtained by finding the Wilson-

Fisher spectrum on the torus for all possible boundary conditions (4.4), separating the states into even and odd sectors according to (4.3), and then choosing the states corresponding to the sector of interest and discarding the rest. This highly nontrivial matching of states represents a dramatic difference with the normal Wilson-Fisher spectrum considered in the previous chapters, and is thus of possible use in distinguishing states nearby topological order from states nearby trivial phases, whereas certain critical exponents do not distinguish these transitions.

We now comment on the effect of modular transformations. Modular transformations are discrete diffeomorphisms on the torus, so we need the spectrum to be invariant under the modular group. This group is generated by the two transformations [5]

$$\begin{aligned} \mathcal{T}: \quad & \tau \rightarrow \tau + 1 \\ \mathcal{S}: \quad & \tau \rightarrow -\frac{1}{\tau}. \end{aligned} \tag{4.5}$$

Under these transformations, the area $\tau_2 L^2$ is left unchanged. To see how our spectrum transforms under these operations, we can look at how the loop sums over the momenta $|k_{n,m}|^2$ in Eq. (A.28) given in Appendix A.3 transform. We find that modular transformations map between the different topological sectors as follows:

$$\begin{aligned} \mathcal{T}: \quad & (\eta_1, \eta_2) \rightarrow (\eta_1\eta_2, \eta_2) \\ \mathcal{S}: \quad & (\eta_1, \eta_2) \rightarrow (\eta_2, \eta_1) \end{aligned} \tag{4.6}$$

where $\eta_{1,2} = \pm 1$, and the notation (η_1, η_2) refers to whether the field picks up a plus or minus sign around the two cycles. These results imply that if we include any of the antiperiodic sectors, modular invariance forces us to include the other two. In contrast, the fully periodic sector $(+1, +1)$ is modular invariant by itself.

We note that modular invariance will cause extra degeneracies to arise for special values of τ. For example, the square torus $\tau = i$ satisfies $\tau = -1/\tau$. Since the full spectrum must

be invariant under $\mathcal{S}$, the $(-1,0)$ and $(0,-1)$ sectors are degenerate. Another special case is the triangular torus $\tau = e^{i\pi/3}$, which satisfies $\tau = -1/(\tau - 1)$. Then the invariance of the full spectrum under $\mathcal{T}^{-1}\mathcal{S}$ means all three nontrivial sectors have exactly degenerate spectra.

4.3.1 Comparison with numerics: Ising* spectrum

Here we will compare the analytic computation of the Ising* spectrum with numerics performed using exact diagonalization. The microscopic Hamiltonian being considered is the toric code in a transverse field,

$$\begin{aligned} H_{\mathrm{TC}} &= -J_a \sum_s A_s - J_b \sum_p B_p - h \sum_i \sigma_i^x \\ A_s &= \prod_{i \in s} \sigma_i^x, \qquad B_p = \prod_{i \in p} \sigma_i^z \end{aligned} \tag{4.7}$$

Here, the Pauli matrices σ live on the links of a square lattice, s denotes a star and p a plaquette on the lattice. For $h = 0$, this is the exactly solvable toric code Hamiltonian [77] which describes a $\mathbb{Z}_2$ spin liquid in the even sector. As one increases h, the system is driven through an Ising* confinement transition into a trivial paramagnet [78–81].

Numerical simulations were performed for $J_a = J_b = 1$ and $h = h_c$. These results were first reported in Reference [34] along with the critical transverse field Ising spectrum described in Section 2.5. Further details on the numerical methods used to obtain the spectrum may be found in both Section 2.5 and the original reference.

A comparison of the numerical spectrum with values obtained from the ϵ expansion are shown in Figure 4.3.1. The agreement is reasonably good, although less so than the critical Ising spectrum. This is somewhat expected from the perspective of the ϵ expansion detailed in Chapter 1, where the P/P sector has a completely different perturbative structure from the antiperiodic sectors. It is only in the fully periodic sector that the torus spectrum requires a mapping to strongly-coupled oscillators and an expansion in $\epsilon^{1/3}$, while the other sectors have

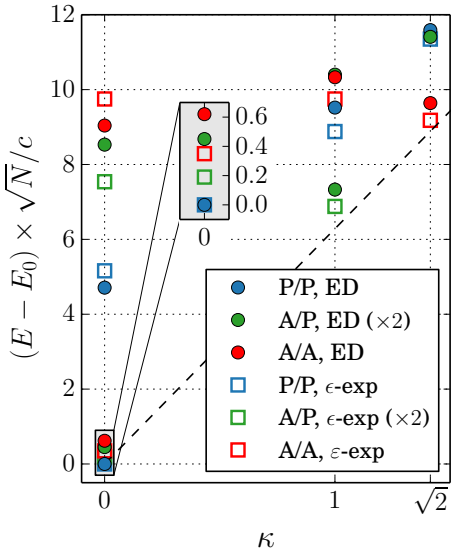

Figure 4.3.1: Comparison of the low-energy spectrum of the toric code in a transverse field with the analytic Ising* spectrum computed in the ϵ expansion. Full symbols denote values obtained from ED while open symbols are values obtained from the ϵ expansion. The notation P(A) refers to whether the boundary conditions around the torus are (anti-)periodic. The inset is a zoom onto the lowest four levels.

a spectrum given by normal weak-coupling perturbation theory and an ordinary expansion in ϵ. The unequal footing of the strength of interactions in the different sectors is a natural source for quantitative disagreement between the different sectors.

4.4 Transition from the $\mathbb{Z}_2$ spin liquid to antiferromagnetic order

Recent numerical studies [82, 83] of the spin $S = 1/2$ antiferromagnet on the triangular lattice have presented convincing evidence for a spin liquid ground state in the presence of a next-nearest neighbor exchange interaction (J_2). They also find an apparently continuous transition to an antiferromagnetically ordered ground state at smaller J_2, with the familiar 3-sublattice coplanar order of the triangular lattice. Here we will assume that this antiferromagnetic state is the same as the conventional state described by the semiclassical spin-wave theory, and possesses only integer spin excitations. So the transition from the spin

liquid to the antiferromagnet is a confinement transition, associated with the confinement of half-integer spin excitations.

An attractive candidate for the observed spin liquid is the $\mathbb{Z}_2$ spin liquid [59, 60, 65, 66] described in Section 4.2. In the terminology used there, the confinement transition is driven by the condensation of spinons, or e particles, carrying nontrivial quantum numbers under spin rotation. A theory for the condensation of spinons from the $\mathbb{Z}_2$ spin liquid on the triangular lattice was presented in Refs. [73, 74], and this theory will form the basis of our computations here. The order parameter of the coplanar antiferromagnet is identified by points on the SO(3) manifold, and so the Landau-Ginzburg-Wilson (LGW) framework suggests a field theory based on such an order parameter. However, the theory of Refs. [73, 74] is a 'deconfined' critical theory beyond the LGW paradigm, and is instead expressed in terms of a spinon field which is identified by points on SU(2)$\equiv S_3$.

The connection between coplanar magnetic order and the spinon in the spin liquid phase can be made explicit. We write the expectation value in the ordered state as

$$\langle \mathbf{S}_j \rangle = S \left[\mathbf{n}_1 \cos\left(\vec{Q}\cdot\vec{x}_j\right) + \mathbf{n}_2 \sin\left(\vec{Q}\cdot\vec{x}_j\right)\right] \tag{4.8}$$

where the ordering wave vector is $\vec{Q} = 4\pi\left(1/3, 1/\sqrt{3}\right)$ for the semiclassical ground state of the Heisenberg model on the triangular lattice. The vectors $\mathbf{n}_{1,2}$ are arbitrary up the constraints

$$\mathbf{n}_1^2 = \mathbf{n}_2^2 = 1, \qquad \mathbf{n}_1 \cdot \mathbf{n}_2 = 0 \tag{4.9}$$

Different orientations of these two vectors are related by a rotation matrix, identifying the order parameter as an element of SO(3). A conventional LGW description of a transition from this magnetically ordered state to a paramagnetic state would begin with an effective action for the fluctuations of the vectors $\mathbf{n}_{1,2}$. However, this phase transition would drive the system into a trivial gapped paramagnetic state with a non-degenerate ground state, which cannot occur in a system with an odd number of half-integer spins per unit cell such as the

triangular antiferromagnet [84]. Therefore, we seek a description in terms of fractionalized degrees of freedom. Following Refs. [73, 74], we write

$$n_{1a} + in_{2a} = \sum_{\alpha,\beta,\gamma=1}^{2} \epsilon_{\alpha\gamma} z_\gamma \sigma^a_{\alpha\beta} z_\beta \tag{4.10}$$

This parametrization explicitly solves the constraints in Eq. (4.9), and it can be checked that the complex bosonic field z_α, with $\alpha = \uparrow, \downarrow$, transforms as an $S = 1/2$ spinor under spin rotations. However, this representation is doubled-valued: one can perform a gauge transformation, $z_\alpha(\mathbf{x}, \tau) \to \eta(\mathbf{x}, \tau) z_\alpha(\mathbf{x}, \tau)$, $\eta = \pm 1$, at any point in space-time and obtain an equivalent representation of the physically observable order parameter. This identifies the order parameter space as $\mathrm{SU}(2)/\mathbb{Z}_2$, which is equivalent to SO(3). This description is complementary to the confinement transition described above, where z_α is identified with the SU(2) spinon of the $\mathbb{Z}_2$ spin liquid. We note that as the spinon condenses, the only remnant of the gapped vison in the spin liquid is the double-valued nature of the spinon field.

We therefore write a critical theory for the complex boson z_α, taking values in SU(2), consistent with the allowed symmetries. Keeping only terms relevant at the critical point, the universal Lagrangian of the transition in 2+1 dimensional spacetime is

$$\mathcal{L} = |\partial_\mu z_\alpha|^2 + s|z_\alpha|^2 + u\left(|z_\alpha|^2\right)^2. \tag{4.11}$$

The 'mass' s has to be tuned to a critical value $s = s_c$ to access the critical point, while u approaches a non-zero value determined by the Wilson-Fisher fixed point [4]. Note that this spin-1/2 relativistic boson is not in contradiction with the spin-statistics theorem, because here 'spin' refers to a global flavor symmetry, rather than the intrinsic angular momentum of relativistic particles. In this section we will allow the index α to range over $1 \ldots N$ and use the $1/N$ expansion. Due to the gauge constraint, this is the critical $\mathrm{O}(2N)^*$ detailed in Section 4.2. Note that Eq. (4.10) implies the physical order parameter has a scaling dimension given by a composite bilinear in the spinon fields, so the anomalous dimension of

$\mathbf{n}_{1,2}$ fields will be much larger than those of the spinons [85].

We now determine whether a given lattice antiferromagnet is in the 'even' or 'odd' sector of the $\mathbb{Z}_2$ gauge theory, determining which of the states we keep after separating the Hilbert space into sectors as in Eq. (4.3). This is determined by noting that the mapping (4.10) implies that the spinons carry $S = 1/2$, so every excitation of the even (odd) sector of the gauge theory will carry integer (half-odd-integer) spin. Considering the realization of this model as the low-energy theory of a microscopic spin Hamiltonian, we know that the excitations of an antiferromagnet with an even (odd) total number of half-odd-integer spins will also only have physical excitations which carry integer (half-odd-integer) spin. Therefore, the relevant sector of the gauge theory is given by the total number of half-odd-integer spins in the underlying lattice antiferromagnet.

In the application to the lattice antiferromagnet, we also have to consider the fact that the O($2N$) symmetry of $\mathcal{L}$ is an emergent symmetry of the critical point, and is not a symmetry of the underlying Hamiltonian. So we have to consider operators which break the O($2N$) symmetry. All operators which break the O($2N$) symmetry down to SU(N) are irrelevant at the critical point, and we will consider here only the leading irrelevant operator. This is given by [73, 74]

$$\mathcal{L}' = \gamma |z_\alpha^* \nabla z_\alpha|^2 \tag{4.12}$$

Below, we will describe the leading perturbative effect of γ on the critical spectrum.

4.4.1 Critical O$(2N)^*$ spectrum at large N

We now consider the large N limit of the O$(2N)^*$ model. This is very similar to the computation in Section 3.3, but the fields can take anti-periodic boundary conditions along either direction of the torus. We treat the four topological sectors as separate decoupled theories. The boundary conditions can be taken into account by noticing that momentum quantization is shifted by a half-integer in the anti-periodic direction. We parametrize the momentum

(ω_1, ω_2)	(a_1, a_2)
(P,P)	$(0, 0)$
(P,A)	$\left(0, \frac{1}{2}\right)$
(A,P)	$\left(\frac{1}{2}, 0\right)$
(A,A)	$\left(\frac{1}{2}, \frac{1}{2}\right)$

Table 4.4.1: The definitions of a_1 and a_2 appearing in (4.13) for different boundary conditions. The left column denotes whether the boundary conditions are periodic (P) or anti-periodic (A) in the ω_1 or ω_2 directions respectively, while the right column gives the values of a_1 and a_2 for these boundary conditions.

as

$$k_{n,m} = 2\pi \left[(n + a_1)k_1 + (m + a_2)k_2\right], \qquad n, m \in \mathbb{Z}, \tag{4.13}$$

where the k_i are defined in Eq. (A.26), and the values of a_1, a_2 are determined by the boundary conditions, see Table 4.4.1.

This redefinition of allowed momenta is all that is needed to reproduce the calculations in 3.2. We can still use the special functions defined in the appendix (which are defined for arbitrary boundary conditions), and we solve the same gap equation for Δ,

$$g^{(2)}_{1/2}(\Delta, \tau) = -2\pi L(s - s_c), \tag{4.14}$$

and have the same formula for the ground state energy,

$$E_0 = \frac{2\pi N}{\tau_2 L} g^{(2)}_{-1/2}(\Delta, \tau) + \frac{N(s - s_c)}{2} \tau_2 L^2 \Delta^2. \tag{4.15}$$

However, we can now find the gap and the ground state energies in all four topological sectors of the theory, and we will see below that the splitting between the ground-state energies is important. The ground-state energies are proportional to N, so the energy splittings in the O$(2N)^*$ theory will be N-dependent in the $1/N$ expansion, unlike the O$(2N)$ case of Chapter 3. This N-dependence is a physical property of a system with $2N$ spinons, since the ground state configuration of each field with a twist will each contribute equally to shift the energy

Deg.	$\kappa = 0$	$\kappa = 1$
1	0	
2	1.921	
9	3.0239	
1	3.0244	
25	6.048	
66	7.111	7.111
60		7.975
1	8.126	
49	9.072	

Table 4.4.2: Energy splittings $L(E - E_0)$ and their degeneracies at $s = s_c$ for the $O(4)^*$ transition from the large-N expansion with $\tau = i$. Here, $\kappa = L|k|/2\pi$. The ground state energy relative to $L = \infty$ is $LE_0 = -1.317$. Here, we restrict to states that are even in the fields z_α, which corresponds to an antiferromagnet with an even number of $S = 1/2$ spins.

above the ground state of the system without a twist.

One consequence of the anti-periodic sectors is that there is no zero mode, so the massless free particle spectrum $|k|$ already has a gap. As a result, the saddle-point value of $i\tilde{\lambda} = \Delta^2$ determined through Eq. (4.14) can take negative values, provided $\sqrt{|k|^2 - |\Delta^2|}$ is real for all possible values of k.

We now consider the constraint of Eq. (4.3), requiring that the wavefunctional must be either an even or odd function of the z_α. These two cases correspond to an even or odd number of spins in the underlying lattice antiferromagnet of interest. In terms of the results in Section 3.3, this means we need to calculate the full spectrum for all of the relevant boundary conditions, and then separate the spectrum into the states with even particle-number states and odd particle-number states to describe the two possibilities.

4.4.2 Evolution of the spectrum of a function of $s - s_c$

When considering the deviation from the critical point, the topologically nontrivial sectors correspond to extra features in the two neighboring phases. In a $\mathbb{Z}_2$ spin liquid, the ground state on a torus will exhibit a four-fold degeneracy up to exponential splitting in the sys-

Deg.	$\kappa = 0$	$\kappa = 1/2$	$\kappa = 1/\sqrt{2}$	$\kappa = 1$	$\kappa = \sqrt{5}/2$	$\kappa = \sqrt{2}$
4	1.512					
16		4.516				
16	4.536					
16				6.463		
16			6.694			
36	7.560					
32					8.719	
16						9.013

Table 4.4.3: Energy splittings from $L(E - E_0)$ for the $O(4)^*$ transition from the large-N expansion with $\tau = i$ and $N = \infty$. Here, $\kappa = L|k|/2\pi$, and we restrict to states that are odd in the fields z_α, which corresponds to an antiferromagnet with an odd number of $S = 1/2$ spins. We are measuring the energies with respect to the lowest energy in the O(4) model, $LE_0 = -1.317$, for comparison with Table 4.4.2.

tem size. In addition, excited states in each topological sector will also contain a four-fold degeneracy corresponding to excitations in the background of different flux sectors through the holes of the torus. This topological degeneracy is the only remnant of the vison particle, which has been integrated out to obtain the O($2N$)* model, so our theory only captures the spectrum at energies well below the vison mass.

Topological phase

This degeneracy is easily verified in our model; as shown above, the phase with $s > s_c$ will have an energy gap even in an infinite volume, which results in the spectrum showing a weak dependence on boundary conditions. This will cause the different topological sectors to become degenerate up to an exponential splitting of magnitude e^{-mL} where $m = 2\pi(s - s_c)$. From solving Eq. (4.14) for $s \gg s_c$, one find that in all four sectors the gap approaches $\Delta = m$ up to exponential corrections in the system size, and similarly the ground state energies in this limit will become exponentially close.

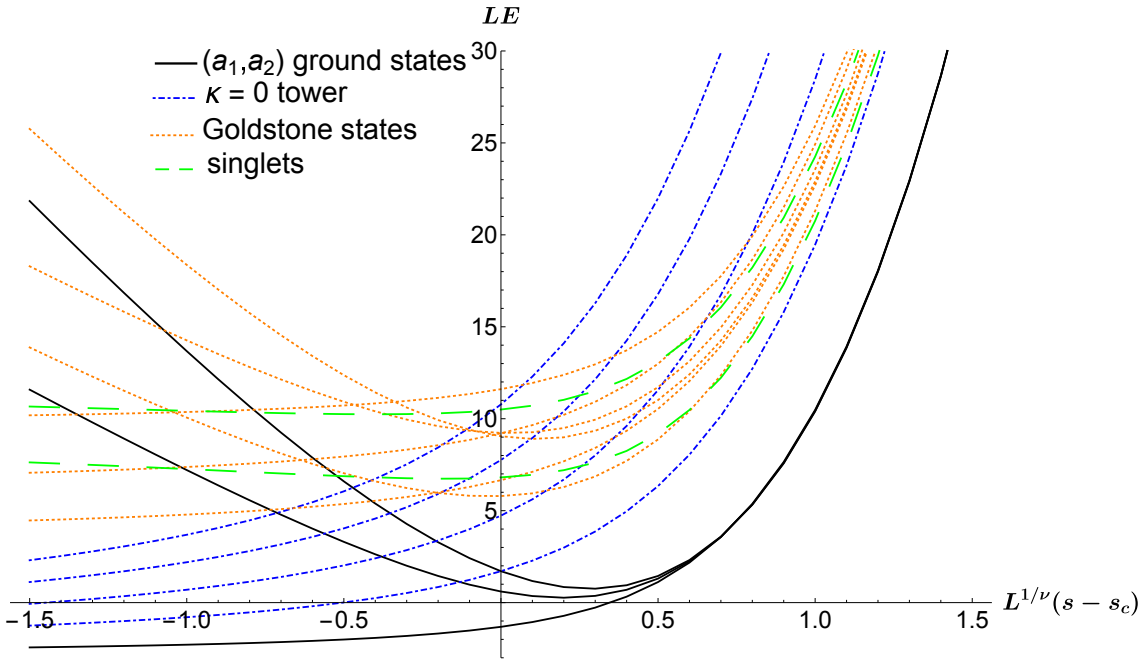

Figure 4.4.1: (Color online) The evolution of the spectrum LE for the O$(4)^*$ model as a function of the tuning parameter $L^{1/\nu}(s - s_c)$ on the square torus, $\tau = i$. Note that $\nu = 1$ to leading order in $1/N$. The energy levels are defined so that $E = 0$ at $s = s_c$ and $L = \infty$. We label the states by their behavior in the ordered region, distinguishing between the tower, the Goldstone modes, and the singlet states. We also distinguish the four "ground states" of the different sectors (a_1, a_2) according to Table 4.4.1, though the (A,P) and (P,A) sectors are degenerate for the square geometry. These states become degenerate in the topological phase, while they represent $\mathbb{Z}_2$ vortices in the magnetic phase. Our choice of states is not exhaustive, but highlights the main features of the proximate phases.

Magnetically ordered phase

In the magnetically ordered phase, $s < s_c$, the antiperiodic boundary conditions have an interpretation as vortices of the order parameter. This can be seen from the parametrization of the order parameter in terms of the spinon degrees of freedom in Eq. (4.10). As the spinon field undergoes a smooth non-contractible twist around a cycle of the torus, $z_\alpha \to -z_\alpha$, the physical order parameter returns to its original configuration after traversing a topologically nontrivial path in order parameter space. These correspond to vortices associated with the first homotopy group, $\pi_1(SO(3)) = \mathbb{Z}_2$. Note that by only allowing twists in the order parameter around the torus, we are ignoring local vortex configurations. This simplification is analogous to ignoring the local vison excitations in the spin liquid phase, since a local vortex will have some extra energy cost due to its core.

The energy cost of a vortex can be estimated by dimensional analysis. On general grounds, in the ordered phase we can write the energy functional for the phase $\theta(x)$ of the order parameter as

$$\mathcal{E} = \frac{\rho_s}{2} \int d^2x \, (\nabla \theta_\alpha)^2 \tag{4.16}$$

where ρ_s is a "spin stiffness" (really the stiffness of the condensed z_α fields rather than the physical spin order parameter), given by $\rho_s \sim N(s_c - s)$ close to the large-N critical point [73, 74]. We consider a smooth configuration of the field from $z_\alpha \to -z_\alpha$ as the order parameter winds around either cycle, which have lengths $|\omega_{1,2}|$. This contributes a gradient of order $\nabla z_\alpha \sim 1/|\omega_{1,2}|$, and the energy cost will be

$$\mathcal{E} \sim N(s_c - s) \frac{\mathcal{A}}{|\omega_{1,2}|^2}. \tag{4.17}$$

The estimate can be checked against the current model. For $s \ll s_c$, the solution of of gap equation becomes

$$\Delta^2 = \frac{1}{\mathcal{A}^2 (s_c - s)^2} - |k_{\min}|^2 \tag{4.18}$$

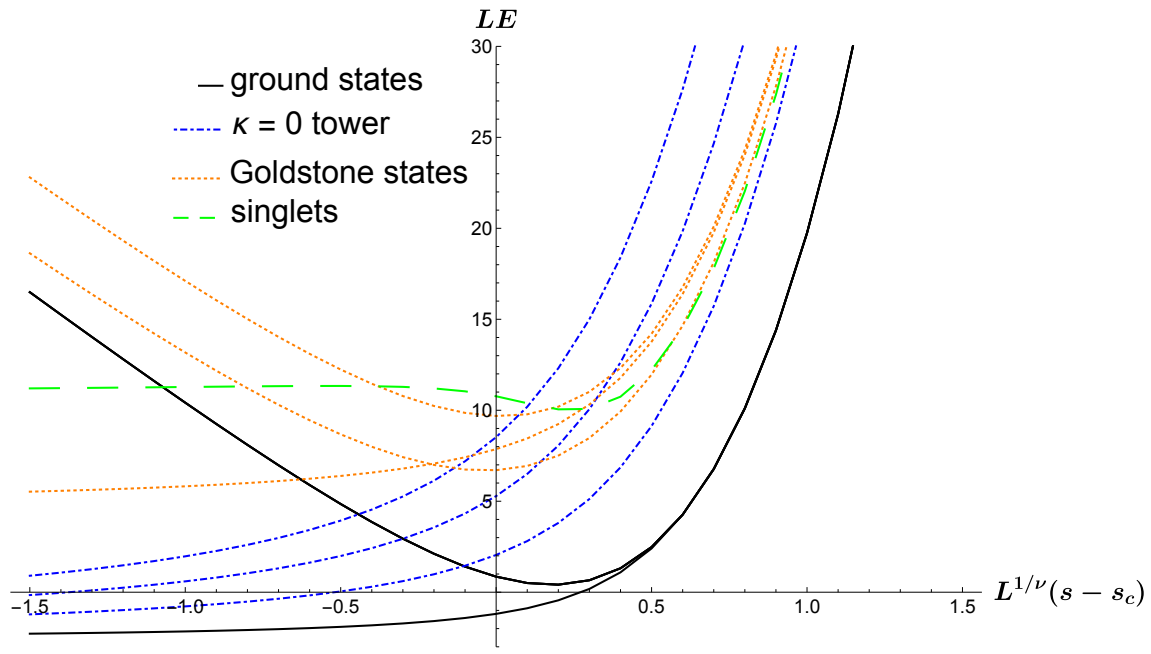

Figure 4.4.2: (Color online) The evolution of the spectrum LE for the O(4)* model as a function of the tuning parameter $L^{1/\nu}(s-s_c)$ on the triangular torus, $\tau = e^{i\pi/3}$. Note that $\nu = 1$ to leading order in $1/N$. The energy levels are defined so that $E = 0$ at $s = s_c$ and $L = \infty$. We label the states by their behavior in the ordered region, distinguishing between the tower, the Goldstone modes, and the singlet states. Note that the three sectors (A,P), (P,A), and (A,A) are degenerate in this geometry. Our choice of states is not exhaustive, but highlights the main features of the proximate phases.

where $|k_{\rm min}|$ is the minimum value of $|k|$ allowed in a given topological sector (so $k_{\rm min}$ is always zero in the (P,P) sector). Solving Eq. (4.15) for the energy of a vortex in this limit gives

$$E_{\rm vortex} \equiv E_0 - E_{0,(P,P)} = \frac{N\mathcal{A}(s_c - s)}{2}|k_{\rm min}|^2 \qquad s \ll s_c \tag{4.19}$$

This agrees with the above estimate since $|k_{\rm min}|^2 \sim 1/|\omega_{1,2}|^2$ in the different sectors.

Results

We give the results for the low-lying O(4)* spectrum on a square torus at criticality in Tables 4.4.2 and 4.4.3, which contain the even and odd spin results respectively. We also give the evolution of the spectrum as a function of $s-s_c$ in Figure 4.4.1, choosing some representative states to depict the nature of the two phases.

We also comment on the triangular torus, $\tau = e^{i\pi/3}$. This is an interesting case because

numerical simulations on the triangular lattice are more easily performed using this boundary condition, so these results have relevance to future studies on the J_1-J_2 Heisenberg model where the antiferromagnetic-spin liquid transition has been reported. For this special value of the modular parameter, it turns out that all three nontrivial topological sectors are exactly degenerate. This is due to the choice $\tau = e^{i\pi/3}$ being invariant under the modular transformation $\tau \to -1/(\tau - 1)$, see the discussion below Eq. (4.6). In addition, this torus has a discrete six-fold rotational symmetry, resulting in a highly degenerate spectrum for finite-momentum states. The evolution of the spectrum for the triangular torus is shown in Figure 4.4.2.

4.4.3 Anisotropic corrections

We now consider to the leading irrelevant operator in our theory,

$$\mathcal{L}' = \gamma |z_\alpha^* \nabla z_\alpha|^2. \tag{4.20}$$

Asymptotically close to the critical point, this term is irrelevant and will not contribute to universal physics. However, this term is *dangerously* irrelevant because it breaks the O($2N$) symmetry down to SU(N) for any deviation from the scaling limit. Therefore, the actual energy levels for the transition will organize into SU(N) multiplets for any lattice model, with a splitting determined by γ. The coefficient γ is non-universal and will be determined by microscopics, so in principle one must fit its value to a given spectrum.

We begin by discussing the nature of the splitting in terms of representation theory. The real and imaginary parts of z_α transform together as an O($2N$) vector, but this representation will transform reducibly under the SU(N) symmetry of Eq. (4.20). Labelling the irreducible representations by their dimension, the splitting of the O($2N$) vector into SU(N) representations is

$$2N \longrightarrow N \oplus \overline{N}, \tag{4.21}$$

where N and $\overline{N}$ are the fundamental and anti-fundamental representations of SU(N), which we will shortly associate with spinons and anti-spinons. We can analyze the breaking of higher representations of O($2N$) by taking tensor products of the fundamental representation. For example, the splitting of the two-particle states can be obtained by taking the antisymmetric or symmetric tensor product of the O($2N$) vector, and use the known properties for adding SU(N) representations

$$\begin{aligned}\left[\left(N\oplus\overline{N}\right)\otimes\left(N\oplus\overline{N}\right)\right]_A &= \frac{N(N-1)}{2}\oplus\overline{\frac{N(N-1)}{2}}\oplus\left(N^2-1\right)\oplus 1\\ \left[\left(N\oplus\overline{N}\right)\otimes\left(N\oplus\overline{N}\right)\right]_S &= \frac{N(N+1)}{2}\oplus\overline{\frac{N(N+1)}{2}}\oplus\left(N^2-1\right)\oplus 1\end{aligned} \tag{4.22}$$

where the subscripts indicate antisymmetrizing or symmetrizing the direct product with respect to the ordering of the O($2N$) indices. Since the symmetric representation of O($2N$) contains an irreducible singlet, it must coincide with the singlet state in the last line of Eq. (4.22).

We can make contact with our expressions in Section 3.3 by defining spinon and anti-spinon operators and relating them to the O($2N$) vector operators $b_\alpha^\dagger$. We expand the z_α field as

$$z_\alpha = \frac{1}{\mathcal{A}^{1/2}}\sum_{k\neq 0}\frac{e^{ik\cdot x}}{\sqrt{2E_1(k)}}\left(a_\alpha(k)+c_\alpha^\dagger(-k)\right). \tag{4.23}$$

Here, the dot product is given by $k\cdot x\equiv \mathrm{Re}(kx^*)$, and $E_1(k)=\sqrt{|k|^2+\Delta^2}$ is the single-particle energy at $N=\infty$. Here, we are assuming that the perturbation γ does not shift the saddle-point value of the path integral, so we can perturb around the $N=\infty$ spectrum. Since z_α transforms as an SU(N) vector, the particles created by $c_\alpha^\dagger$ are spinons and the particles created by $a_\alpha^\dagger$ are anti-spinons. We can identify these with the O($2N$) bosons

defined earlier

$$\begin{aligned} c_\alpha^\dagger &= \frac{1}{\sqrt{2}}\left(b_\alpha^\dagger + i b_{\alpha+N}^\dagger\right) \\ a_\alpha^\dagger &= \frac{1}{\sqrt{2}}\left(b_\alpha^\dagger - i b_{\alpha+N}^\dagger\right). \end{aligned} \tag{4.24}$$

From these relations it is straight-forward to check that the embedding in Eq. (4.21) holds. The decomposition of the two-particle states can be written

$$\begin{aligned} b_{[\alpha}^\dagger b_{\beta]}^\dagger &\longrightarrow c_{[\alpha}^\dagger c_{\beta]}^\dagger + a_{[\alpha}^\dagger a_{\beta]}^\dagger + \left(c_\alpha^\dagger a_\beta^\dagger - a_\beta^\dagger c_\alpha^\dagger - \frac{\delta_{\alpha\beta}}{N}\left(c_\gamma^\dagger a_\gamma^\dagger - a_\gamma^\dagger c_\gamma^\dagger\right)\right) + \frac{\delta_{\alpha\beta}}{N}\left(c_\gamma^\dagger a_\gamma^\dagger - a_\gamma^\dagger c_\gamma^\dagger\right) \\ b_{(\alpha}^\dagger b_{\beta)}^\dagger &\longrightarrow c_{(\alpha}^\dagger c_{\beta)}^\dagger + a_{(\alpha}^\dagger a_{\beta)}^\dagger + \left(c_\alpha^\dagger a_\beta^\dagger + a_\beta^\dagger c_\alpha^\dagger - \frac{\delta_{\alpha\beta}}{N}\left(c_\gamma^\dagger a_\gamma^\dagger + a_\gamma^\dagger c_\gamma^\dagger\right)\right) \\ b_\gamma^\dagger b_\gamma^\dagger &\longrightarrow c_\gamma^\dagger a_\gamma^\dagger + a_\gamma^\dagger c_\gamma^\dagger \end{aligned} \tag{4.25}$$

where the indices on the left run to $2N$ while the indices on the right run to N. If the two states carry the same momentum there is no antisymmetric contribution.

We now apply perturbation theory on the degenerate states, using Eq. (4.25) to diagonalize the perturbation. We define the dimensionless coupling $\tilde{\gamma} \equiv \gamma/L$ as well as the shorthand $\chi_\alpha(k) \equiv a_\alpha(k) + c_\alpha^\dagger(-k)$, and obtain the interaction Hamiltonian

$$V_\gamma = \frac{\tilde{\gamma}}{\tau_2 L} \sum_{k_1,k_2,k_3 \neq 0} \frac{(k_2 \cdot k_3)\, \chi_\alpha^\dagger(k_1)\chi_\alpha(k_2)\chi_\beta^\dagger(k_3)\chi_\beta(k_1 - k_2 + k_3)}{4\sqrt{E_1(k_1)E_1(k_2)E_1(k_3)E_1(k_1 - k_2 + k_3)}} \tag{4.26}$$

The single particle energies of spinons and anti-spinons are shifted by the same amount, so there is no splitting to one-particle states to leading order.

We will explicitly compute the shift in energies for the two-particle states in Eq. (4.25), which are all degenerate at $N = \infty$ except for the singlet state in the last line. The perturbation will split these states, and can also split any possible degeneracy between states with the same total momentum. We first ignore the latter possibility, which does not occur for any of the states listed in the above tables. Recall that the two-particle state energies

can be written as $E_2(k) = E_1(q) + E_1(k-q)$ for some value of q. Then the splitting of the antisymmetric representation is

$$\begin{aligned}
\frac{N(N-1)}{2}, \overline{\frac{N(N-1)}{2}} : &\qquad \Delta E_{\text{asym}}(k) = -\frac{\tilde{\gamma}}{\tau_2 L}\frac{|k-2q|^2}{4E_1(q)E_1(k-q)} \\
N^2-1 : &\qquad \Delta E_{\text{adj}}(k) = -\frac{\tilde{\gamma}}{\tau_2 L}\frac{2q\cdot(k-q)}{4E_1(q)E_1(k-q)} \\
1 : &\qquad \Delta E_{\text{s}}(k) = \frac{\tilde{\gamma}}{\tau_2 L}\frac{N\left(|q|^2+|k-q|^2\right)-2q\cdot(k-q)}{4E_1(q)E_1(k-q)},
\end{aligned} \tag{4.27}$$

while for the symmetric representation,

$$\begin{aligned}
\frac{N(N+1)}{2}, \overline{\frac{N(N+1)}{2}} : &\qquad \Delta E_{\text{sym}}(k) = \frac{\tilde{\gamma}}{\tau_2 L}\frac{|k|^2}{4E_1(q)E_1(k-q)} \\
N^2-1 : &\qquad \Delta E_{\text{adj}}(k) = -\frac{\tilde{\gamma}}{\tau_2 L}\frac{2q\cdot(k-q)}{4E_1(q)E_1(k-q)}.
\end{aligned} \tag{4.28}$$

The subscripts refer to the states being in the symmetric, antisymmetric, singlet, or adjoint representations of SU(N).

Summarizing the results to first order in γ, the degeneracy of the antisymmetric representation breaks down from $N(2N-1)$ to $N(N-1)$, N^2-1, and 1, while the degeneracy of the symmetric traceless tensor representation breaks down from $(2N-1)(2N+2)/2$ to $N(N+1)$ and N^2-1.

Note that the first-order correction is zero if the unperturbed particles all have zero momentum. Therefore, to first order there is no splitting of the "tower of states" in the antiferromagnetic phase. Although we do not compute the magnitude for the splitting of the states in the tower, we comment on the expected representations which should appear. In Section 3.3.1 we saw that the tower of states for the O($2N$) model all belong to the symmetric traceless tensor representations. For the case of interest, $N = 2$, the allowed degeneracies in the tower becomes $(2\ell+1)^2$ for $\ell = 0, 1, 2, ...$ where we use the constraint that only an even number of particles are allowed. Repeating the above analysis by forming symmetric products and subtracting out the traces, one finds that each of these states decomposes into

deg. at $\gamma = 0$	$\sqrt{\mathcal{A}}E_2$	κ	$\tilde{q}$	deg. at $\mathcal{O}(\gamma)$	$\sqrt{\mathcal{A}}\Delta E$
9	3.0239	0	0	9	0
30	7.111	0	1/2	4	$-1.47\tilde{\gamma}$
				12	0
				12	$0.73\tilde{\gamma}$
				2	$1.47\tilde{\gamma}$
36	7.111	1	1/2	12	$-0.73\tilde{\gamma}$
				24	0
60	7.975	1	0	8	$-1.01\tilde{\gamma}$
				24	0
				24	$1.01\tilde{\gamma}$
				4	$2.02\tilde{\gamma}$

Table 4.4.4: The two-particle states in the even sector of the critical O(4)* spectrum, taken from Table 4.4.2, and their splitting due to the perturbation. The energies of these states are written as $E_2(k) = E_{gs} + E_1(q) + E_1(k-q)$, and we list the scaled momenta, $\kappa = L|k|/2\pi$ and $\tilde{q} = L|q|/2\pi$. For further details, see the text.

$(2\ell+1)$ different SU(2) representations each with spin-ℓ. We also note that the spacing of the even-particle spectrum for the O(4)* model should be proportional to $2\ell(2\ell+2) \propto \ell(\ell+1)$, which agrees with the spacing for the tower in an SU(2) antiferromagnet [52]. This qualitative structure of the spectrum, with $(2\ell+1)$ inequivalent spin-ℓ multiplets in the tower becoming approximately degenerate close to the critical point, is an interesting feature of this theory which could give good evidence for the existence of an O(4)* transition and a neighboring spin liquid phase.

For a definite example, we revisit the results for the even sector of the O(4)* model on the square torus. In Table 4.4.4, we explicitly show all the two-particle states from Table 4.4.2 which are split by the perturbation, and give the magnitude of the splitting. Note that the numerical value of all energies will be shifted from their unperturbed values, but here we only give the energy splitting between states. The states listed in Table 4.4.4 turn out to be the only states in Table 4.4.2 which are split at first-order in γ.

In principle, one can continue this process to higher-particle states, and to higher order in γ. For a more complex O($2N$) multiplet, one finds how the SU(N) representations fit inside the larger group, and use this to diagonalize the perturbation within the degenerate

multiplet.

4.5 Conclusions

In the present chapter, we have presented results on the finite size torus spectrum of a class of critical points which are beyond the LGW paradigm. We related their spectra to the Wilson-Fisher spectra considered in Chapters 2 and 3, and we compared analytic and numerical results for the Ising* transition between a $\mathbb{Z}_2$ spin liquid and a trivial paramagnet.

We also examined a two-dimensional antiferromagnet, with global SU(2) spin rotation symmetry, which undergoes a transition between a gapped $\mathbb{Z}_2$ spin liquid and coplanar antiferromagnetic order. Such a transition is described by a O(4)* conformal field theory in 2+1 dimensions, which is closely related to the O(4) Wilson-Fisher conformal field theory. We showed that its spectrum contains features which descend from the phases found on either side of the critical point. The topological degeneracy on the gapped side evolves into non-trivial boundary conditions and selection rules on the operators of the conformal field theory. And the spontaneously broken spin-rotation symmetry on the other side yields low-lying states with non-zero spin at the critical point.

We hope that our results will aid in analyzing numerical data on lattice models which undergo transitions to ordered to spin liquid states. With the available data on the manner in which the "tower of states" evolve into the spin liquid across a quantum critical point, strong constraints become available on identifying the topological order in the spin liquid.

Chapter 5

Entanglement entropy of the large N Wilson-Fisher conformal field theory

5.1 Introduction

The entanglement entropy (EE) has emerged as an important tool in characterizing strongly interacting quantum systems [11, 86–94]. In the context of relativistic theories in 2 spatial dimensions, the so-called F theorem uses the EE on a circular disk to place constraints on allowed renormalization group flows [11, 95–100]. For quantum systems with holographic duals, the EE can be computed via the Ryu-Takayanagi formula [87], and this is a valuable tool in restricting possible holographic duals of strongly interacting theories [101, 102].

Despite its importance, the list of results for the EE of strongly interacting gapless field theories in 2+1 dimensions is sparse. The most extensive results are for CFTs on a circular disk geometry in the vector large-N and small-ϵ expansions [98, 99, 103–107]. Some results have also been obtained [93] in the infinite cylinder geometry in an expansion in $\epsilon = (3-d)$, where d is the spatial dimension, but the extrapolation of these results to $d = 2$ is not

straightforward.

In this chapter we show how the vector large N expansion can be used to obtain the EE in essentially all entanglement geometries, generalizing results that were only available so far in the circular disk geometry. The large N expansion was also used in Ref. [93] in the infinite cylinder geometry, but the results were limited to the universal deviation of the EE when the CFT is tuned away from the critical point by a relevant operator. For a region with a smooth boundary, the groundstate of a CFT has an EE S which obeys

$$S = C\frac{L}{\delta} - \gamma \tag{5.1}$$

where δ is a short-distance UV length scale, C is the area law coefficient depending on the regulator, L is an infrared length scale associated with the entangling geometry, and γ is the universal part of the EE we are interested in. We will compute γ for the Wilson-Fisher CFT with O(N) symmetry on arbitrary smooth regions in the plane, and in the cylinder and torus geometries. Our methods generalize to other geometries, and also to other CFTs with a vector large N limit. We also obtain universal entanglement entropies associated with geometries with sharp corners.

Our analysis relies on a general result which will be established in Section 5.2. We consider the large N limit of the Wilson-Fisher CFT on a general geometry using the replica method, which requires the determination of the partition function on a space which is a n-sheeted Riemann surface. The large N limit maps the CFT to a Gaussian field theory with a self-consistent, spatially dependent mass [93]. Determining this mass for general n is a problem of great complexity, given the singular and non-translationally invariant n-sheeted geometry; complete results for such a spatially dependent mass are not available. However, we shall show that a key simplification occurs in the limit $n \to 1$ required for the computation of the EE: the spatially dependent part of the mass does not influence the value of the EE. This simplification leads to our main results. We note here that the simplification does not extend

to the Rényi entropies $n \neq 1$, so we shall not obtain any results for the Rényi entropies of the Wilson-Fisher CFT in the large N limit.

Section 5.2 will compute the EE for the Wilson-Fisher CFT on arbitrary smooth regions in an infinite plane, and for regions containing a sharp corner, in which case (5.1) is modified. In both these cases, and for other entangling regions in the infinite plane, the EE is equal to that of a CFT of N free scalar fields. Section 5.3.2 will consider the case of an entanglement cut on an infinite cylinder. A non-zero limit of γ/N as $N \to \infty$ was obtained in Ref. [93] for the free field case. We will show that a very different result applies to the Wilson-Fisher CFT, with $\gamma/N = \mathcal{O}(1/N)$. Section 5.3.3 considers the case of a torus with two cuts: here γ/N is non-zero for both the free field and Wilson-Fisher cases, but the values are distinct from each other.

5.2 Mapping to a Gaussian theory

In this section we consider the EE of the critical O(N) model at large-N, and show that it can be mapped to the EE of a Gaussian scalar field.

5.2.1 Replica method

We first recall how the EE can be computed in a quantum field theory using the replica method introduced in Refs. [86, 108]. The EE associated with a region A is given by

$$S = -\mathrm{Tr}\left(\rho_A \log \rho_A\right) \tag{5.2}$$

where ρ_A is the reduced density matrix in A. A closely related measure of the entanglement is the n-th Rényi entropy, which is defined as

$$S_n = \frac{1}{1-n} \log \mathrm{Tr} \rho_A^n \tag{5.3}$$

where $n > 1$ is an integer. In the replica method, outlined below, the Rényi entropies are directly computed from a path integral construction. One can then analytically continue n to non-integer values, and obtain the EE as a limit

$$\lim_{n\to 1} S_n = S \tag{5.4}$$

Equivalently, one can consider expanding $\log \mathrm{Tr}\rho_A^n$ to leading order in $(n-1)$, obtaining

$$\log \mathrm{Tr}\rho_A^n = -(n-1)S + \mathcal{O}\big((n-1)^2\big) \tag{5.5}$$

Thus, the small $(n-1)$ behavior of $\mathrm{Tr}\rho_A^n$ is sufficient to compute the entropy S.

The computation of $\mathrm{Tr}\rho_A^n$ proceeds as follows. We first consider the matrix element of the reduced density matrix between two field configurations on A, $\phi'_A(\mathbf{x})$ and $\phi''_A(\mathbf{x})$. This can be computed using the Euclidean path integral

$$\langle \phi'_A(\mathbf{x})|\rho_A|\phi''_A(\mathbf{x})\rangle = \mathcal{Z}_1^{-1} \int_{\phi(\mathbf{x}\in A, t_E=0^-)=\phi'_A(\mathbf{x})}^{\phi(\mathbf{x}\in A, t_E=0^+)=\phi''_A(\mathbf{x})} \mathcal{D}\phi(\mathbf{x}, t_E) e^{-\mathcal{S}_E} \tag{5.6}$$

where $\mathcal{S}_E$ is the Euclidean action of the system. We then write the trace over ρ_A^n in terms of these matrix elements

$$\mathrm{Tr}\rho_A^n = \int \mathcal{D}\phi'_A \mathcal{D}\phi''_A \cdots \mathcal{D}\phi_A^{(n)} \ \langle \phi'_A|\rho_A|\phi''_A\rangle \langle \phi''_A|\rho_A|\phi'''_A\rangle \cdots \langle \phi_A^{(n)}|\rho_A|\phi'_A\rangle \tag{5.7}$$

Combining Eqns. (5.6) and (5.7), we obtain the path integral expression for $\mathrm{Tr}\rho_A^n$ as

$$\mathrm{Tr}\rho_A^n = \frac{\mathcal{Z}_n}{\mathcal{Z}_1^n} \tag{5.8}$$

Here, $\mathcal{Z}_n$ is the partition function over the n-sheeted Riemann surface obtained by performing the integrations in Eq. (5.7). In particular, we consider n copies of our Euclidean field theory, but we glue the spatial region $(\mathbf{x} \in A, t_E = 0^+)$ of the kth copy to the spatial region

($\mathbf{x} \in A, t_E = 0^-$) of the $(k+1)$th copy, repeating until we glue the nth copy to the first copy. This construction introduces conical singularities at the boundary of A.

5.2.2 Entanglement entropy for the O(N) model at large N

We now specialize to the critical O(N) model in $(2+1)$-dimensions. We use a non-linear σ model formulation, writing the n-sheeted action as

$$\begin{aligned} \mathcal{S}_n &= \int d^3x_n \, \mathcal{L}_n \\ \mathcal{L}_n &= \frac{1}{2}\phi_\alpha \left(-\partial_n^2 + i\lambda\right) \phi_\alpha - \frac{N}{2g_c} i\lambda \end{aligned} \tag{5.9}$$

where α runs from 1 to N and is summed over. Here, d^3x_n and ∂_n^2 denote the integration measure and the Laplacian on the n-sheeted Riemann surface, respectively. The field $\lambda(x)$ is a Lagrange multiplier enforcing the local constraint $\phi(x)^2 = N/g_c$. In the $N = \infty$ limit, the path integral is evaluated using the saddle point method:

$$\begin{aligned} \mathcal{Z}_n &= \int \mathcal{D}\phi\mathcal{D}\lambda \; e^{-\mathcal{S}_n} \\ &= \int \mathcal{D}\lambda \; \exp\left[-\frac{N}{2}\mathrm{Tr}\log\left(-\partial_n^2 + i\lambda\right) + \frac{N}{2g_c}\int d^3x \; i\lambda\right] \\ \Longrightarrow \log \mathcal{Z}_n &= -\frac{N}{2}\mathrm{Tr}\log\left(-\partial_n^2 + \langle i\lambda\rangle_n\right) + \frac{N}{2g_c}\int d^3x_n \; \langle i\lambda\rangle_n + \mathcal{O}(1/N) \end{aligned} \tag{5.10}$$

In the last equality, the saddle point configuration of the field λ is determined by solving the gap equation

$$G_n(x, x; \langle i\lambda\rangle_n) = \frac{1}{N}\langle\phi(x)^2\rangle_n = \frac{1}{g_c} \tag{5.11}$$

where $G_n(x, x')$ is the Green's function on the n-sheeted surface:

$$\left(-\partial_n^2 + \langle i\lambda(x)\rangle_n\right) G_n(x, x'; \langle i\lambda\rangle_n) = \delta^3(x - x') \tag{5.12}$$

and the critical coupling is determined by demanding that the gap vanishes for the infinite volume theory on the plane:

$$\frac{1}{g_c} = \int \frac{d^3p}{(2\pi)^3} \frac{1}{p^2} \tag{5.13}$$

In the absence of the entangling cut, $n = 1$, we denote the saddle point value of λ as

$$\langle i\lambda \rangle_1 = m_1^2 \tag{5.14}$$

We assume that the one-sheeted geometry is translation-invariant, so m_1 is independent of position. On the infinite plane we have $m_1 = 0$, but we will also consider geometries where one or both dimensions are finite, in which case m_1 becomes a universal function of the geometry of the system determined by

$$G_1(x, x; m_1^2) = \frac{1}{g_c} \tag{5.15}$$

On the n-sheeted Riemann surface, $\langle i\lambda(x) \rangle_n$ is always a nontrivial function of position, and the exact form of this function depends on the shape of the entangling surface and the number of Riemann sheets n. The problem of determining this function can be addressed numerically for fixed n, but for the purposes of obtaining the EE, we only need its spatial dependence to first-order in $(n-1)$. In particular, we assume that we can write

$$\langle i\lambda(x) \rangle_n \approx m_1^2 + (n-1) f(x) \tag{5.16}$$

for some function of space-time $f(x)$. Then to leading order in N and $(n-1)$, we have

$$\begin{aligned} -\log \mathcal{Z}_n &\approx \frac{N}{2} \mathrm{Tr} \log \left(-\partial_n^2 + m_1^2 \right) - \frac{N}{2g_c} \int d^3x_n \; m_1^2 \\ &+ (n-1) \frac{N}{2} \mathrm{Tr} \left(\frac{f(x)}{-\partial_1^2 + m_1^2} \right) - (n-1) \frac{N}{2g_c} \int d^3x \; f(x) \end{aligned} \tag{5.17}$$

Then using the definition of G_1 and m_1,

$$\mathrm{Tr}\left(\frac{f(x)}{-\partial_1^2+m_1^2}\right)=\int d^3x\; G_1(x,x;m_1^2)f(x)=\frac{1}{g_c}\int d^3x f(x) \tag{5.18}$$

implying that that last line of Eq. (5.17) vanishes, and $f(x)$ does not contribute to the EE. After using $\int d^3x_n = n\int d^3x$, we can write

$$-\log\frac{\mathcal{Z}_n}{\mathcal{Z}_1^n}=\frac{N}{2}\left[\mathrm{Tr}\log\left(-\partial_n^2+m_1^2\right)-n\mathrm{Tr}\log\left(-\partial_1^2+m_1^2\right)\right] \tag{5.19}$$

This final expression is equal to the quantity $-\log\mathrm{Tr}\rho_A^n$ computed for N free scalars with mass m_1 and the action

$$\mathcal{L}_n'=\phi_\alpha\left(-\partial_n^2+m_1^2\right)\phi_\alpha \tag{5.20}$$

Therefore, the EE of the critical O(N) model at order N is equal to the EE of N free scalar fields, where the free fields have the same mass gap as the O(N) model on the physical, one-sheeted surface. Similar results will apply to other large-N vector models. For instance, in Appendix B.2 we follow very similar steps to show that the EE of the fermionic Gross-Neveu model maps to that of N free Dirac fermions. The mass of the free fermions is determined self-consistently by the spatial geometry of the physical single-sheeted spacetime.

5.3 Entanglement entropy in particular geometries

5.3.1 Entanglement entropy on the infinite plane

We first consider the EE when the system is on the infinite plane. In this case, $m_1 = 0$, and the EE associated with a region A is equal to the EE of N massless free scalars in the same region.

One entangling region for which there are known results is the circular disk. According to

the F-theorem [11], the universal part of the EE for the disk is given by

$$\gamma_{\text{disk}} = F \equiv -\log|\mathcal{Z}_{S^3}| \tag{5.21}$$

Here, $\mathcal{Z}_{S^3}$ is the finite part of the Euclidean partition function on a three-sphere spacetime. This quantity was computed in Ref. [98] for massless free scalar fields and for the large-N O(N) model, and they were found to be equal at order N in agreement with our general result given above. Explicitly,

$$\gamma_{\text{disk}} = \frac{N}{16}\left(2\log 2 - 3\frac{\zeta(3)}{\pi^2}\right) \tag{5.22}$$

where $\zeta(3) \approx 1.202$. Our results also apply to regions with sharp corners, in which case we can make non-trivial checks of our general result, as we now discuss.

Entanglement entropy of regions with corners

When region A (embedded in the infinite plane) contains a sharp corner of opening angle θ, the EE of a CFT (5.1) is modified by a subleading logarithmic correction [109, 110]

$$S = C\frac{L}{\delta} - a(\theta)\log(L/\delta) + \cdots \tag{5.23}$$

where the dimensionless coefficient $a(\theta) \geq 0$ is universal, and encodes non-trivial information about the quantum system. Since we work in the infinite plane, according to our analysis above, the large-N value of $a(\theta)$ will be the same as for N free scalars, namely

$$a_{\text{WF}}(\theta) = N\, a_{\text{free}}(\theta) + \mathcal{O}(N^0) \tag{5.24}$$

The non-trivial function $a_{\text{free}}(\theta)$ for a single free scalar was studied numerically and analytically by a number of authors for a wide range of angles [109, 111–115]. Interestingly, we can make an analytical verification of the relation (5.24) in the nearly smooth limit, by virtue of

the following identity that holds for any CFT [111, 116, 117]

$$a(\theta \approx \pi) = \frac{\pi^2 C_T}{24} (\theta - \pi)^2 + \mathcal{O}\big((\theta - \pi)^4\big) \tag{5.25}$$

Here, C_T is a non-negative coefficient determining the groundstate two-point function of the stress tensor $T_{\mu\nu}$:

$$\langle T_{\mu\nu}(x) T_{\eta\kappa}(0)\rangle = \frac{C_T}{x^6} \mathcal{I}_{\mu\nu,\eta\kappa}(x) \tag{5.26}$$

where $\mathcal{I}_{\mu\nu,\eta\kappa}(x)$ is a dimensionless tensor fixed by conformal symmetry [118]. Eq. (5.25) was conjectured [111] for general CFTs in two spatial dimensions, and subsequently proved using non-perturbative CFT methods [117]. Now, C_T is the same at the Wilson-Fisher and Gaussian fixed points [119] at leading order in N:

$$C_T^{\mathrm{WF}} = N C_T^{\mathrm{free}} + \mathcal{O}(N^0) \tag{5.27}$$

which, when combined with Eq. (5.25), leads to a non-trivial confirmation of (5.24) in the nearly smooth limit $\theta \approx \pi$. (We note that $C_T^{\mathrm{free}} = \frac{3}{32\pi^2}$ using conventional normalization [118].)

The knowledge of C_T can be used to make a statement about $a(\theta)$ away from the nearly smooth limit because the existence of the following lower bound [114]: $a(\theta) \geq C_T \frac{\pi^2}{3} \log\left[1/\sin(\theta/2)\right]$, which follows from the strong subadditivity of the EE, and (5.25). We see that applying this bound to the large-N Wilson-Fisher fixed point is consistent with our result (5.24).

5.3.2 Infinite cylinder

We now compute the EE of the semi-infinite region obtained by tracing out half of an infinite cylinder. The relevant geometry is pictured in Fig. 5.3.1. We can take the position of the

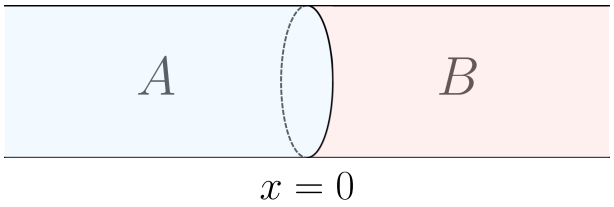

Figure 5.3.1: The geometry considered in calculating the entanglement entropy on the infinite cylinder.

cut to be at $x = 0$ by translation invariance. As for the disk, we can write the EE as

$$S = C\frac{L}{\delta} - \gamma_{\rm cyl} \tag{5.28}$$

where $\gamma_{\rm cyl}$ is the universal part. The existence of a universal $\gamma_{\rm cyl}$ in critical theories was first established [92, 120, 121] for the $z = 2$ quantum Lifshitz model using the methods of Ref. [90]. In the context of CFTs, this geometry was considered in Ref. [93], where the entropy γ was computed for massless free fields and for the Wilson-Fisher fixed point in the $\epsilon = (3 - d)$ expansion (where the extra dimensions introduced in the ϵ-expansion are made periodic with circumference L).

We first review the calculation of the entropy for free massive fields, which will allow us to calculate the EE for the Wilson-Fisher fixed point for large N. We allow for twisted boundary conditions along the finite direction

$$\phi(x, y + L) = e^{i\varphi_y}\phi(x, y) \tag{5.29}$$

Here, $\varphi_y \in [0, 2\pi)$. We note that unless $\varphi_y = 0, \pi$, the fields ϕ are complex. In this case, we are considering $N/2$ complex fields, and the O(N) symmetry of the theory breaks down to U(1)×SU($N/2$).

This geometry allows a direct analytic computation of the n-sheeted partition function for free fields by mapping to radial coordinates, $(t_E, x) = (r\cos\theta, r\sin\theta)$. In these coordinates, the n-sheeted surface is fully parametrized by giving the angular coordinate a periodicity of

$2\pi n$. In Refs. [86, 93], it was shown that the n-sheeted partition function for free fields can be written in terms of the one-sheeted Green's function:

$$\begin{aligned} -\log\frac{\mathcal{Z}_n}{\mathcal{Z}_1^n} &= \frac{N}{2}\left[\mathrm{Tr}\log\left(-\partial_n^2+m^2\right)-n\mathrm{Tr}\log\left(-\partial_n^2+m^2\right)\right] \\ &= \frac{\pi N}{6}\left(n-\frac{1}{n}\right)LG_1(x,x;m^2) \end{aligned} \tag{5.30}$$

Then using Eq. (5.5), the EE is given by

$$S=\frac{\pi N}{3}LG_1(x,x;m^2) \tag{5.31}$$

In Appendix B.1, we compute the Green's function for a massive free field on the cylinder. Using Eq. (B.5), and making the cutoff dependence explicit, we find the regularized part of the EE to be (see also Ref. [122])

$$\gamma_{\mathrm{cyl}} = \frac{N}{12}\log\left[2\left(\cosh mL-\cos\varphi_y\right)\right] \tag{5.32}$$

For $m=0$, this reduces to Eq. (5.12) of Ref. [93], and indeed displays a divergence for a periodic boundary condition $\varphi_y=0$ due to the zero mode. We note that the universal contribution to the EE of $N/2$ complex free scalar fields is of order N, as one would expect from a free field theory with N degrees of freedom.

We now turn to the Wilson-Fisher fixed point. In a finite geometry, the Wilson-Fisher fixed point will acquire a mass gap m_1 which is proportional to $1/L$ and depends only on φ_y. This is computed by solving $G_1(x,x;m_1^2)=1/g_c$, which is done in Appendix B.1. The result is

$$m_1=\frac{1}{L}\mathrm{arccosh}\left(\frac{1}{2}+\cos\varphi_y\right) \tag{5.33}$$

Then from the arguments of Section 5.2,

$$\gamma_{\text{cyl}} = \frac{N}{12} \log \left[2 \left(\cosh m_1 L - \cos \varphi_y \right) \right] = 0 \tag{5.34}$$

It happens that for the saddle point value of the mass, the universal part of the EE vanishes for all values of the twist φ_y. The leading contribution to γ_{cyl} will be of $\mathcal{O}(N^0)$, a drastic reduction from Gaussian fixed point which is of order N.

This result can be seen more directly from Eq. (5.31). The gap equation implies that $G_1(x, x; m_1^2) = 1/g_c$, so without even solving for m_1, the EE can immediately be written

$$S = \frac{\pi N}{3} \frac{L}{g_c} \tag{5.35}$$

However, the critical coupling is completely non-universal and independent of L. Using a hard UV momentum cutoff $1/\delta$,

$$\frac{1}{g_c} = \int^{1/\delta} \frac{d^3p}{(2\pi)^3} \frac{1}{p^2} = \frac{1}{2\pi^2 \delta} \tag{5.36}$$

and the EE is pure area law, $S \propto L/\delta$.

In fact, this result can be extended to other geometries. The result $\gamma_{\text{cyl}} = 0$ for the large-N Wilson-Fisher fixed point occurred because the entropy is proportional to $G_1(x, x; m^2)$. However, the results of Refs. [86, 93] imply that the expression for the free-field entropy given in Eq. (5.31) holds for *any* system where the entangling cut is perpendicular to an infinite, translationally-invariant direction. Thus, if we consider the large-N Wilson-Fisher CFT on any d-dimensional spatial geometry with at least one infinite dimension, the universal part of the EE obtained by tracing out over half of that dimension is $\mathcal{O}(N^0)$. This argument only holds in dimensions where the Wilson-Fisher CFT exists, so for $1 < d < 3$. In particular, this result agrees with the large-N limit of the ϵ-expansion calculation in Ref. [93], which considered the Wilson-Fisher CFT on the $(3-\epsilon)$-dimensional spatial region $\mathbb{R} \times \mathbb{T}^{2-\epsilon}$, where

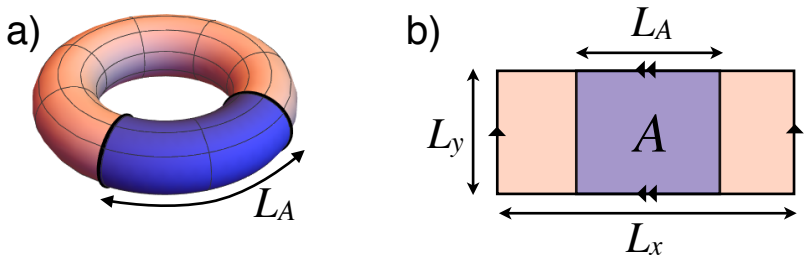

Figure 5.3.2: a) Two dimensional (flat) torus. b) Its representation in the plane. We analyze the entanglement entropy of region A.

$\mathbb{T}^d$ is the d-dimensional torus. This constitutes a non-trivial consistency check on both calculations.

Finally, we note that similar results apply to other large N models. As shown in Appendix B.2, the EE for the Gross-Neveu CFT maps to that of N free Dirac fermions, where the mass of the fermions is determined by the spatial geometry of the one-sheeted spacetime, Tr $G_1^F(x, x; m_1) = m_1/g_c^2$. Here, the critical coupling $1/g_c^2$ is again a non-universal quantity which cannot depend on the spatial geometry of the system, and is proportional to the UV cutoff. Then using the results of Ref. [86], it can be shown that $S \propto G_1^F$ for free fermions on the spatial geometries discussed in the previous paragraph, and therefore $\gamma = \mathcal{O}(N^0)$ for the large-N Gross-Neveu CFT on the infinite cylinder.

5.3.3 Torus

We study the EE of the large-N fixed point on a spatial torus, as shown in Fig. 5.3.2. For a CFT, we expect the following form for S [123, 124]

$$S = C\frac{2L_y}{\delta} - \gamma_{\text{tor}}(u;\tau) \tag{5.37}$$

where we have defined the ratio

$$u = L_A/L_x \tag{5.38}$$

and τ is the modular parameter, $\tau = iL_x/L_y$, for the rectangular torus we work with. $\gamma_{\rm tor}$ is a universal term that we shall study at the large-N Wilson-Fisher fixed point.

As discussed in Section 5.2.2, the EE at leading order in N is given by that of $N/2$ free complex scalars with a mass m_1 determined by the geometry. m_1 is thus the self-consistent mass on the torus for a single copy of the theory. It obeys the scaling relation $m_1 L_y = g(\tau)$, where τ is the aspect ratio of the torus, and g is a non-trivial dimensionless function given in Chapter 3. m_1 depends on both twists along the x- and y-cycles of the torus, φ_x, φ_y. Since $\gamma_{\rm tor}^{\rm free}$ for a massive free boson is not known, we will numerically study the (u, τ)-dependence of $\gamma_{\rm tor}^{\rm WF}$ by working on the lattice.

However, before doing so, we describe two limits in which we can make statements about $\gamma_{\rm tor}$. First, we consider the so-called thin torus limit for which $L_y \to 0$, while L_A, L_x remain finite, i.e. $\tau \to i\infty$ and u is fixed. For generic boundary conditions, we have that the torus EE approaches twice the semi-infinite cylinder value [123, 124] discussed above, $\gamma_{\rm tor} \to 2\gamma_{\rm cyl}$. This holds in the absence of zero modes, which is the generic case. Our result Eq. (5.34) implies that $\gamma_{\rm tor} = \mathcal{O}(N^0)$ in that limit. However, this cannot hold at all values of τ. Indeed, for any fixed τ let us consider the "thin slice" limit $L_A \to 0$. There, $\gamma_{\rm tor}$ reduces to the universal contribution of a thin strip of width L_A in the infinite plane [123, 124], $\gamma_{\rm tor} = \kappa L_y/L_A$, where the universal constant $\kappa \geq 0$ can be computed in the infinite plane. κ is thus independent of the boundary conditions along x, y. Applying our mapping to free fields, this means that at leading order in N

$$\kappa^{\rm WF} = N\kappa^{\rm free} \tag{5.39}$$

where $\kappa^{\rm free} \simeq 0.0397$ for a free scalar [109]. By continuity, we thus expect that for general u and τ, $\gamma_{\rm tor}^{\rm WF}$ will scale linearly with N in the large-N limit. We now verify this statement via a direct calculation.

Lattice numerics

The lattice Hamiltonian for a free boson of mass m_1 can be taken to be

$$H = \frac{1}{2}\sum_{k_y}\sum_{i=0}^{L_x-1}\left(|\pi_{k_y}(i)|^2 + |\phi_{k_y}(i+1) - \phi_{k_y}(i)|^2 + \omega_{k_y}^2|\phi_{k_y}(i)|^2\right) \tag{5.40}$$

$$\omega_{k_y}^2 = 4\sin^2(k_y/2) + m_1^2 \tag{5.41}$$

where the theory is defined on a square lattice with unit spacing, $\pi_{k_y}(i)$ is the operator canonically conjugate to $\phi_{k_y}(i)$, and $|A|^2 = A^\dagger A$. The index i runs over the L_x lattice sites in the x-direction. Crystal momentum along the y-direction remains a good quantum number in the presence of the entanglement cut, and is quantized as follows

$$k_y = \frac{2\pi n_y}{L_y} + \frac{\varphi_y}{L_y}\,, \tag{5.42}$$

where the integer n_y runs from 0 to $L_y - 1$, and φ_y is the twist along the y-direction. We note that the Hamiltonian (5.40) corresponds to L_y decoupled 1d massive boson chains: $H = \sum_{k_y} H_{1\mathrm{d}}(k_y)$, each with an effective mass ω_{k_y}. This means that the EE is the sum over the corresponding 1d EEs: $S = \sum_{k_y} S_{1\mathrm{d}}(k_y)$. For each 1d chain, the EE for the interval of length $L_A \leq L_x$ is obtained from the correlation functions $X_{ij} = \langle\phi^\dagger(i)\phi(j)\rangle$ and $P_{ij} = \langle\pi^\dagger(i)\pi(j)\rangle$, where we have suppressed the k_y label. The prescription for the EE is then [109]

$$S_{1\mathrm{d}} = \sum_\ell \left[(\nu_\ell + \tfrac{1}{2})\log(\nu_\ell + \tfrac{1}{2}) - (\nu_\ell - \tfrac{1}{2})\log(\nu_\ell - \tfrac{1}{2})\right] \tag{5.43}$$

where ν_ℓ are eigenvalues of the matrix $\sqrt{X_A P_A}$, with the A meaning that X_{ij} and P_{ij} are restricted to region A. This method was previously used to study the EE of free fields on the torus [122–125].

To obtain the universal part of the entropy we first need to numerically determine the area

law coefficient C (5.37), which we find is $C \simeq 0.07745$. We can then isolate the universal part, $\gamma_{\rm tor}$, by subtracting the area law contribution. The result for a square torus, i.e. $\tau = i$, is shown in Fig. 5.3.3, where we compare the Wilson-Fisher fixed point with the Gaussian fixed point. Only $0 < u < 1/2$ is shown because the other half is redundant by virtue of the identity $\gamma_{\rm tor}(1-u) = \gamma_{\rm tor}(u)$, true for pure states. We set $\varphi_x = 0$ and $\varphi_y = \pi$ (since fully periodic boundary conditions yield a divergent $\gamma_{\rm tor}^{\rm Gauss}$), which leads to a purely imaginary mass $m_1 L_y \simeq i\,1.77078$ for the Wilson-Fisher theory, while m_1 is naturally zero at the Gaussian fixed point. The imaginary mass does not cause a problem since $k_y^2 + m_1^2 > 0$ in the presence of the twist, (5.42). From Fig. 5.3.3, we see that $\gamma_{\rm tor}^{\rm WF}$ scales linearly with N as was anticipated above. However, contrary to the case of the infinite plane, the EE of the Wilson-Fisher fixed point is reduced compared to the Gaussian fixed point, $\gamma_{\rm tor}^{\rm WF}(u) < \gamma_{\rm tor}^{\rm Gauss}(u)$ for all values of u. The difference between the EE of the two theories decreases in the thin slice limit $u \to 0$, where we have the divergence $\gamma_{\rm tor} = \kappa/u$, with the same constant κ for both theories, Eq. (5.39). This constant has been calculated in a different context [109], $\kappa = N\kappa^{\rm free} = N\,0.0397$, and fits our data very well. Another consistency check is that $\gamma_{\rm tor}(u)$ should be convex decreasing [124] for $0 < u < 1/2$, which is indeed the case in Fig. 5.3.3.

5.4 Conclusions

The large N limit of the Wilson-Fisher theory yields the simplest tractable strongly-interacting CFT in 2+1 dimensions. In this chapter, we have succeeded in computing the entanglement entropy of this theory using a method which can be applied to essentially any entanglement geometry. In particular, for any region in the infinite plane, the EE of the large-N Wilson-Fisher fixed point is the same as that of N free massless bosons. In contrast, when space is compactified into a cylinder or a torus, the results will differ in general as we have illustrated using cylindrical entangling regions. Our results naturally extend to other large-N vector theories, like the fermionic Gross-Neveu CFT (Appendix B.2).

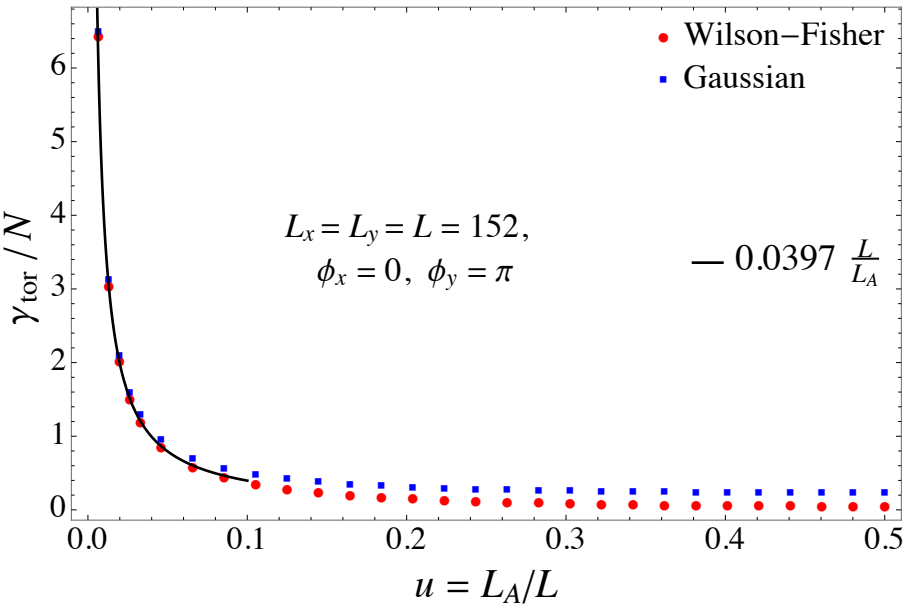

Figure 5.3.3: The universal EE $\gamma_{\rm tor}$ of a cylindrical region, $L_A \times L$, cut out of a square torus, $L \times L$. The red dots correspond to the interacting fixed point of the O(N) model at large N, while the blue squares to the Gaussian fixed point (N free relativistic scalars). We have normalized $\gamma_{\rm tor}$ by N. The data points were obtained numerically on a square lattice of linear size $L = 152$. The line shows the expected divergence in the small u limit, the same for both theories.

In the case of the EE of the semi-infinite cylinder, $\gamma_{\rm cyl}$, Ref. [93] has compared its value at the UV Gaussian fixed point and the IR Wilson-Fisher one using the ϵ expansion. For these two specific fixed points, it was found that $|\gamma_{\rm cyl}^{\rm UV}| > |\gamma_{\rm cyl}^{\rm IR}|$, suggestive of the potential of $\gamma_{\rm cyl}$ to "count" degrees of freedom. Our results at large N, however, show that the opposite can occur for certain RG flows. Namely, $|\gamma_{\rm cyl}^{\rm UV}| < |\gamma_{\rm cyl}^{\rm IR}|$ is possible. Indeed, let us consider the flow from the Wilson-Fisher critical point to the stable fixed point describing the phase where the O(N) symmetry is spontaneously broken [9]. In the UV, we see that $\gamma_{\rm cyl}^{\rm WF} \sim N^0$ does not grow with N, while at the IR fixed point $\gamma_{\rm cyl}^{\rm broken} \sim N$ due to the $(N-1)$ Goldstone bosons [126]. This holds for generic boundary conditions $\varphi_y \neq 0$.

It is also of interest to obtain the Rényi entropies of such an interacting CFT, notably for comparison with large-scale quantum Monte Carlo simulations which can usually only yield the second Rényi entropy [127, 128]. Unfortunately, this is a much more challenging problem, because the full x-dependence of the saddle-point $\langle i\lambda(x)\rangle_n$ in (5.12) is needed on

a n-sheeted Riemann surface. Numerical analysis will surely be required, supplemented by analytic results in the limit of large and small x.

Chapter 6

Critical behavior of an impurity at the boson superfluid-Mott insulator transition

6.1 Introduction

The quantum phase transition between a superfluid and a Mott insulator in two dimensions represents one of the best studied examples of quantum critical matter, both theoretically and experimentally. The critical properties of this transition are described by a strongly interacting relativistic quantum field theory in the O(2) Wilson-Fisher universality class [9, 129]. This phase transition can be realized experimentally using cold atoms trapped in optical lattices [12, 130, 131].

In this chapter, we study the superfluid-insulator transition in the presence of an impurity degree of freedom, motivated by recent numerical work by Huang *et al.* [132] of the lattice Bose-Hubbard model. Their study models the presence of an impurity in terms of a trapping potential, representing the attachment of charge to the impurity. With the bulk taken to be at the superfluid-insulator quantum critical point, they found a remarkable quantum transition

at the impurity, where the total boson number trapped by the impurity jumped by unity. Despite the jump in the boson number, the transition is second order because it is associated with divergence in the size of the screening cloud. They find the emergence of scale-invariant behavior for a critical value of the trapping potential, suggesting the emergence of a new universality class associated with the impurity degree of freedom.

Models of impurities coupled to an interacting bulk critical theory were considered in References [133, 134]. Furthermore, a model of impurities coupled to a bulk interacting critical theory was investigated in Refs. [135–137]. The latter model describes the effect of impurities coupled to quantum antiferromagnets close to their critical point. In that work, the impurities are represented by a localized spin degree of freedom which coupled to the bulk quantum field theory, and a stable interacting fixed point was found perturbatively in the $\epsilon = 3 - d$ expansion. This novel impurity-driven critical behavior led to new observables associated with the impurity degree of freedom.

Here we take a similar approach in studying the superfluid-insulator transition coupled to impurities. We will argue for the particular form of an impurity-bulk interaction to model the critical behavior, and study the resulting theory in the ϵ expansion. Working with a slightly generalized model, we will find an interacting fixed point, and calculate the new critical exponents associated with the theory. Unlike the case with the antiferromagnet, this impurity fixed point has a single relevant perturbation which does not break any symmetries: this relevant direction corresponds to the tuning of the magnitude of the trapping potential. We will also determine the universal dependence of the finite temperature compressibility on the impurity degree of freedom at the fixed point. The exponents and the compressibility can be related to those calculated numerically in Refs. [132, 138].

The chapter is arranged as follows. In Section 6.2 we discuss the microscopic model of Ref. [132], and argue for the form of the universal quantum field theory describing its universal properties. We set up the form of the ϵ expansion of a generalized form of the theory. Section 6.3 describes how the diagrammatic expansion of the model is constructed,

and gives the expansion to two-loop order. We give a summary of the renormalization group equations in Section 6.4, and give our predictions for the critical exponents of the model. In Section 6.5, we determine the universal contribution of the impurity to the finite temperature compressibility of the model, and we conclude in Section 6.6.

6.2 The model

6.2.1 Continuum field theory

We seek the critical theory describing the microscopic model studied numerically in Ref. [132]. This is given by

$$\mathcal{H}_1 = \sum_{\langle ij \rangle} b_i^\dagger b_j + \frac{U}{2} \sum_i n_i \left(n_i - 1 \right) - \mu \sum_i n_i + V n_0 \tag{6.1}$$

where $b_i^\dagger$ is a boson creation operator on site i, $\langle \cdots \rangle$ denotes nearest-neigbors, and $n_i \equiv b_i^\dagger b_i$. The model is studied at constant density with unit filling fraction, where a bulk critical point between a superfluid and insulating state is known to exist at the values $U_c = 16.7424(1)$ and $\mu_c = 6.21(2)$ [139, 140]. For $V = 0$, it is known that the bulk transition is described by the relativistically-invariant $O(2)$-symmetric Wilson-Fisher conformal field theory [129], given by the Hamiltonian

$$\mathcal{H}'_\phi = \int d^3x \left\{ \frac{\pi_{\alpha'}^2 + c^2 \left(\nabla \phi_{\alpha'} \right)^2 + s_c \, \phi_{\alpha'}^2}{2} + \frac{u_0}{4!} \left(\phi_{\alpha'}^2 \right)^2 \right\} \tag{6.2}$$

where the index runs from $\alpha' = 1, 2$. The coupling s_c has been fine-tuned to its critical value, and u_0 flows to a universal value in the infrared. The fields $\phi_{\alpha'}(x,t)$ and $\pi_{\alpha'}(x,t)$ represent the bulk order parameter and its canonical conjugate respectively, obeying the commutation relation

$$[\phi_{\alpha'}(x,t), \pi_{\beta'}(x',t)] = \delta_{\alpha'\beta'} \delta^d(x - x') \tag{6.3}$$

The velocity scale c depends on microscopic details of the system, and will henceforth be set to unity.

In Ref. [132], it was found that the addition of the impurity potential V leads to new critical behavior. As the potential is turned on, it is found that charge is either depleted or concentrated at the origin depending on the sign of V. The density profile is characterized by a half-integer charged core, and a half-integer charged halo located at a radius ξ_h from the origin. The sign of the halo charge flips across the critical point.

At a critical value of V, the halo size, ξ_h, diverges to infinity, indicating the onset of scale invariance. If the coupling V continues to increase, the charge of the halo changes sign and contracts back to the origin; so this is a transition between a system with total charge Q and $Q \pm 1$. The radius of the halo is observed to have the universal behavior

$$\xi_h \propto |V - V_c|^{-\nu_z} \tag{6.4}$$

with $\nu_z = 2.33(5)$ [132].

In seeking the critical theory, we need to couple the bulk Hamiltonian Eq. (6.2) to a field describing the impurity degree of freedom. This theory retains the $O(2)$ invariance. We claim that the correct impurity coupling is given by

$$\mathcal{H}_{\text{imp}} = -\gamma_0 \left[\phi_1(x=0)\hat{S}_x + \phi_2(x=0)\hat{S}_y\right] + h_z \hat{S}_z \tag{6.5}$$

where $\hat{S}_\alpha$ represents a spin-1/2 degree of freedom defined at $x = 0$; a spin $S = 1/2$ impurity model has also been proposed and studied independently by Chen *et al.* [138]. The impurity site density n_0, is related to the spin via $\hat{S}_z = n_0 - Q + 1/2$ for a transition between Q and $Q - 1$. We also note that a scalar-spin interaction of this form was studied in a different context by Zaránd and Demler [141]. Here, the two couplings γ_0 and h_z are both relevant in $d = 2$. The $O(2)$ symmetry of the impurity is generated by $\hat{S}_z$, and at $h_z = 0$, there is an exact two-fold degeneracy between the $\hat{S}_z = \pm 1/2$ states, which reproduces the two-fold

degeneracy of the microscopic theory at the critical impurity potential $V = V_c$ between the different charge sectors. We will argue below that the coupling γ_0 flows to a universal value which controls the critical behavior of the impurity degree of freedom.

Our analysis will also consider the case where the impurity $\hat{S}_\alpha$ has a generic spin S. This corresponds to possible multicritical points where $2S + 1$ states become degenerate at the impurity. In the Bose-Hubbard model, we would have to tune $2S$ couplings to achieve this. In the field theory, the $2S$ relevant couplings correspond to the operators $\hat{S}_z^p$, with $1 \leq p \leq 2S$. We will only consider the scaling dimension of the $p = 1$ operator here.

6.2.2 Expansion in ϵ

We will work with a generalization of the above theory, given by

$$\mathcal{H} = \mathcal{H}_\phi - \gamma_0 \phi_{\alpha'}(x = 0)\hat{S}_{\alpha'} \tag{6.6}$$

Here, the first term is the Hamiltonian for the $O(N)$-symmetric scalar field theory in d spatial dimensions,

$$\mathcal{H}_\phi = \int d^d x \left\{ \frac{\pi_\alpha^2 + (\nabla\phi_\alpha)^2 + s_c\ \phi_\alpha^2}{2} + \frac{u_0}{4!}\left(\phi_\alpha^2\right)^2 \right\} \tag{6.7}$$

We use the notation where unprimed indices run from $\alpha = 1, 2, ..., N$, while primed indices only take the values $\alpha' = 1, 2$. Summation is implied over repeated indices, and it is understood that $\phi_\alpha^2 = \phi_\alpha \phi_\alpha$. The operators $\hat{S}_\alpha(t)$ satisfy the $SU(2)$ algebra,

$$\begin{aligned} [\hat{S}_\alpha, \hat{S}_\beta] &= i\epsilon_{\alpha\beta\gamma}\hat{S}_\gamma \\ \mathrm{Tr}\left(\hat{S}_\alpha \hat{S}_\beta\right) &= \frac{1}{3}(2S+1)S(S+1)\delta_{\alpha\beta} \end{aligned} \tag{6.8}$$

where the spin operator only takes the values $\alpha = 1, 2, 3$. We continue to label the $1 - 2$ directions with primed indices, and refer to the third direction as the $z-$direction. We note that the total Hamiltonian in Eq. (6.6) has $O(2) \times O(N-2)$ symmetry. Here we will

allow arbitrary values of spin, S, and give results for $S = 1/2$ at the end of the calculation. Although the operator $\hat{S}_z$ does not appear in this Hamiltonian, it has nontrivial correlations in the interacting theory due to the commutation relations. Its scaling dimensions will then determine the critical exponent associated with perturbing this theory by a term $h_z \hat{S}_z$.

We will study this system in the $\epsilon = 3 - d$ expansion. We will use the minimal subtraction renormalization scheme of Ref. [24], where $s_c = 0$ and the bare fields and interaction strength are replaced by

$$\begin{aligned} \phi_\alpha &= \sqrt{Z}\phi_{R\alpha} \\ u_0 &= \frac{\mu^\epsilon Z_4}{S_{d+1} Z^2} g \end{aligned} \tag{6.9}$$

Here, μ is an arbitrary energy scale, g is a dimensionless coupling constant, and

$$S_d = \frac{2}{\Gamma(d/2)(4\pi)^{d/2}} \tag{6.10}$$

is a convenient phase factor. To leading order in g, the renormalization constants are given by

$$\begin{aligned} Z &= 1 - \frac{(N+2)}{144\epsilon} g^2 \\ Z_4 &= 1 + \frac{(N+8)}{6\epsilon} g + \left(\frac{(N+8)^2}{36\epsilon^2} - \frac{(5N+22)}{36\epsilon} \right) g^2 \end{aligned} \tag{6.11}$$

The beta function follows immediately from Eqns. (6.9) and (6.11)

$$\beta_g \equiv \mu \frac{dg}{d\mu}\bigg|_{u_0} = -\epsilon g + \frac{(N+8)}{6} g^2 - \frac{(3N+14)}{12} g^3 \tag{6.12}$$

from which we determine the bulk fixed point by finding the value of g where the beta function vanishes:

$$g^* = \frac{6\epsilon}{(N+8)} \left[1 + \frac{3(3N+14)}{(N+8)^2} \epsilon \right] \tag{6.13}$$

The addition of a localized bulk-impurity interaction cannot significantly alter the bulk correlation functions, so the above results also hold for the full theory $\mathcal{H}$. However, we must now consider the renormalization of the impurity operators and their interaction with the bulk order parameter. We define the constants

$$\begin{aligned} \hat{S}_{\alpha'} &= \sqrt{Z'}\hat{S}_{R\alpha'} \\ \hat{S}_z &= \sqrt{Z_z}\,\hat{S}_{Rz} \\ \gamma_0 &= \frac{\mu^{\epsilon/2} Z_\gamma}{\sqrt{ZZ'\tilde{S}_{d+1}}}\gamma \end{aligned} \tag{6.14}$$

Here, γ is another dimensionless renormalized interaction, and we have introduced another convenient phase factor

$$\tilde{S}_d = \frac{\Gamma(d/2-1)}{4\pi^{d/2}} \tag{6.15}$$

In terms of the above constants, we find that the impurity beta function is given by

$$\beta_\gamma \equiv \mu \frac{d\gamma}{d\mu}\bigg|_{u_0,\gamma_0} = -\frac{\frac{\epsilon}{2}\gamma + \gamma\beta_g \frac{d}{dg}\log\left(Z_\gamma/\sqrt{ZZ'}\right)}{1+\gamma\frac{d}{d\gamma}\log\left(Z_\gamma/\sqrt{ZZ'}\right)} \tag{6.16}$$

One major result of this paper is the determination of the beta function to two-loop order, from which we find an infrared fixed point at a critical value of γ^* which is perturbative in ϵ. The major observables associated with this fixed point are the universal decay of the spin operators. We introduce the anomalous dimensions,

$$\begin{aligned} \left\langle \hat{S}_{\alpha'}(t)\hat{S}_{\alpha'}(0)\right\rangle &\sim \frac{1}{t^{\eta'}} \\ \left\langle \hat{S}_z(t)\hat{S}_z(0)\right\rangle &\sim \frac{1}{t^{\eta_z}} \end{aligned} \tag{6.17}$$

where algebraic decay is forced by scale invariance, and the exponents are given by

$$\begin{aligned} \eta' &= \beta_\gamma \frac{d}{d\gamma} \log Z' + \beta_g \frac{d}{dg} \log Z' \\ \eta_z &= \beta_\gamma \frac{d}{d\gamma} \log Z_z + \beta_g \frac{d}{dg} \log Z_z \end{aligned} \tag{6.18}$$

These anomalous dimensions, which are twice the scaling dimension of the spin operators, are new data associated with the universality class of this phase transition.

Once the anomalous dimension of $\hat{S}_z$ is determined, we can also determine the critical exponents associated with perturbing the critical theory. The leading relevant perturbations to Eq. (6.6) are given by

$$\begin{aligned} \Delta\mathcal{H}' &= h' \hat{S}_{\alpha'} \\ \Delta\mathcal{H}_z &= h_z \hat{S}_z \end{aligned} \tag{6.19}$$

for any of the three $\hat{S}_\alpha$. This perturbation will introduce a large timescale ξ characterizing an exponential decay of the spin correlation functions, and by scaling arguments, it is straightforward to show that

$$\begin{aligned} \xi' &= |h'|^{-\nu'} \\ \xi_z &= |h'|^{-\nu_z} \end{aligned} \tag{6.20}$$

where

$$\begin{aligned} \nu' &= \frac{1}{1 - \eta'/2} \\ \nu_z &= \frac{1}{1 - \eta_z/2} \end{aligned} \tag{6.21}$$

Here, exponent ν_z corresponds to the critical exponent defined in the microscopic model above.

6.3 Renormalization

We determine the renormalization parameters above using bare perturbation theory. In particular, we will work in imaginary time τ, and compute the following correlation functions to two-loop order:

$$\begin{aligned} \mathcal{G}'(\tau)\delta_{\alpha'\beta'} &= \left\langle \hat{S}_{\alpha'}(\tau)\hat{S}_{\beta'}(0)\right\rangle \\ \mathcal{G}^z(\tau) &= \left\langle \hat{S}_z(\tau)\hat{S}_z(0)\right\rangle \\ \mathcal{V}(x,\tau)\delta_{\alpha'\beta'} &= \left\langle \phi_{\alpha'}(x,\tau)\hat{S}_{\beta'}(0)\right\rangle \end{aligned} \tag{6.22}$$

All correlation functions are understood to be imaginary time-ordered, we take $\tau > 0$, and a trace is taken over the spin indices. This calculation will result in divergences in the form of poles in ϵ, but we choose the constants Z', Z_3, and Z_4 such that these poles cancel when the correlation functions are expressed in terms of renormalized operators and couplings.

Due to the nontrivial commutator in Eq. (6.8), the perturbative expansion for these correlation functions does not obey Wick's theorem, nor do disconnected diagrams cancel. We must expand the numerator and denominator of the correlation functions separately as a series in u_0 and γ_0, and by carefully keeping track of the time-ordering of the spin operators we can obtain the desired correlation functions. This procedure can be represented by a form of diagrammatic perturbation theory developed in Ref. [136].

We first write the correlation function of the interacting theory in terms of free correlators, where the free part of our theory is the quadratic part of $\mathcal{H}_\phi$.

$$\langle \mathcal{O}\rangle = \frac{\left\langle \mathcal{O}e^{-\beta\mathcal{H}_I}\right\rangle_0}{\left\langle e^{-\beta\mathcal{H}_I}\right\rangle_0} \tag{6.23}$$

We introduce a finite inverse temperature β as an intermediate step. The Hamiltonian which

appears on the right-hand side is the interaction Hamiltonian,

$$\mathcal{H}_I = \frac{u_0}{4!}\int d^d x \left(\phi_{I\alpha}(x)^2\right)^2 - \gamma_0 \phi_{I\alpha'}(x=0)\hat{S}_{\alpha'} \tag{6.24}$$

The operators $\phi_{I\alpha}$ are the familiar interaction representation of our original bosonic fields (the interaction and Schrödinger representations of $\hat{S}_\alpha$ are equivalent in our model). Then we expand the exponentials in the numerator and denominator, and the expectation values break into simple products of bosonic correlators and spin correlators. The bosonic operators obey Wick's theorem, so we obtain integrals over products of the free finite-temperature bosonic Green's function:

$$D_T(x,\tau) = \langle \phi_\alpha(x,\tau)\phi_\beta(0,0)\rangle_0 \tag{6.25}$$

However, the time-ordering over spin expectation values will result in a corresponding time-ordering over dummy integration variables.

We represent the imaginary time-ordered expectation value of an arbitrary operator $\langle A\rangle_0$ with the following diagrammatic rules:

- Every diagram contains a single directed loop along which imaginary time runs periodically from 0 to β, represented by a full line.
- External factors of $\hat{S}_\alpha(\tau)$ contained in A are represented by open circles placed on the directed loop at the appropriate external value of τ.
- External factors of $\phi_\alpha(\tau, x)$ contained in A are represented by open boxes which are placed outside of the directed loop.
- Factors of the interaction γ_0 are represented by closed circles placed on the directed loop, and a bosonic propagator always emerges from this vertex.
- Factors of the interaction u_0 are represented by a filled square, which connects to four bosonic propagators.

- Internal bosonic propagators connecting vertices placed at (x_i, τ_i) and (x_j, τ_j) give a factor of $D_T(x_i - x_j, \tau_i - \tau_j)$, and we integrate over all internal x_i and τ_i. However, the ordering of all the τ_i's appearing on the directed loop must be kept in determining the integration region.

- We trace over the spins along the directed line. If there are no spin operators inserted, this is interpreted at $\mathrm{Tr}\,\mathbb{I} = (2S+1)$.

We obtain the correction to $\langle A \rangle$ at a given order of u_0 and γ_0 by writing down all possible diagrams which obey the above rules and have the correct number of interaction vertices, and then sum them. We will demonstrate how to apply these rules in detail for the relatively simple one-loop case, before giving the full two-loop results.

6.3.1 Spin-spin correlation function

We show the lowest-order diagrams contributing to the spin-spin correlation functions in Fig. 6.3.1.(b). Below we will evaluate spin traces using the identities enumerated in Appendix C.1. We first write out the diagrams in the denominator, obtaining from the above rules

$$\mathcal{Z} = (2S+1) + \mathrm{Tr}\left(\hat{S}_{\alpha'}\hat{S}_{\alpha'}\right)\gamma_0^2 \int_0^\beta d\tau_1 \int_{\tau_1}^\beta d\tau_2 D_T(\tau_1 - \tau_2) + \cdots \tag{6.26}$$

We then rewrite this expression for reasons which will become clear shortly:

$$\begin{aligned}\mathcal{Z} \;=\; & (2S+1) + \;(2S+1)\frac{2S(S+1)}{3}\gamma_0^2\Bigg[\int_0^\tau d\tau_1 \int_{\tau_1}^\tau d\tau_2 + \int_\tau^\beta d\tau_1 \int_{\tau_1}^\beta d\tau_2 \\ & + \int_0^\tau d\tau_1 \int_\tau^\beta d\tau_2\Bigg] D_T(\tau_1 - \tau_2) + \cdots \end{aligned} \tag{6.27}$$

We now consider the numerator of the spin-spin correlator in Eq. (6.22), given by the

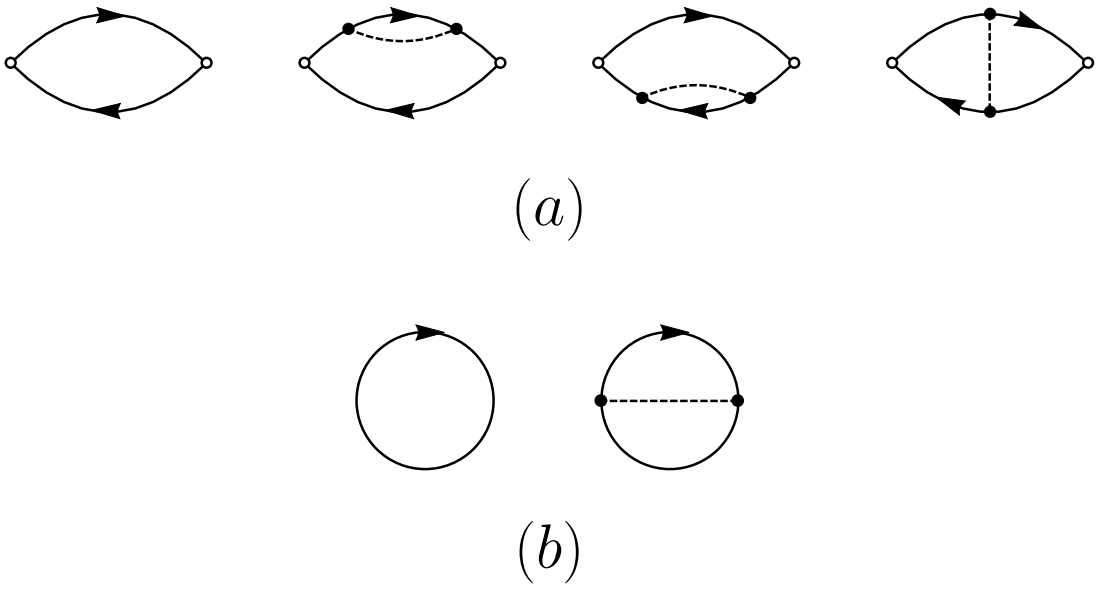

Figure 6.3.1: The diagrammatic expansion for the spin-spin correlation function at one-loop, using the Feynman rules specified in the Section 6.3. The diagrams contributing to the numerator and denominator of the correlation function are pictured in (a) and (b) respectively. As described in the main text, the integrals contributing to the numerator and denominator can be combined, so that we only need to keep track of differing spin traces.

diagrams in Fig. 6.3.1.(a).

$$\begin{aligned}\mathcal{Z}\mathcal{G}(\tau) &= \mathrm{Tr}\left(\hat{S}_\alpha \hat{S}_\beta\right) + \mathrm{Tr}\left(\hat{S}_\alpha \hat{S}_{\sigma'} \hat{S}_{\sigma'} \hat{S}_\beta\right) \gamma_0^2 \int_0^\tau d\tau_1 \int_{\tau_1}^\tau d\tau_2 D_T(\tau_1 - \tau_2) \\ &+ \mathrm{Tr}\left(\hat{S}_\alpha \hat{S}_\beta \hat{S}_{\sigma'} \hat{S}_{\sigma'}\right) \gamma_0^2 \int_\tau^\beta d\tau_1 \int_{\tau_1}^\beta d\tau_2 D_T(\tau_1 - \tau_2) \\ &+ \mathrm{Tr}\left(\hat{S}_\alpha \hat{S}_{\sigma'} \hat{S}_\beta \hat{S}_{\sigma'}\right) \gamma_0^2 \int_0^\tau d\tau_1 \int_\tau^\beta d\tau_2 D_T(\tau_1 - \tau_2) + \cdots \end{aligned} \tag{6.28}$$

Here, we take the external indices to either be α', β' to define $\mathcal{G}'(\tau)$, or 3 to denote $\mathcal{G}_3(\tau)$. We notice that the three integrals contributing to the numerator are identical to the three we used to split up the denominator. Thus, to calculate the full correlation function, we only need to compute these three integrals and keep track of the difference in spin traces which appear in the numerator and denominator. This simplification is minor for the one-loop case, but it simplifies the two-loop calculation enormously.

We now write the one-loop correlation function in terms of the spin traces given in Appendix C.1. Here, the traces on the right-hand side correspond to either the $\mathcal{S}_i'$ or $\mathcal{S}_i^z$ in the appendix depending on whether the left-hand side represents the correlator $\mathcal{G}'(\tau)$ or $\mathcal{G}^z(\tau)$ respectively.

$$\begin{aligned}\mathcal{G}(\tau) &= \frac{S(S+1)}{3}\Bigg\{1+\left[\mathcal{S}_1-\frac{2S(S+1)}{3}\right]\gamma_0^2\int_0^\tau d\tau_1\int_{\tau_1}^\tau d\tau_2 D_T(\tau_1-\tau_2)\\ &+\left[\mathcal{S}_1-\frac{2S(S+1)}{3}\right]\gamma_0^2\int_\tau^\beta d\tau_1\int_{\tau_1}^\beta d\tau_2 D_T(\tau_1-\tau_2)\\ &+\left[\mathcal{S}_2-\frac{2S(S+1)}{3}\right]\gamma_0^2\int_0^\tau d\tau_1\int_\tau^\beta d\tau_2 D_T(\tau_1-\tau_2)+\cdots\Bigg\}\end{aligned} \tag{6.29}$$

We now consider the evaluation of these integrals. For the purpose of renormalizing our theory, we can work in the $T=0$ limit, where the bosonic propagator takes the form

$$D_0(\tau)=\int\frac{d^dk}{(2\pi)^d}\frac{d\omega}{2\pi}\frac{e^{-i\omega\tau}}{k^2+\omega^2}=\frac{\tilde{S}_{d+1}}{|\tau|^{d-1}} \tag{6.30}$$

Finally, the integrations over imaginary time must be extended with care, since imaginary time is really compact: $\beta\sim 0$. Therefore, we need to extend the integration domain as

$$\int_0^\beta \longrightarrow \int_0^\infty+\int_{-\infty}^0 \tag{6.31}$$

so that the integration still forms a loop in imaginary time. So the three integrals appearing in Eq. (6.29) respectively become

$$\int_0^\tau d\tau_1\int_{\tau_1}^\tau d\tau_2 D_0(\tau_1-\tau_2)=-\frac{\tilde{S}_{d+1}\tau^\epsilon}{\epsilon(1-\epsilon)} \tag{6.32}$$

$$\left[\int_\tau^\infty d\tau_1\int_{\tau_1}^\infty d\tau_2+\int_\tau^\infty d\tau_1\int_{-\infty}^0 d\tau_2+\int_{-\infty}^0 d\tau_1\int_{\tau_1}^0 d\tau_2\right]D_0(\tau_1-\tau_2)=-\frac{\tilde{S}_{d+1}\tau^\epsilon}{\epsilon(1-\epsilon)} \tag{6.33}$$

$$\left[\int_0^\tau d\tau_1 \int_\tau^\infty d\tau_2 + \int_0^\tau d\tau_1 \int_{-\infty}^0 d\tau_2\right] D_0(\tau_1 - \tau_2) = \frac{2\tilde{S}_{d+1}\tau^\epsilon}{\epsilon(1-\epsilon)} \tag{6.34}$$

where we have used the dimensional regularization "identity" $\int_0^\infty d\tau \tau^\alpha = 0$.

Collecting all of the above results, we find that the leading-order spin-spin correlation functions are given by

$$\mathcal{G}'(\tau) = \frac{S(S+1)}{3}\left[1 - \frac{\gamma_0^2 \tilde{S}_{d+1}\tau^\epsilon}{\epsilon(1-\epsilon)} + \cdots\right] \tag{6.35}$$

$$\mathcal{G}^z(\tau) = \frac{S(S+1)}{3}\left[1 - \frac{2\gamma_0^2 \tilde{S}_{d+1}\tau^\epsilon}{\epsilon(1-\epsilon)} + \cdots\right] \tag{6.36}$$

The procedure at two-loop is done using the same procedure; we fill in the intermediate steps in Appendix C.2. Our final result is

$$\begin{aligned}\left\langle \hat{S}_{\alpha'}(\tau)\hat{S}_{\beta'}(0)\right\rangle &= \delta_{\alpha'\beta'}\frac{S(S+1)}{3}\left[1 - \frac{\gamma_0^2\tilde{S}_{d+1}\tau^\epsilon}{\epsilon(1-\epsilon)}\right. \\ &\quad \left. + \left(\gamma_0^2\tilde{S}_{d+1}\tau^\epsilon\right)^2\left(\frac{1}{\epsilon^2} + \frac{5}{2\epsilon} + \cdots\right)\right]\end{aligned} \tag{6.37}$$

$$\begin{aligned}\left\langle \hat{S}_z(\tau)\hat{S}_z(0)\right\rangle &= \frac{S(S+1)}{3}\left[1 - \frac{2\gamma_0^2\tilde{S}_{d+1}\tau^\epsilon}{\epsilon(1-\epsilon)}\right. \\ &\quad \left. + \left(\gamma_0^2\tilde{S}_{d+1}\tau^\epsilon\right)^2\left(\frac{3}{\epsilon^2} + \frac{6}{\epsilon} + \cdots\right)\right]\end{aligned} \tag{6.38}$$

where we only keep the divergent part of the γ_0^4 term.

6.3.2 Vertex renormalization

We now consider the renormalization of the vertex function $\mathcal{V}(x,\tau)$, defined in Eq. (6.22). In writing down all possible diagrams up to two-loop order, it becomes apparent that every

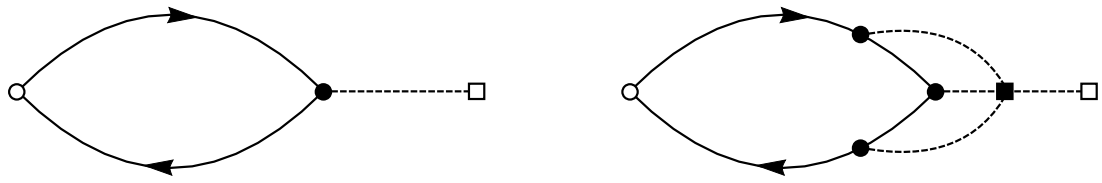

Figure 6.3.2: The diagrams which renormalize the impurity interaction γ.

diagram which does not depend on u_0 is identical to a diagram appearing in Fig. 6.3.1, but with the insertion of an external boson. Therefore, the only loop diagrams which contribute to renormalizing the bare interaction γ_0 are those which involve the bulk interaction; these are shown in Fig. 6.3.2. This implies the *exact* relation

$$Z_\gamma = 1 \quad \text{at} \quad g = 0 \tag{6.39}$$

We now evaluate the diagrams in Fig. 6.3.2 using the Feynman rules specified above. There is only one loop diagram which corrects the tree-level interaction, but there are three distinct ways to evaluate the spin traces. We find

$$\begin{aligned} \mathcal{V}(x,\tau) &= \frac{S(S+1)}{3}\gamma_0 \int \frac{d^d k}{(2\pi)^d}\frac{e^{ikx}}{k^2} \\ &\quad - \frac{S(S+1)}{3}\frac{\gamma_0^3 u_0}{18}\int \frac{d^d k}{(2\pi)^d}\frac{e^{ikx}}{k^2}\int \frac{d^d k_1}{(2\pi)^d}\int \frac{d^d k_2}{(2\pi)^d}\frac{2\mathcal{S}_1' + \mathcal{S}_2'}{k_1^2 k_2^2 (k+k_1+k_2)^2} \end{aligned} \tag{6.40}$$

where the spin traces $\mathcal{S}_i'$ are specified in Appendix C.1. Evaluating the divergent part of the integral,

$$\begin{aligned} \mathcal{V}(x,\tau) &= \frac{S(S+1)}{3}\int \frac{d^d k}{(2\pi)^d}\frac{e^{ikx}}{k^2}\Bigg[\gamma_0 \\ &\quad - \gamma_0^3 u_0 \left(S(S+1) - \frac{1}{3}\right)\left(k^2\right)^{-\epsilon}\tilde{S}_{d+1}^2\left(\frac{2\pi^2}{15\epsilon} + \cdots\right)\Bigg] \end{aligned} \tag{6.41}$$

6.4 Renormalization group summary

The RG equations can be obtained directly from the Eqns. (6.37), (6.38), (6.41), along with the definitions of the renormalization constants in Section 6.2. After some algebra, we obtain

$$\begin{aligned} Z' &= 1 - \frac{\gamma^2}{\epsilon} + \frac{1}{2\epsilon}\gamma^4 \\ Z_z &= 1 - \frac{2\gamma^2}{\epsilon} + \frac{1}{\epsilon^2}\gamma^4 \\ Z_\gamma &= 1 + \frac{2\pi^2\left[S(S+1) - \frac{1}{3}\right]}{15\epsilon} g\gamma^2 \end{aligned} \tag{6.42}$$

The beta function now follows from Eq. (6.16):

$$\beta_\gamma = -\frac{\epsilon}{2}\gamma + \frac{1}{2}\gamma^3 - \frac{1}{2}\gamma^5 + \frac{(N+2)}{144} g^2\gamma + \frac{4\pi^2}{15}\left[S(S+1) - \frac{1}{3}\right] g\gamma^3 \tag{6.43}$$

Tuning the bulk interactions to their fixed point, $g = g^*$, we find a fixed point for the impurity interactions which is also perturbative in ϵ. To leading order,

$$\gamma^{*2} = \epsilon + \left[1 - \frac{N+2}{2(N+8)^2} - \frac{16\pi^2}{5(N+8)}\left(S(S+1) - \frac{1}{3}\right)\right]\epsilon^2 \tag{6.44}$$

Since our model is symmetric under $\gamma \to -\gamma$, all physical quantities only depend on γ^2. The initial flow depends on the sign of the bare value of γ_0, after which the theory will flow to either γ^* or $-\gamma^*$.

The anomalous dimensions of the spin operators follow from Eq. (6.18):

$$\eta' = \gamma^2 - \gamma^4 \tag{6.45}$$

$$\eta_z = 2\gamma^2 \tag{6.46}$$

where the $\mathcal{O}(\gamma^4)$ contribution to η_z vanishes. Evaluating these at $\gamma = \gamma^*$:

$$\eta' = \epsilon - \left(\frac{N+2}{2(N+8)^2} + \frac{16\pi^2}{5(N+8)} \left[S(S+1) - \frac{1}{3} \right] \right) \epsilon^2 \tag{6.47}$$

$$\eta_z = 2\epsilon + \left(2 - \frac{N+2}{(N+8)^2} - \frac{32\pi^2}{5(N+8)} \left[S(S+1) - \frac{1}{3} \right] \right) \epsilon^2 \tag{6.48}$$

As an aside, we mention the model with a Gaussian bulk, $g = 0$. This theory is infrared unstable to interactions, but the simple relation $Z_\gamma = 1$ allows us to derive an exact result for the anomalous dimension of the spin operators. Since the beta function for γ only depends on Z' in this theory, and $\beta_\gamma = 0$ at the interacting fixed point, Eqns. (6.16)-(6.18) imply

$$\eta' = \epsilon \quad \text{at} \quad g = 0 \tag{6.49}$$

to all orders in ϵ. In contrast, η_z will generically receive corrections at every order in ϵ at the Gaussian fixed point.

From Eqn. (6.21), we find the critical exponents

$$\nu' = 1 + \frac{\epsilon}{2} + \left(\frac{1}{4} - \frac{N+2}{4(N+8)^2} - \frac{8\pi^2}{5(N+8)} \left[S(S+1) - \frac{1}{3} \right] \right) \epsilon^2 \tag{6.50}$$

$$\nu_z = 1 + \epsilon + \left(2 - \frac{N+2}{2(N+8)^2} - \frac{16\pi^2}{5(N+8)} \left[S(S+1) - \frac{1}{3} \right] \right) \epsilon^2 \tag{6.51}$$

We now compare these to numerical results. For $N = 2$ and $S = 1/2$, we predict the critical exponents

$$\begin{aligned} \nu' &\approx 1.08 \\ \nu_z &\approx 2.66 \end{aligned} \tag{6.52}$$

In Refs [132, 138], both the microscopic model of Eqn. (6.1) and the field theory model of Eqn. (6.5) were studied in numerical simulations. These authors calculated the above critical exponents to be

$$\begin{aligned} \nu' &\approx 1.13(2) \\ \nu_z &\approx 2.33(5) \end{aligned} \tag{6.53}$$

The numerics show impressive agreement with the ϵ expansion.

6.5 Compressibility

In this section, we consider the finite-temperature response of the critical theory to an external probe coupled to the conserved $O(2)$ charge associated with particle number in the superfluid. Physically, this corresponds to the compressibility of the superfluid. We compute this by altering our Lagrangian,

$$\frac{1}{2}\int d^dx \left[(\partial_\tau\phi_1)^2 + (\partial_\tau\phi_2)^2\right] \longrightarrow \frac{1}{2}\int d^dx \left[(\partial_\tau\phi_1 + iH\phi_2)^2 + (\partial_\tau\phi_2 - iH\phi_1)^2\right] - H\hat{S}_z \tag{6.54}$$

and then taking variational derivatives of the free energy

$$\chi = \left.\frac{\delta^2 (T\log Z)}{\delta H^2}\right|_{H=0} \tag{6.55}$$

Here, we will continue working with our generalized theory, Eq. (6.6), with $O(2)\times O(N-2)$ symmetry, where the probe field H couples to the $O(2)$ charge. The contribution of the bulk degrees of freedom to this quantity were computed in Ref. [142], so here we focus only on terms which depend on γ, and we denote this part of the compressibility by $\chi_{\rm imp}$. Because this is a correlation function of a conserved current, its scaling dimension cannot renormalize,

so at finite temperature it must take the form

$$\chi_{\rm imp} = \frac{\mathcal{C}_1}{T} \tag{6.56}$$

where $\mathcal{C}_1$ is a *universal* number. We can also interpret $\mathcal{C}_1 = S_{\rm eff}(S_{\rm eff}+1)/3$ as the "effective spin" in the presence of interactions with the bulk, since for $\gamma = 0$,

$$\chi_{\rm imp}\Big|_{\gamma=0} = \frac{S(S+1)}{3T} \tag{6.57}$$

In our calculations at $T = 0$, we found that bulk interactions did not contribute to the impurity critical exponents until two-loop order. However, the structure of the ϵ-expansion for the bulk theory is rather different at finite temperature. In the critical regime, physical quantities become an expansion in $\sqrt{\epsilon}$ (with possible extra factors of $\ln \epsilon$) [142]. This dependence enters through the finite-temperature bosonic propagator, which is now given by

$$D_T(x,\tau) = T\sum_{i\omega_n}\int \frac{d^dk}{(2\pi)^d}\frac{e^{ikx}e^{-i\omega_n\tau}}{\omega_n^2+k^2+m^2} \tag{6.58}$$

with

$$m^2 = \left(\frac{N+2}{N+8}\right)\frac{2\pi^2 T}{3}\epsilon \tag{6.59}$$

We will see that this leads to a $\sqrt{\epsilon}$-expansion for $\chi_{\rm imp}$ as well.

Performing the functional derivative in Eq. (6.55), the compressibility is given by

$$\begin{aligned}\chi_{\rm imp} &= \frac{1}{\beta}\int_0^\beta d\tau\int_0^\beta d\tau'\left\langle \hat{S}_z(\tau)\hat{S}_z(\tau')\right\rangle + \frac{1}{\beta}\int_0^\beta d\tau\int d^dx\ \left\langle \phi_{\alpha'}^2(\tau,x)\right\rangle \\ &\quad - \frac{1}{\beta}\int_0^\beta d\tau\int_0^\beta d\tau'\int d^dx\int d^dx'\left\langle \left[\phi_2\partial_\tau\phi_1 - \phi_1\partial_\tau\phi_2\right](\tau,x)\left[\phi_2\partial_{\tau'}\phi_1 - \phi_1\partial_{\tau'}\phi_2\right](\tau',x')\right\rangle \\ &\quad - \frac{2i}{\beta}\int_0^\beta d\tau\int_0^\beta d\tau'\int d^dx\left\langle \hat{S}_z(\tau)\left[\phi_2\partial_{\tau'}\phi_1 - \phi_1\partial_{\tau'}\phi_2\right](\tau',x)\right\rangle\end{aligned} \tag{6.60}$$

These correlation functions can be computed using the same diagrammatic technique used

in Section 6.3, we simply do not take the zero temperature limit. A straight-forward computation leads to the expression

$$\chi_{\rm imp} = \frac{S(S+1)}{3T}\left[1+\frac{\gamma_0^2}{2T}\int\frac{d^dk}{(2\pi)^d}\frac{\mathrm{csch}^2\left(\beta\sqrt{k^2+m^2}/2\right)}{k^2+m^2}\right] \tag{6.61}$$

Here we see why keeping the temperature-dependent mass in the bosonic propagator was crucial: for $m \to 0$ this expression in infrared singular, and an evaluation at finite m gives (at leading order)

$$\chi_{\rm imp} = \frac{S(S+1)}{3T}\left[1+\gamma^2\frac{\pi}{\beta m}\right] \tag{6.62}$$

which lowers the order of the leading correction to

$$\chi_{\rm imp} = \frac{S(S+1)}{3T}\left[1+\left(\frac{3(N+8)}{2(N+2)}\right)^{1/2}\sqrt{\epsilon}\right] \tag{6.63}$$

As has been seen in previous work on the finite temperature ϵ-expansion, the leading correction is not particularly small, so this may not give a good numerical estimate. For $S = 1/2$ and $N = 2$, we find

$$\mathcal{C}_1 \approx .734 \tag{6.64}$$

In Reference [138], the constant $\mathcal{C}_1$ is computed numerically in a finite volume geometry, with a result close to the free value. Due to finite size effects, their result cannot be directly compared to ours.

6.6 Conclusions

Huang *et al.* [132] recently found a novel impurity quantum critical point in their study of the Bose-Hubbard model on the square lattice. They held the bulk square lattice at the superfluid-insulator quantum critical point, and then varied the strength of the trapping potential at a single site. They found a quantum phase transition, with a diverging length

scale, at a critical value of the trapping potential where the impurity site occupation number jumped by unity.

In an earlier study of quantum antiferromagnets with SU(2) spin rotation symmetry, Ref. [135] examined impurities in dimerized, two-dimensional antiferromagnets at the bulk critical point point between a spin-gap state and Néel order described by the O(3) Wilson-Fisher conformal field theory. They found that impurities were universally characterized by a single spin quantum number, S, which specified a renormalization group fixed point with *no* relevant directions in the impurity field theory.

In this chapter, we proposed that impurity criticality of the Bose-Hubbard model [132] is described by the $S = 1/2$ impurity fixed point found in Ref. [135], after the O(3) symmetry is reduced to O(2) in both the bulk and the impurity. We showed that with only O(2) symmetry, the impurity fixed point does allow for a *single* relevant perturbation in the impurity field theory: this relevant perturbation is associated with a longitudinal field acting on the $S = 1/2$ spin on the impurity site. We note that a model of $S = 1/2$ impurity has also been recently studied by Chen *et al.* [138]. With the presence of this relevant impurity perturbation, we can understand the need for a critical trapping potential in the numerical study of Huang *et al.* [132].

We computed critical exponents and universal amplitudes associated with the O(2)-symmetric impurity fixed point in an expansion in $\epsilon = 3 - d$, where d is the bulk spatial dimensionality. Associated with two different relevant perturbations, we estimated from a computation to order ϵ^2 that the impurity length scale diverged with the exponents $\nu_z \approx 2.66$ and $\nu' \approx 1.08$; this compares well with the numerical results [132, 138] $\nu_z \approx 2.33$ and $\nu' \approx 1.13$. Additional tests of the ϵ-expansion results will be possible in further numerical studies.

Finally, we note that this novel impurity quantum criticality should be accessible in cold atom experiments, and we hope it will be studied in the near future.

Appendix A

Appendix to Chapters 2-4

A.1 Infinite volume computations

Here we recall some properties of the Wilson-Fisher fixed point in an infinite volume. We will need the resulting expressions to renormalize the theory in a finite volume, and we relate the couplings to universal observables of the infinite-volume theory. The computations are standard [24], so we will be brief. Here we express the theory as a Euclidean action,

$$\mathcal{S} = \int d\tau d^d x \left[\frac{1}{2} \left(\partial_\tau \phi_\alpha \right)^2 + \frac{1}{2} \left(\nabla \phi_\alpha \right)^2 + \frac{s_0}{2} \phi_\alpha^2 + \frac{u}{4!} \phi_\alpha^4 + \Lambda \right] \tag{A.1}$$

where $d = 3 - \epsilon$, but now we integrate over infinite volume. At one-loop, we need to renormalize the couplings s, u, and the energy density Λ (there is no field renormalization until two-loop). To this end, we introduce the renormalized couplings

$$\begin{aligned} s_0 &= s_c + Z_2 s \\ u &= Z_4 \frac{\mu^\epsilon g}{S_{d+1}} \end{aligned} \tag{A.2}$$

where $S_d = 2/(\Gamma(d/2)(4\pi)^{d/2})$ is a convenient factor, and μ is an arbitrary renormalization scale. The renormalized coupling s has been defined so that $s = 0$ at criticality by defini-

tion. We renormalize the theory using a modified minimal subtraction scheme as detailed in Ref. [24], where the renormalization constants are given by

$$\begin{aligned} Z_2 &= 1 + \frac{N+2}{6\epsilon} g \\ Z_4 &= 1 + \frac{N+8}{6\epsilon} g \end{aligned} \tag{A.3}$$

and the critical coupling is $s_c = 0$. The Wilson-Fisher fixed point is obtained when the couplings take the values

$$\begin{aligned} s &= 0 \\ g^* &= \frac{6\epsilon}{N+8}\left(1 + \frac{3(3N+14)}{(N+8)^2}\epsilon\right) \end{aligned} \tag{A.4}$$

We are also interested in the vacuum energy in the vicinity of the Wilson-Fisher fixed point. To this end, we have included the additive constant Λ which we choose to make the ground state energy density finite in an infinite volume. This constant also depends on the renormalization scale, and is given by

$$\begin{aligned} \Lambda &= \frac{s^2 Z_2^2 S_{d+1}}{\mu^\epsilon} Z_\Lambda \\ Z_\Lambda &= \frac{N}{4\epsilon} - \frac{N(N+2)}{24\epsilon^2} g \end{aligned} \tag{A.5}$$

Our choice of regularization leads to the vanishing of the ground state energy density at $L = \infty$ and $s = s_c$, where the system has full conformal invariance.

We note that computations will involve the arbitrary energy scale μ. This dependence can always be eliminated in favor of physical quantities. As an example, we can consider the exact energy gap in an infinite volume when $s > 0$. The inverse propagator can be written as a function of the Euclidean momentum $p = (\omega, k)$ as

$$G(p)^{-1} = p^2 + s - \Sigma(p^2) \tag{A.6}$$

Then the exact energy gap m is given by

$$m^2 = s - \Sigma(m^2) \tag{A.7}$$

At one loop this gives

$$m^2 = s\left[1 + \frac{\epsilon}{2}\left(\frac{N+2}{N+8}\right)\ln(s/\mu^2)\right] \tag{A.8}$$

where we have taken $g = g^*$. We can then always use this to rewrite dependence on s and μ in terms of the physical parameter m by inverting this expression,

$$s = m^2\left[1 - \frac{\epsilon}{2}\left(\frac{N+2}{N+8}\right)\ln(m^2/\mu^2)\right] \tag{A.9}$$

In an infinite volume, we can calculate the vacuum energy density. Setting $g = g^*$, this is given by

$$\begin{aligned}\frac{E_0}{\mathcal{A}^{d/2}} &= \frac{Ns^2}{64\pi^2\mu^\epsilon}\left[\ln\left(s/\mu^2\right) - \frac{1}{2}\right] + \frac{Ns^2\epsilon}{128\pi^2\mu^\epsilon}\left[1 - E_\gamma + \ln 4\pi\right]\left[\ln\left(s/\mu^2\right) - \frac{1}{2}\right] \\ &- \frac{Ns^2\epsilon}{256\pi^2\mu^\epsilon}\left[\ln^2\left(s/\mu^2\right) - \ln\left(s/\mu^2\right) + \frac{\pi^2}{3} + \frac{1}{2}\right] + \frac{N(N+2)}{(N+8)}\frac{s^2\epsilon}{\mu^\epsilon}\left[\ln\left(s/\mu^2\right) + \frac{\pi^2}{3}\right]\end{aligned} \tag{A.10}$$

where E_γ is the Euler-Mascheroni constant and $s > 0$.

We note that our finite-volume calculations must be analytic through the critical point $s = 0$, and the system remains disordered for $s < 0$. Therefore, any singularities or branch cuts present in these expressions must cancel out in final results. Therefore we prefer to give our expressions in terms of s and μ rather than m and E_0, which are both non-analytic for $s = 0$, and undefined for $s < 0$.

A.2 Derivation of the Bloch effective Hamiltonian

Here, we give a derivation of Eq. (2.14), the effective Hamiltonian from Bloch's perturbation theory [29]. For the relation between this approach and other effective Hamiltonian

approaches to perturbation theory, we direct the reader to Ref. [143].

We begin by considering a degenerate subspace of the unperturbed spectrum, $\Omega_0 = \text{Span}\{|\epsilon_0\rangle\}$, where the states $|\epsilon_0\rangle$ satisfy

$$H_0|\epsilon_0\rangle = \epsilon_0|\epsilon_0\rangle \tag{A.11}$$

These states are split into distinct energies by the exact Hamiltonian $H = H_0 + V$,

$$H|\alpha\rangle = E_\alpha|\alpha\rangle, \qquad E_\alpha = \epsilon_0 + \mathcal{O}(V) \tag{A.12}$$

Here, we have defined the orthonormal basis of states $|\alpha\rangle$ which diagonalize the exact Hamiltonian and reduce to the degenerate manifold $|\epsilon_0\rangle$ in the $V = 0$ limit. We will define the space spanned by these states by $\Omega = \text{Span}\{|\alpha\rangle\}$. If the perturbation is small, there should be a one-to-one correspondence between the spaces Ω_0 and Ω. We will assume the latter fact in what follows.

Let P_0 be the projection operator onto the space Ω_0, and define the states

$$|\alpha_0\rangle = P_0|\alpha\rangle \tag{A.13}$$

The set of states $|\alpha_0\rangle$ are a particular basis spanning Ω_0, although this basis is not orthonormal in general. We now claim that we can define a linear operator U such that

$$\begin{aligned} U|\alpha_0\rangle &= |\alpha\rangle \\ U|\phi\rangle &= 0 \quad \forall|\phi\rangle \notin \Omega_0 \end{aligned} \tag{A.14}$$

Once the operator U is found, we can construct an effective Hamiltonian which acts on the

unperturbed subspace but gives the exact energy spectrum,

$$H_{\text{eff}} = P_0 H U$$
$$H_{\text{eff}}|\alpha_0\rangle = E_\alpha|\alpha_0\rangle \tag{A.15}$$

This Hamiltonian acts on the unperturbed subspace, but gives the exact spectrum of the interacting Hamiltonian. We can also obtain the exact eigenstates by $|\alpha\rangle = U|\alpha_0\rangle$.

We now make a few clarifying comments on the above operators and states. We note that Ω_0 and Ω represent subspaces within the same Hilbert space, and that these subspaces overlap by assumption. Since the linearly independent basis $|\alpha_0\rangle$ defined via (A.13) is not necessarily orthogonal, the operator U is not unitary, so the standard intuition on changes of basis does not apply here. For example, since we can decompose any state $|\phi\rangle$ in the Hilbert space as

$$|\phi\rangle = P_0|\phi\rangle + (1 - P_0)\,|\phi\rangle \tag{A.16}$$

it follows that

$$U|\phi\rangle = UP_0|\phi\rangle \tag{A.17}$$

so

$$UP_0 = U \tag{A.18}$$

is an exact operator identity. In particular, this implies $U|\alpha\rangle = |\alpha\rangle$. Furthermore, the effective Hamiltonian defined in Eq. (A.15) is not necessarily Hermitian. Thus, even though the vectors $|\alpha_0\rangle$ are eigenvectors of H_{eff}, it does not follow that the effective Hamiltonian is diagonal in the $|\alpha_0\rangle$ basis. This can also be inferred from the fact that the $|\alpha_0\rangle$ may not be orthogonal. Below, we will define a similarity transform which does allow the definition of a Hermitian effective Hamiltonian from Eq. (A.15).

We now find an explicit expression for U for a completely general Hamiltonian. Starting

from Schrödinger's equation,

$$\begin{aligned} H|\alpha\rangle &= E_\alpha|\alpha\rangle \\ \Rightarrow UP_0H|\alpha\rangle &= E_\alpha|\alpha\rangle. \end{aligned} \tag{A.19}$$

Since $UP_0 = U$,

$$(H - UH)\,|\alpha\rangle = 0 \tag{A.20}$$

for all $|\alpha\rangle \in \Omega$. Furthermore, for any state $|\alpha\rangle \in \Omega$, we have $U|\alpha\rangle = |\alpha\rangle$ and $UH_0|\alpha\rangle = \epsilon_0|\alpha\rangle$, from which we have the general operator relation on the entire Hilbert space:

$$\begin{aligned} &(H_0 + V - \epsilon_0 - UV)\,U = 0 \\ \Rightarrow\ &(\epsilon_0 - H_0)\,U = VU - UVU \end{aligned} \tag{A.21}$$

We can invert the left-hand side of this equation by using the fact that the operator $(\epsilon_0 - H_0)$ satisfies $(\epsilon_0 - H_0)\,P_0 = 0$ and has a well-defined inverse in the space orthogonal to Ω_0. This gives the implicit equation

$$U = P_0 + \frac{1 - P_0}{\epsilon_0 - H_0}\,(VU - UVU) \tag{A.22}$$

This allows an expansion in powers of V. Up to third order in V, this is given by

$$\begin{aligned} H_{\text{eff}} &= \epsilon_0 P_0 + P_0 V P_0 + P_0 V \frac{1 - P_0}{\epsilon_0 - H_0} V P_0 \\ &+ P_0 V \frac{1 - P_0}{\epsilon_0 - H_0} V \frac{1 - P_0}{\epsilon_0 - H_0} V P_0 - P_0 V \frac{1 - P_0}{(\epsilon_0 - H_0)^2} V P_0 V P_0 + \cdots \end{aligned} \tag{A.23}$$

For higher order expressions, see Refs. [28, 29]. As seen in Section 2.3.2, the leading non-trivial two-loop diagram is of order $\epsilon^{5/3}$. We can now check explicitly by putting V from Eq. (2.10) that the last term in Eq. (A.23) is of order $\epsilon^{5/3}$ or higher, justifying our truncation of the effective Hamiltonian in the main body of our paper.

We note that the effective Hamiltonian defined above will not be Hermitian in general without a redefinition, although we will not encounter this problem at one-loop. In general, we have

$$BH_{\text{eff}}^{\dagger} = H_{\text{eff}}B, \qquad B \equiv P_0 P P_0 \tag{A.24}$$

where P is the projection operator onto the space Ω. Then the redefined Hermitian Hamiltonian

$$H'_{\text{eff}} \equiv B^{-1/2} H_{\text{eff}} B^{1/2} \tag{A.25}$$

acts on Ω_0 and has the same spectrum as H_{eff}.

A.3 Loops sums

In this appendix we give the calculation of the relevant loop diagrams on a torus in fractional dimensions. The torus is parametrized by complex coordinates, $x = x_1 + ix_2$, with two complex periods ω_1 and ω_2, see Fig. 2.2.1. We define the modular parameter, $\tau = \omega_2/\omega_1 = \tau_1 + i\tau_2$, and the length scale $L \equiv |\omega_1|$. The area of the torus is given by $\mathcal{A} = \tau_2 L^2$.

In this geometry, the basis vectors of the dual lattice are

$$k_1 = -i\omega_2/\mathcal{A}, \qquad k_2 = i\omega_1/\mathcal{A} \tag{A.26}$$

We consider the eigenvalues of the Laplacian on the torus. We will allow twisted boundary conditions along the two cycles of the torus.

$$\begin{aligned} \phi_\alpha(x+\omega_1) &= e^{2\pi i a_1}\phi_\alpha(x) \\ \phi_\alpha(x+\omega_2) &= e^{2\pi i a_2}\phi_\alpha(x) \end{aligned} \tag{A.27}$$

The parameters a_1 and a_2 take values in the range $[0, 1)$. For $a_{1,2}$ not equal to either an 1 or 1/2, the fields ϕ_α are actually complex and our symmetry breaks down from O(N) to

$SU(N) \times U(1)$. In Chapters 1 and 2 we always take $a_1 = a_2 = 0$, while the calculation of loop sums on the torus with twisted boundary conditions is used in Chapters 3 and 4.

The eigenvalues of the Laplacian are

$$|k_{n,m}|^2 = (2\pi)^2 \left|(n+a_1)k_1 + (m+a_2)k_2\right|^2, \qquad n,m \in \mathbb{Z} \tag{A.28}$$

and a general one-loop diagram will take the form

$$\sum_{n,m\in\mathbb{Z}}{}' \frac{1}{\left(|k_{n,m}|^2 + s\right)^\nu} = \left(\frac{\tau_2 L}{2\pi}\right)^{2\nu} \sum_{n,m\in\mathbb{Z}}{}' \frac{1}{\left(|m+a_2+(n+a_1)\tau|^2+\gamma\right)^\nu} \tag{A.29}$$

where $\gamma = \tau_2^2 L^2 s/4\pi^2$, and the primed summation indicates that the $n = m = 0$ term is omitted in the fully periodic case $(a_1, a_2) = (0, 0)$.

We now generalize this sum to an arbitrary number of dimensions. This is done by promoting the two-vector $(n + a_1, m + a_2)$ to a d-dimensional vector where the first $d/2$ components are $n + a_1$ and the last $d/2$ components are $m + a_2$. Then in (A.29) the sums are taken over $n, m \in \mathbb{Z}^{d/2}$. We write the sums as

$$S_\nu^{(d)}(s,\tau) = \sum_{n,m\in\mathbb{Z}^{d/2}}{}' \frac{1}{\left(|m+a_2+(n+a_1)\tau|^2+\gamma\right)^\nu}. \tag{A.30}$$

The summand is rewritten using the identity

$$\frac{1}{A^\nu} = \frac{\pi^\nu}{\Gamma(\nu)} \int_0^\infty d\lambda \lambda^{\nu-1} e^{-\pi\lambda A} \tag{A.31}$$

giving

$$S_\nu^{(d)} = \frac{\pi^\nu}{\Gamma(\nu)} \int_0^\infty d\lambda \lambda^{\nu-1} e^{-\pi\lambda\gamma} \sum_{n,m\in\mathbb{Z}^{d/2}}{}' \exp\left(-\pi\lambda|m+a_2+(n+a_1)\tau|^2\right). \tag{A.32}$$

We can now write the sum in terms of the two-dimensional Riemann theta function, defined

as

$$\Theta\left(\lambda, \mathbf{\Omega}, \mathbf{u}\right) \equiv \sum_{\mathbf{n}\in\mathbb{Z}^2} \exp\left(-\pi\lambda \mathbf{n}^{\intercal}\cdot\mathbf{\Omega}\cdot\mathbf{n} - 2\pi\mathbf{n}^{T}\cdot\mathbf{u}\right) \tag{A.33}$$

where Ω is a 2×2 matrix and $\mathbf{u}$ is a two-dimensional vector. Then

$$S_{\nu}^{(d)} = \frac{\pi^{\nu}}{\Gamma(\nu)}\int_0^{\infty} d\lambda\lambda^{\nu-1}e^{-\pi\lambda\gamma}\left[\exp\left(-\frac{d\pi\lambda\eta}{2}\right)\Theta\left(\lambda,\mathbf{\Omega}(\tau),\mathbf{v}_1\right)^{d/2} - \delta_{a_1 0}\delta_{a_2 0}\right] \tag{A.34}$$

where

$$\mathbf{\Omega}(\tau) = \begin{pmatrix} |\tau|^2 & \tau_1 \\ \tau_1 & 1 \end{pmatrix}, \qquad \mathbf{v}_1 = \lambda\begin{pmatrix} \tau_1\left(a_2 + a_1\tau_1\right) + a_1\tau_2^2 \\ a_2 + a_1\tau_1 \end{pmatrix}, \qquad \eta = (a_1\tau_2)^2 + (a_2 + a_1\tau_1)^2. \tag{A.35}$$

The function $S_{\nu}^{(d)}(s,\tau)$ has a divergence for small λ whenever $\nu < d/2$. We evaluate the sums by dimensional regularization: we separate out the divergent parts and and evaluate them in the convergent regime $\nu > d/2$, and then analytically continue them to the physical values of ν and d of interest, taking care to renormalize any poles in ϵ which arise. For our purposes, it is also crucial that we obtain final expressions which are regular at $s = 0$ and remain finite for $s < 0$, since the finite-volume theory should be analytic through the critical point.

We proceed by splitting the integral in Eq (A.34) into two parts, $\int_0^{\infty} = \int_0^1 + \int_1^{\infty}$, and studying the divergent part. Using the mathematical identity

$$\Theta\left(\lambda,\mathbf{\Omega},\mathbf{u}\right) = \frac{1}{\lambda\sqrt{\det\mathbf{\Omega}}}\exp\left(\frac{\pi}{\lambda}\mathbf{u}^{T}\cdot\mathbf{\Omega}^{-1}\cdot\mathbf{u}\right)\Theta\left(\frac{1}{\lambda},\mathbf{\Omega}^{-1},-\frac{i}{\lambda}\mathbf{\Omega}^{-1}\cdot\mathbf{u}\right), \tag{A.36}$$

we write the lower portion of the integral as

$$\begin{aligned}
&\frac{\pi^\nu}{\Gamma(\nu)}\int_0^1 d\lambda\lambda^{\nu-1}e^{-\pi\lambda\gamma}\left[\tau_2^{-d/2}\lambda^{-d/2}\Theta\left(\frac{1}{\lambda},\mathbf{\Omega}(\tau)^{-1},\mathbf{v}_2\right)^{d/2}-\delta_{a_10}\delta_{a_20}\right]\\
=\;&\tau_2^{-d/2}\frac{\pi^\nu}{\Gamma(\nu)}\int_1^\infty d\lambda\lambda^{d/2-\nu-1}\left[e^{-\pi\gamma/\lambda}\Theta\left(\lambda,\mathbf{\Omega}(\tau)^{-1},\mathbf{v}_2\right)^{d/2}-1+\frac{\pi\gamma}{\lambda}-\frac{(\pi\gamma)^2}{2\lambda^2}\right] \qquad \text{(A.37)}\\
+\;&\tau_2^{-d/2}\frac{\pi^\nu}{\Gamma(\nu)}\int_1^\infty d\lambda\lambda^{d/2-\nu-1}\left(1-\frac{\pi\gamma}{\lambda}+\frac{(\pi\gamma)^2}{2\lambda^2}\right)-\frac{\pi^\nu}{\Gamma(\nu)}\delta_{a_10}\delta_{a_20}\int_1^\infty d\lambda\lambda^{-\nu-1}e^{-\pi\gamma/\nu}
\end{aligned}$$

where we define the vector $\mathbf{v}_2 = -i(a_1, a_2)$. For $d = 3$ and $\nu \geq -1/2$, the UV divergences are entirely contained in the last line of Eq (A.38). The very last term can be integrated in its convergent regime, obtaining

$$\frac{1}{\Gamma(\nu)}\int_1^\infty d\lambda\lambda^{-\nu-1}e^{-\pi\gamma/\nu} = e^{-\pi\gamma}\sum_{k=0}^{\infty}\frac{(\pi\gamma)^k}{\Gamma(\nu+k+1)} \qquad \text{(A.38)}$$

This expression was obtained by evaluating the integral for $\nu > 0$ and $\gamma > 0$, obtaining an expression involving incomplete gamma functions, and then expressing these functions as a power series. The final expression is a single-valued analytic function for all γ and ν with no singularities [144], and evaluating this series numerically is trivial.

When $\nu > d/2$ we can evaluate

$$\int_1^\infty d\lambda\lambda^{d/2-\nu-1}\left(1-\frac{\pi\gamma}{\lambda}+\frac{(\pi\gamma)^2}{2\lambda^2}\right) = \frac{1}{\nu-d/2}-\frac{\pi\gamma}{1+\nu-d/2}+\frac{(\pi\gamma)^2}{4+2\nu-d} \qquad \text{(A.39)}$$

Since we are expanding around $d = 3$, the three terms will contribute poles for $\nu = 3/2$, $\nu = 1/2$, and $\nu = -1/2$ respectively. We will see that these three poles are related to the renormalization of u, s_0, and $\mathcal{E}_0$.

To summarize our results so far, we have written the loop sum as

$$\sum_{n,m\in\mathbb{Z}}{}' \frac{1}{\left(|k_{n,m}|^2+s\right)^\nu} = \left(\frac{\tau_2 L}{2\pi}\right)^{2\nu} S_\nu^{(d)}(s,\tau), \qquad \text{(A.40)}$$

$$
\begin{aligned}
S_\nu^{(d)} &= \frac{\pi^\nu}{\Gamma(\nu)}\int_1^\infty d\lambda\lambda^{\nu-1}e^{-\pi\lambda\gamma}\left[\exp\left(-\frac{d\pi\lambda\eta}{2}\right)\Theta\left(\lambda,\mathbf{\Omega}(\tau),\mathbf{v}_1\right)^{d/2}-\delta_{a_10}\delta_{a_20}\right] \\
&+ \tau_2^{-d/2}\frac{\pi^\nu}{\Gamma(\nu)}\int_1^\infty d\lambda\lambda^{d/2-\nu-1}\left[e^{-\pi\gamma/\lambda}\Theta\left(\lambda,\mathbf{\Omega}(\tau)^{-1},\mathbf{v}_2\right)^{d/2}-1+\frac{\pi\gamma}{\lambda}-\frac{(\pi\gamma)^2}{2\lambda^2}\right] \quad \text{(A.41)} \\
&+ \tau_2^{-d/2}\frac{\pi^\nu}{\Gamma(\nu)}\left(\frac{1}{\nu-d/2}-\frac{\pi\gamma}{1+\nu-d/2}+\frac{(\pi\gamma)^2}{4+2\nu-d}\right)-\delta_{a_10}\delta_{a_20}e^{-\pi\gamma}\sum_{k=0}^\infty\frac{\pi^{k+\nu}\gamma^k}{\Gamma(\nu+k+1)}
\end{aligned}
$$

where $\gamma=\tau_2^2L^2s/4\pi^2$, the Riemann theta function Θ is defined in (A.33), and

$$
\mathbf{\Omega}(\tau)=\begin{pmatrix}|\tau|^2 & \tau_1\\ \tau_1 & 1\end{pmatrix}, \qquad \mathbf{\Omega}(\tau)^{-1}=\frac{1}{\tau_2^2}\begin{pmatrix}1 & -\tau_1\\ -\tau_1 & |\tau|^2\end{pmatrix} \qquad \text{(A.42)}
$$

$$
\mathbf{v}_1=\lambda\begin{pmatrix}\tau_1\left(a_2+a_1\tau_1\right)+a_1\tau_2^2\\ a_2+a_1\tau_1\end{pmatrix}, \qquad \mathbf{v}_2=-i\begin{pmatrix}a_1\\ a_2\end{pmatrix}, \qquad \eta=(a_1\tau_2)^2+(a_2+a_1\tau_1)^2
$$

From these expressions we define finite functions. They are given in terms of the $S_\nu^{(d)}$, but with their poles around $d=3$ removed.

$$
\begin{aligned}
f_{-1/2}^{(3-\epsilon)}(\tau,s,\mu) &= S_{-1/2}^{(3-\epsilon)}+\frac{\tau_2^{5/2}L^4s^2}{4\pi\mu^\epsilon\mathcal{A}^{\epsilon/2}\epsilon}S_{4-\epsilon} \\
f_{1/2}^{(3-\epsilon)}(\tau,s,\mu) &= S_{1/2}^{(3-\epsilon)}+\frac{4\pi\tau_2^{1/2}L^2s}{\mu^\epsilon\mathcal{A}^{\epsilon/2}\epsilon}S_{4-\epsilon} \\
\tilde{f}_{3/2}^{(3-\epsilon)}(\tau,s,\mu) &= S_{3/2}^{(3-\epsilon)}-\frac{32\pi^3\tau_2^{-3/2}}{\mu^\epsilon\mathcal{A}^{\epsilon/2}\epsilon}S_{4-\epsilon} \qquad \text{(A.43)}
\end{aligned}
$$

The three functions $f_\nu^{(d)}$ have a regular power series about $s=0$ and $\epsilon=0$, and the extra factors are defined to simplify expressions in our renormalization scheme. We note that these functions are all dependent on μ, but the first two functions are independent of μ at $s=0$, while the third function will be exchanged for a μ-independent function below. We note the

identities

$$\begin{aligned}
\frac{\partial}{\partial s} f_\nu^{(d)}(\tau, s, \mu) &= -\frac{\nu \tau_2^2 L^2}{4\pi^2} f_{\nu+1}^{(d)}(\tau, s, \mu) \\
f_\nu^{(d)}(\tau+1, 0, \mu) &= f_\nu^{(d)}(\tau, 0, \mu) \\
\tau_2^\nu f_\nu^{(d)}(\tau, 0, \mu) &= \frac{\tau_2^\nu}{|\tau|^{2\nu}} f_\nu^{(d)}(1/\tau, 0, \mu)
\end{aligned} \tag{A.44}$$

The first identity will be useful for renormalizing the bare mass, while the other two are a consequence of modular invariance.

A.3.1 Loop sums with zero mode

In the large N computation in Chapter 3, we find that we will not need to separate out the zero-momentum mode in the fully periodic case, $(a_1, a_2) = 0$. This is because the gap is always finite, so every sum is IR safe. Our leading order results also do not need to be renormalized in dimensional regularization. In this subsection, we define variants of the above functions useful for our large N computations.

If we do not separate out the zero mode in the periodic case, we simply need to omit the terms proportional to $\delta_{a_1 0}\delta_{a_2 0}$ in Eq. (A.41). The resulting expression is finite for all $1 < d < 3$ in the cases $\nu = \pm 1/2$ which we need. We also do not need to separate out the same poles we did in Eq. (A.41).

With these comments, we give the relevant expressions needed in the large N computation.

$$\sum_{n,m\in\mathbb{Z}} \frac{1}{\left(|k_{n,m}|^2 + \Delta^2\right)^\nu} = \left(\frac{\tau_2 L}{2\pi}\right)^{2\nu} g_\nu^{(d)}(\Delta, \tau), \tag{A.45}$$

$$\begin{aligned} g_\nu^{(d)}(\Delta,\tau) &= \frac{\pi^\nu}{\Gamma(\nu)}\int_1^\infty d\lambda\lambda^{\nu-1}e^{-\pi\lambda\gamma}\exp\left(-\frac{d\pi\lambda\eta}{2}\right)\Theta\left(\lambda,\mathbf{\Omega}(\tau),\mathbf{v}_1\right)^{d/2} \\ &+ \tau_2^{-d/2}\frac{\pi^\nu}{\Gamma(\nu)}\int_1^\infty d\lambda\lambda^{d/2-\nu-1}\left[e^{-\pi\gamma/\lambda}\Theta\left(\lambda,\mathbf{\Omega}(\tau)^{-1},\mathbf{v}_2\right)^{d/2}-1+\frac{\pi\gamma}{\lambda}\right] \\ &+ \tau_2^{-d/2}\frac{\pi^\nu}{\Gamma(\nu)}\left(\frac{1}{\nu-d/2}-\frac{\pi\gamma}{1+\nu-d/2}\right) \end{aligned} \tag{A.46}$$

where $\gamma=\tau_2^2L^2\Delta^2/4\pi^2$, the Riemann theta function Θ is defined in (A.33), and

$$\mathbf{\Omega}(\tau)=\begin{pmatrix}|\tau|^2 & \tau_1\\ \tau_1 & 1\end{pmatrix}, \qquad \mathbf{\Omega}(\tau)^{-1}=\frac{1}{\tau_2^2}\begin{pmatrix}1 & -\tau_1\\ -\tau_1 & |\tau|^2\end{pmatrix} \tag{A.47}$$

$$\mathbf{v}_1=\lambda\begin{pmatrix}\tau_1\left(a_2+a_1\tau_1\right)+a_1\tau_2^2\\ a_2+a_1\tau_1\end{pmatrix}, \qquad \mathbf{v}_2=-i\begin{pmatrix}a_1\\ a_2\end{pmatrix}, \qquad \eta=(a_1\tau_2)^2+(a_2+a_1\tau_1)^2$$

A.4 Renormalization of the effective Hamiltonian

Here we consider the renormalization of physical quantities. To this end, we calculate the effective Hamiltonian for the splitting of the Fock vacuum, $h_{k=0}$, which contains most of the divergences which need to be considered.

We calculate each individual expression in Eq. (2.30). The constant term is

$$\begin{aligned} h_{k=0}^{(0)} &= \mathcal{A}^{(3-\epsilon)/2}\Lambda+\frac{N}{2}\sum_{k\neq0}\sqrt{|k|^2+s_0}+\frac{u\mathcal{A}^{\epsilon/2}}{\mathcal{A}^{3/2}}\frac{N(N+2)}{4(4!)}\left[\sum_{k\neq0}\frac{1}{\sqrt{|k|^2+s_0}}\right]^2 \\ &= \mathcal{A}^{(3-\epsilon)/2}\Lambda+\frac{\pi N}{\tau_2 L}\left[f_{-1/2}^{(3-\epsilon)}(\tau,sZ_2,\mu)-\frac{\tau_2^{5/2}L^4s^2}{4\pi\mu^\epsilon\mathcal{A}^{\epsilon/2}\epsilon}S_{4-\epsilon}\right] \\ &+ \frac{g\mu^\epsilon}{S_{4-\epsilon}}\frac{\mathcal{A}^{\epsilon/2}}{\tau_2^{3/2}L^3}\frac{N(N+2)}{4(4!)}\frac{\tau_2^2L^2}{4\pi^2}\left[f_{1/2}^{(3-\epsilon)}(\tau,s,\mu)-\frac{4\pi\tau_2^{1/2}L^2s}{\mu^\epsilon\mathcal{A}^{\epsilon/2}\epsilon}S_{4-\epsilon}\right]^2 \end{aligned} \tag{A.48}$$

By expanding out all of the terms, including the g-dependent Z_2 factor using Eq. (A.3), and using the definition of Λ from Eq. (A.5), we find that all poles in ϵ cancel, as well as all

factors of $S_{4-\epsilon}$. Once the poles cancel, we set $g = g^*$, obtaining

$$h^{(0)}_{k=0} = \frac{\pi N}{\tau_2 L} f^{(3-\epsilon)}_{-1/2}(\tau, s, \mu) + \frac{N(N+2)}{(N+8)} \frac{\epsilon}{8L} \tau_2^{1/2} f^{(3)}_{1/2}(\tau, s, \mu)^2 \tag{A.49}$$

The coefficient of φ_α^2 is

$$\begin{aligned} h^{(2)}_{k=0} &= \frac{\varphi^2}{2} \tau_2^{1/2} L s Z_2 + \frac{u\mathcal{A}^{\epsilon/2}}{2\tau_2 L^2} \left(\frac{\delta_{\alpha\beta}}{12} \varphi^2 + \frac{1}{6} \varphi_\alpha \varphi_\beta \right) \sum_{\mathbf{k} \neq 0} \frac{\delta_{\alpha\beta}}{\sqrt{|k|^2 + s}} \\ &= \frac{\varphi^2}{2} \left\{ \tau_2^{1/2} L s \left(1 + \frac{N+2}{6\epsilon} g \right) + \left(\frac{N+2}{12} \right) \frac{g \mu^\epsilon \mathcal{A}^{\epsilon/2}}{\tau_2 L^2 S_{4-\epsilon}} \left[f^{(3-\epsilon)}_{1/2}(\tau, s, \mu) - \frac{4\pi \tau_2^{1/2} L^2 s}{\mu^\epsilon \mathcal{A}^{\epsilon/2} \epsilon} S_{4-\epsilon} \right] \right\} \end{aligned}$$

The poles in ϵ and factors of $S_{4-\epsilon}$ cancel, and after setting $g = g^*$ we obtain

$$h^{(2)}_{k=0} = \frac{1}{\sqrt{\tau_2} L} \frac{\varphi^2}{2} \left\{ \tau_2 L^2 s + 2\pi\epsilon \left(\frac{N+2}{N+8} \right) \tau_2^{1/2} f^{(3)}_{1/2}(\tau, s, \mu) \right\} \tag{A.50}$$

Finally, the divergence in the quartic term cancels similarly, and after setting $g = g^*$ we find

$$\begin{aligned} h^{(4)}_{k=0} &= \frac{u\mathcal{A}^{\epsilon/2}}{\sqrt{\tau_2} L} \frac{\varphi^4}{4!} - \frac{\left(u\mathcal{A}^{\epsilon/2}\right)^2}{8\tau_2^2 L^4} \left(\frac{\delta_{\alpha\beta}}{12} \varphi^2 + \frac{1}{6} \varphi_\alpha \varphi_\beta \right) \left(\frac{\delta_{\gamma\delta}}{12} \varphi^2 + \frac{1}{6} \varphi_\gamma \varphi_\delta \right) \sum_{k \neq 0} \frac{\delta_{\alpha\gamma}\delta_{\beta\delta} + \delta_{\alpha\delta}\delta_{\beta\gamma}}{(|k|^2 + s)^{3/2}} \\ &\Rightarrow \frac{1}{\sqrt{\tau_2} L} \frac{\varphi^4}{4!} \left(\frac{48\pi^2 \epsilon}{N+8} \right) \left\{ \frac{\mu^\epsilon \mathcal{A}^{\epsilon/2}}{8\pi^2 S_{4-\epsilon}} - \frac{\tau_2^{3/2} \epsilon}{4\pi} \tilde{f}^{(3)}_{3/2}(\tau, s, \mu) + \frac{3\,(3N+14)}{(N+8)^2} \epsilon \right\} \end{aligned} \tag{A.51}$$

We note all of these expressions appear to depend on the arbitrary scale μ. This dependence actually drops out of $h^{(4)}_{k=0}$ to this order in ϵ, and it drops out of all quantities at the critical point $s = 0$. We can write

$$\frac{\mu^\epsilon \mathcal{A}^{\epsilon/2}}{8\pi^2 S_{4-\epsilon}} - \frac{\tau_2^{3/2} \epsilon}{4\pi} \tilde{f}^{(3)}_{3/2}(\tau, s, \mu) = 1 - \frac{\tau_2^{3/2} \epsilon}{4\pi} f^{(3)}_{3/2}(\tau, s) + \mathcal{O}(\epsilon^2) \tag{A.52}$$

where $f^{(3)}_{3/2}(\tau, s)$ is μ-independent. The fact that all μ dependence vanishes at $g = g^*$ and $s = 0$ is a manifestation of the scale invariance of the critical theory.

Combining the above results, the effective Hamiltonian takes the form given in Eq. (2.31):

$$\begin{aligned} h_{k=0} &= \mathcal{E}_{k=0} + \frac{1}{\sqrt{\tau_2}L}\left(\frac{\pi_\alpha^2}{2} + \frac{R}{2}\varphi_\alpha^2 + \frac{U}{4!}\left(\varphi_\alpha^2\right)^2\right) \\ \mathcal{E}_{k=0} &\equiv \frac{\pi N}{\tau_2 L} f_{-1/2}^{(3-\epsilon)}(\tau,s,\mu) + \frac{1}{\sqrt{\tau_2}L}\frac{N(N+2)}{N+8}\frac{\epsilon}{8}\tau_2 f_{1/2}^{(3)}(\tau,s,\mu)^2 \\ R &\equiv \tau_2 L^2 s + 2\pi\epsilon\left(\frac{N+2}{N+8}\right)\tau_2^{1/2} f_{1/2}^{(3)}(\tau,s,\mu) \\ U &\equiv \frac{48\pi^2\epsilon}{N+8}\left\{1 - \frac{\tau_2^{3/2}\epsilon}{4\pi} f_{3/2}^{(3)}(\tau,s) + \frac{3\left(3N+14\right)}{\left(N+8\right)^2}\epsilon\right\} \end{aligned} \tag{A.53}$$

To the order required, the special functions are

$$\begin{aligned} f_{-1/2}^{(3-\epsilon)} &= -\frac{1}{2\pi}\int_1^\infty d\lambda\lambda^{-3/2}\exp\left(-\frac{\lambda\tau_2^2L^2s}{4\pi}\right)\left[\exp\left(-\frac{(3-\epsilon)\pi\lambda\eta}{2}\right)\Theta\left(\lambda,\mathbf{\Omega}(\tau),\mathbf{v}_1\right)^{(3-\epsilon)/2} - \delta_{a_10}\delta_{a_20}\right] \\ &- \frac{\tau_2^{-(3-\epsilon)/2}}{2\pi}\int_1^\infty d\lambda\lambda^{1-\epsilon/2}\left[\exp\left(-\frac{\tau_2^2L^2s}{4\pi\lambda}\right)\Theta\left(\lambda,\mathbf{\Omega}(\tau)^{-1},\mathbf{v}_2\right)^{(3-\epsilon)/2} - 1 + \frac{\tau_2^2L^2s}{4\pi\lambda} - \frac{\tau_2^4L^4s^2}{32\pi^2\lambda^2}\right] \\ &- \frac{\tau_2^{-(3-\epsilon)/2}}{\pi} + \frac{\tau_2^{(1+\epsilon)/2}L^2s}{8\pi^2} - \frac{\delta_{a_10}\delta_{a_20}}{\sqrt{\pi}}\exp\left(-\frac{\lambda\tau_2^2L^2s}{4\pi}\right)\sum_{k=0}^\infty\frac{\left(\tau_2^2L^2s/4\pi\right)^k}{\Gamma(k+1/2)} \\ &+ \frac{\tau_2^{5/2}L^4s^2}{64\pi^3}\left[1 - E_\gamma - \ln\left(\frac{\tau_2^2L^2\mu^2}{4\pi}\right)\right] + \frac{\tau_2^{5/2}L^4s^2\epsilon}{128\pi^3}\Bigg\{1 + 2\ln^2 2 + \ln 4\pi - \frac{\pi^2}{12} \\ &+ \frac{1}{2}E_\gamma\left[E_\gamma - 2(1+\ln 4\pi)\right] + \frac{1}{2}\ln\pi\ln 16\pi - \left[1 - E_\gamma - \ln\left(\frac{\sqrt{\tau_2}L\mu}{4\pi}\right)\right]\ln\left(\sqrt{\tau_2}L\mu\right) \\ &- \frac{1}{2}\ln^2\tau_2\Bigg\} + \mathcal{O}(\epsilon^2) \end{aligned} \tag{A.54}$$

$$\begin{aligned} f_{1/2}^{(3)} &= \int_1^\infty d\lambda\lambda^{-1/2}\exp\left(-\frac{\lambda\tau_2^2L^2s}{4\pi}\right)\left[\exp\left(-\frac{3\pi\lambda\eta}{2}\right)\Theta\left(\lambda,\mathbf{\Omega}(\tau),\mathbf{v}_1\right)^{3/2} - \delta_{a_10}\delta_{a_20}\right] \\ &+ \tau_2^{-3/2}\int_1^\infty d\lambda\left[\exp\left(-\frac{\tau_2^2L^2s}{4\pi\lambda}\right)\Theta\left(\lambda,\mathbf{\Omega}(\tau)^{-1},\mathbf{v}_2\right)^{3/2} - 1 + \frac{\tau_2^2L^2s}{4\pi\lambda}\right] - \tau_2^{-3/2} \\ &- \delta_{a_10}\delta_{a_20}\sqrt{\pi}\exp\left(-\frac{\lambda\tau_2^2L^2s}{4\pi}\right)\sum_{k=0}^\infty\frac{\left(\tau_2^2L^2s/4\pi\right)^k}{\Gamma(k+3/2)} + \frac{\sqrt{\tau_2}L^2s}{4\pi}\left[1 - E_\gamma - \ln\left(\frac{\tau_2^2L^2\mu^2}{4\pi}\right)\right] \end{aligned} \tag{A.55}$$

$$
\begin{aligned}
f_{3/2}^{(3)} &= 2\pi \int_1^\infty d\lambda \lambda^{1/2} \exp\left(-\frac{\lambda \tau_2^2 L^2 s}{4\pi}\right) \left[\exp\left(-\frac{3\pi\lambda\eta}{2}\right) \Theta\left(\lambda, \mathbf{\Omega}(\tau), \mathbf{v}_1\right)^{3/2} - \delta_{a_1 0}\delta_{a_2 0}\right] \\
&+ 2\pi\tau_2^{-d/2} \int_1^\infty d\lambda \lambda^{-1} \left[\exp\left(-\frac{\tau_2^2 L^2 s}{4\pi\lambda}\right) \Theta\left(\lambda, \mathbf{\Omega}(\tau)^{-1}, \mathbf{v}_2\right)^{3/2} - 1\right] \\
&+ 2\pi\tau_2^{-3/2} \ln\tau_2 - \delta_{a_1 0}\delta_{a_2 0}\pi^{3/2} \exp\left(-\frac{\lambda\tau_2^2 L^2 s}{4\pi}\right) \sum_{k=0}^\infty \frac{\left(\tau_2^2 L^2 s/4\pi\right)^k}{\Gamma(k+5/2)}
\end{aligned} \tag{A.56}
$$

The function $f_{-1/2}^{(3-\epsilon)}$ should be expanded to first order in ϵ. It is possible to exchange the parameters s and μ for the infinite volume gap and ground state energies, but the latter are not analytic through the critical point so we keep the μ dependence in our final expressions.

A.5 Strong-coupling expansion of isotropic quartic oscillators

In this appendix we give details of the numerical calculation of the spectrum of the isotropic quartic oscillator

$$
\frac{1}{2}\left(-\frac{1}{\rho^{N-1}}\frac{\partial}{\partial r}\rho^{N-1}\frac{\partial}{\partial\rho} - \frac{\ell\left(\ell+N-2\right)}{\rho^{N-1}} + r\rho^2 + 2\rho^4\right) R_{n,\ell}(\rho) = E_{n,\ell} R_{n,\ell}(\rho) \tag{A.57}
$$

in the strong-coupling limit, finding the coefficients

$$
E_{n,\ell} = \sum_{m=1}^\infty c_{n,\ell,m} r^m \tag{A.58}
$$

We tabulate the values of $c_{n,\ell,m}$ which we have calculated in Tables A.5.1-A.5.3.

We begin by solving Eq. (A.57) numerically for $r = 0$. We first fix the asymptotic behavior by writing

$$
R_{n,\ell}(\rho) = \psi_{n,\ell}(\rho) e^{-\sqrt{2}\rho^3/3} \tag{A.59}
$$

The exponential factor takes into account the large-ρ behavior implied by Eq. (A.57). We then use a shooting method, using known boundary conditions on the wave function at

$N=2$	ℓ				
	0	1	2	3	4
$c_{0,\ell,0}$	1.47715	3.39815	5.65434	8.09067	10.7583
$c_{0,\ell,1}$	0.258539	0.447039	0.605913	0.747439	0.877189
$c_{0,\ell,2}$	-0.012345	-0.015633	-0.017109	-0.017109	-0.018469
$c_{0,\ell,3}$	0.000903	0.000806	0.000697	0.000613	0.000548
$c_{1,\ell,0}$	6.00339	8.70045	11.53475	14.50868	17.61616
$c_{1,\ell,1}$	0.554312	0.682554	0.80824713	0.92837	1.04294
$c_{1,\ell,2}$	-0.011291	-0.012457	-0.013714	-0.014705	-0.015489
$c_{1,\ell,3}$	0.000133	0.000236	0.000293	0.000315	0.000320

Table A.5.1: The coefficients of the strong-coupling expansion for the two-dimensional quartic oscillator.

$N=3$	ℓ				
	0	1	2	3	4
$c_{0,\ell,0}$	2.393644	4.478039	6.830308	9.401160	12.159017
$c_{0,\ell,1}$	0.357801	0.529165	0.678421	0.813557	0.938665
$c_{0,\ell,2}$	-0.014371	-0.016492	-0.017576	-0.018230	-0.018667
$c_{0,\ell,3}$	0.000865	0.000749	0.000651	0.000578	0.000521
$c_{1,\ell,0}$	7.335730	10.099944	13.004563	16.046193	19.217579
$c_{1,\ell,1}$	0.618248	0.746036	0.869032	0.986315	1.09832
$c_{1,\ell,2}$	-0.011790	-0.013117	-0.014238	-0.015120	-0.015816
$c_{1,\ell,3}$	0.000188	0.000271	0.000307	0.000319	0.000320

Table A.5.2: The coefficients of the strong-coupling expansion for the three-dimensional quartic oscillator.

$\rho = 0$ (including an arbitrary normalization) to compute $\psi_{n,\ell}$ in Mathematica using DSolve for variable values of the energy until we identify an eigenstate.

Once we find the energy to sufficient accuracy, the function $\psi_{n,\ell}$ will not change much for smaller ρ, but will always blow up after some value of ρ. However, the actual wave function $R_{n,\ell}$ is exponentially suppressed, so we only need to obtain $\psi_{n,\ell}$ accurately for small values of ρ to obtain an accurate wave function.

Once we obtain a numerically accurate energy and wave function for $r = 0$, we use logarithmic perturbation theory to compute the expansion in r. This has the benefit of only needing the unperturbed energy and wave function, whereas the standard Rayleigh-

$N=4$	ℓ				
	0	1	2	3	4
$c_{0,\ell,0}$	3.398150	5.624339	8.090668	10.758265	13.600878
$c_{0,\ell,1}$	0.447038	0.605918	0.747451	0.877202	0.998248
$c_{0,\ell,2}$	-0.015634	-0.017110	-0.017939	-0.018466	-0.018830
$c_{0,\ell,3}$	0.000806	0.000697	0.000612	0.000547	0.000497
$c_{1,\ell,0}$	8.700454	11.534729	14.508675	17.616152	20.849517
$c_{1,\ell,1}$	0.682554	0.808247	0.928370	1.042942	1.152539
$c_{1,\ell,2}$	-0.012457	-0.013714	-0.014704	-0.015489	-0.016111
$c_{1,\ell,3}$	0.000236	0.000293	0.000315	0.000320	0.000319

Table A.5.3: The coefficients of the strong-coupling expansion for the four-dimensional quartic oscillator.

Schrödinger expansion requires knowledge of many excited states to get accurate values for the coefficients. The starting point for logarithmic perturbation theory is to write the wave function as

$$R_{n,\ell} = \prod_{i=1}^{n} (\rho - \rho_i) e^{G(\rho)} \tag{A.60}$$

where ρ_i are the nodes of $R_{n,\ell}$, and then rewrite the eigenvalue equation as an equation for G. Then we assume an expansion in r:

$$\begin{aligned} G(\rho) &= \sum_{m=0} G_m(\rho) r^m \\ \rho_i &= \sum_{m=0} \rho_{i,m} r^m \\ E_{n,\ell} &= \sum_{m=0} c_{n,\ell,m} r^m \end{aligned} \tag{A.61}$$

Inserting these definitions into our eigenvalue equation, the resulting differential equation is linear order-by-order in perturbation theory, so the energies are given in closed form in terms of integrals only involving the unperturbed functions $G_0(\rho)$, $E_{n,\ell,0}$, and $\rho_{i,0}$. For explicit details, we refer the reader to References [32, 33]. We give the coefficients we have calculated in Tables A.5.1-A.5.3.

A.6 $1/N$ CORRECTIONS

Here we mention the form of the leading $1/N$ corrections, following a similar notation to Ref. [47]. First we need to calculate the critical coupling s_c to order $1/N$. This is done by solving the infinite-volume gap equation (3.5), where we write the infinite volume saddle point as $i\tilde{\lambda} = r + i\lambda/\sqrt{N}$:

$$\frac{r}{u} = \frac{s_c}{2} + \int \frac{d^{d+1}p}{(2\pi)^{d+1}} \frac{1}{p^2+r}. \tag{A.62}$$

The coupling s_c should be tuned so that the the energy gap in an infinite volume vanishes. We do this by working backwards: we first calculate the energy gap as a function of r, then tune r such that the energy gap vanishes, and finally define s_c through Eq. (A.62). From the action (3.3), the relevant self-energy diagram corrections to the z_α propagator are

$$\begin{aligned} G_\infty^{-1}(p) &= p^2 + r + \frac{1}{N}\int \frac{d^{d+1}q}{(2\pi)^{d+1}} \frac{1}{\Pi_\infty(q,r)} \frac{1}{((p+q)^2+r)} \\ &- \frac{1}{N}\frac{1}{\Pi_\infty(0,r)} \int \frac{d^{d+1}q_1}{(2\pi)^{d+1}} \frac{d^{d+1}q_2}{(2\pi)^{d+1}} \frac{1}{\Pi_\infty(q_1,r)} \frac{1}{(q_2^2+r)^2((q_1+q_2)^2+r)}, \end{aligned} \tag{A.63}$$

where we have the inverse λ propagators in an infinite volume:

$$\Pi_\infty(q,r) \;=\; \int \frac{d^{d+1}q}{(2\pi)^{d+1}} \frac{1}{(q^2+r)((p+q)^2+r)}. \tag{A.64}$$

The critical point is given by $G_\infty^{-1}(0) = 0$, so to order $1/N$,

$$\begin{aligned} r &= -\frac{1}{N}\int \frac{d^{d+1}q}{(2\pi)^{d+1}} \frac{1}{\Pi_\infty(q,0)} \frac{1}{(p+q)^2} + \frac{1}{N}\frac{1}{\Pi_\infty(0,0)} \int \frac{d^{d+1}q_1}{(2\pi)^{d+1}} \frac{d^{d+1}q_2}{(2\pi)^{d+1}} \frac{1}{\Pi_\infty(q_1,0)} \frac{1}{q_2^4(q_1+q_2)^2} \\ &= \frac{1}{N}\frac{1}{\Pi_\infty(0,0)} \int \frac{d^{d+1}q_1}{(2\pi)^{d+1}} \frac{1}{\Pi_\infty(q_1,0)} \int \frac{d^{d+1}q_2}{(2\pi)^{d+1}} \frac{1}{q_2^4} \left(\frac{1}{(q_1+q_2)^2} - \frac{1}{q_1^2} \right). \end{aligned} \tag{A.65}$$

Note that $\Pi_\infty(0,0)$ is really infrared divergent, but it can be regulated, and it cancels out of physical values [47]. In this case, using dimensional regularization, we notice that

$$\int \frac{d^{d+1}q_2}{(2\pi)^{d+1}} \frac{1}{q_2^4} \left(\frac{1}{(q_1+q_2)^2} - \frac{1}{q_1^2} \right) = \frac{(q_1^2)^{(d+1)/2-3}}{(4\pi)^{(d+1)/2}} \frac{\Gamma(\frac{d-3}{2})\Gamma(\frac{d-1}{2})}{\Gamma(d-2)} \stackrel{d=2}{\Longrightarrow} 0. \tag{A.66}$$

So r is of order $1/N^2$ at the critical point in two spatial dimensions, and from Eq. (A.62), the critical coupling is of order $1/N^2$ in dimensional regularization. Therefore, there is no $1/N$ correction to the finite volume gap equation (3.5).

We can now calculate the self-energy corrections to the z_α in a finite volume. These are given by a similar calculation to the one above, but now with loop sums,

$$\begin{aligned} G^{-1}(k,i\omega) = \omega^2 + k^2 + \Delta^2 + \frac{1}{N\mathcal{A}} \sum_q \int \frac{d\Omega}{2\pi} \frac{D(q,i\Omega)}{((\omega+\Omega)^2 + (k+q)^2 + \Delta^2)} \\ - \frac{D(0,0)}{N\mathcal{A}^2} \int \frac{d\Omega_1 d\Omega_2}{4\pi^2} \sum_{q_1,q_2} \frac{D(q_1,i\Omega_1)}{(\Omega_2^2+q_2^2+\Delta^2)^2((\Omega_1+\Omega_2)^2+(q_1+q_2)^2+\Delta^2)}. \end{aligned} \tag{A.67}$$

The spectrum is then obtained by solving $G^{-1}(k, E(k)) = 0$.

There are also $1/N$ corrections to the singlet states. To compute these, we need the nonlinear terms in the effective action for λ, (3.14). To order $1/N$ these are

$$\begin{aligned} \mathcal{S}_1 = -\frac{i}{6\sqrt{N}} \frac{1}{\mathcal{A}^3} \sum_{k_1,k_2,k_3} \int \prod_{i=1}^{3} \left(\frac{d\omega_i}{2\pi} \right) K_3(p_1,p_2,p_3) \lambda(p_1)\lambda(p_2), \lambda(p_3)\delta(p_1+p_2+p_3) \\ - \frac{1}{24N} \frac{1}{\mathcal{A}^4} \sum_{k_1,k_2,k_3,k_4} \int \prod_{i=1}^{4} \left(\frac{d\omega_i}{2\pi} \right) K_4(p_1,p_2,p_3,p_4) \lambda(p_1)\lambda(p_2)\lambda(p_3)\lambda(p_4)\delta(p_1+p_2+p_3+p_4) \end{aligned} \tag{A.68}$$

using condensed notation where p_i represents k_i and ω_i. The functions in the action are

given by

$$\begin{aligned} K_3 &= 2\sum_q \int d\Omega \frac{1}{(\Omega^2+|q|^2+\Delta^2)((\Omega+\omega_1)^2+|q+k_1|^2+\Delta^2)((\Omega-\omega_2)^2+|q-k_2|^2+\Delta^2)}, \\ K_4 &= 6\sum_q \int d\Omega \frac{1}{(\Omega^2+|q|^2+\Delta^2)((\Omega+\omega_1)^2+|q+k_1|^2+\Delta^2)} \\ &\times \frac{1}{((\Omega+\omega_1+\omega_2)^2+|q+k_1+k_2|^2+\Delta^2)((\Omega-\omega_4)^2+|q-k_4|^2+\Delta^2)} \end{aligned} \tag{A.69}$$

The propagator for λ can then be computed from these interactions terms. One finds that the order $1/N$ correction to the inverse propagator is given by

$$\begin{aligned} D^{-1}(k,i\omega) &= \Pi(k,i\omega) + \frac{1}{2N\mathcal{A}}\sum_q \int \frac{d\Omega}{2\pi}\left[K_3(k,q,|k+q|)\right]^2 D_0(|k+q|,i\omega+i\Omega)D_0(q,i\Omega) \\ &+ \frac{1}{2N\mathcal{A}}\frac{K_3(k,-k,0)}{\Pi(0,0)}\sum_q \int \frac{d\Omega}{2\pi} K_3(q,-q,0)D_0(q,i\Omega) \\ &+ \frac{1}{6N\mathcal{A}}\sum_q \int \frac{d\Omega}{2\pi}\left[K_4(k,q,-k,-q)+2K_4(k,-k,q,-q)\right]D_0(q,i\Omega), \end{aligned} \tag{A.70}$$

and the spectrum of the singlet states is found by solving $D^{-1}(k,E(k))=0$.

A.7 Correspondence between ϵ and large-N expansions

In this Appendix we take the small-ϵ limit of our large-N results (Chapter 3) and compare them to the large-N limit of the ϵ-expansion (Chapter 2). We find exact agreement where possible in both methods. Here we limit ourselves to $s = s_c$.

In the large-N expansion, one begins by solving the gap equation on the torus, which can be written

$$\frac{1}{\mathcal{A}^{d/2}}\sum_k \frac{1}{\sqrt{k^2+\Delta^2}} = \int \frac{d^dk}{(2\pi)^d}\frac{1}{k}. \tag{A.71}$$

We can evaluate this using the methods of Appendix A.3, where dimensional regularization

sets the integral on the right-hand side to zero, obtaining from Eq. (A.43)

$$\frac{1}{\mathcal{A}^{(3-\epsilon)/2}\Delta}+\frac{\tau_2 L}{2\pi\mathcal{A}^{(3-\epsilon)/2}}f_{1/2}^{(3-\epsilon)}(\Delta^2,\tau,\mu)-\frac{\tau_2 L}{2\pi\mathcal{A}^{(3-\epsilon)/2}}\frac{4\pi\tau_2^{1/2}L^2\Delta^2}{\mu^\epsilon\mathcal{A}^{\epsilon/2}\epsilon}S_{4-\epsilon}=0. \tag{A.72}$$

As $\epsilon\to 0$, the function $f_{1/2}^{(3)}$ is regular, while the last term in Eq. (A.72) diverges. This requires the first term to diverge in the same way, from which one already sees that to leading order $\Delta\sim\epsilon^{1/3}$. Continuing this process, one can explicitly solve Eq (A.72) perturbatively in ϵ, making use of identities derived in Appendix A.3. The gap at $N=\infty$ is given by

$$\sqrt{\mathcal{A}}\Delta=\left(4\pi^2\epsilon\right)^{1/3}+\frac{1}{3}\left(2\pi\right)^{1/3}\sqrt{\tau_2}f_{1/2}^{(3)}(0,\tau)\epsilon^{2/3}-\tau_2^{3/2}\frac{2\left(f_{1/2}^{(3)}(0,\tau)\right)^3+27f_{3/2}^{(3)}(0,\tau)}{162\left(2\pi\right)^{1/3}}\epsilon^{4/3}+\mathcal{O}\left(\epsilon^{5/3}\right) \tag{A.73}$$

where the functions are identical to those defined in Eqs. (A.54-A.56), and the μ-dependence has dropped out.

Once the gap equation has been solved, the Hamiltonian of the theory at $N=\infty$ is given by

$$H=\mathcal{E}_0+P\sum_k\sum_\alpha\sqrt{|k|^2+\Delta^2}b_\alpha^\dagger(k)b_\alpha(k)P+(1-P)\sum_{n,k}E_n(k)b_n^\dagger(k)b_n(k)\left(1-P\right). \tag{A.74}$$

Here,

$$\mathcal{E}_0=\frac{N}{2}\sum_k\sqrt{|k|^2+\Delta^2} \tag{A.75}$$

which should be evaluated order-by-order in ϵ using the techniques in Appendix A.3. The operator P projects onto all states which contain no O(N) singlets. Finally, the energies of the singlet states $E_n(k)$ are the solutions to the equation

$$\Pi(k,E_n(k))=0 \tag{A.76}$$

where

$$\Pi(k,\omega) = \frac{1}{\mathcal{A}^{(3-\epsilon)/2}} \sum_{\mathbf{q}} \frac{\sqrt{q^2+\Delta^2} + \sqrt{(k+q)^2+\Delta^2}}{2\sqrt{(q^2+\Delta^2)((k+q)^2+\Delta^2)}((\sqrt{q^2+\Delta^2}+\sqrt{(k+q)^2+\Delta^2})^2-\omega^2)}. \tag{A.77}$$

We now consider a subset of the above spectrum; specifically, the states created by

$$H_{\text{eff},k=0} = \mathcal{E}_0 + P\sum_{\alpha} \Delta b_\alpha^\dagger(0) b_\alpha(0) P + (1-P)\, E_0(0) b_0^\dagger(0) b_0(0)\,(1-P) \tag{A.78}$$

This Hamiltonian creates two kinds of zero-momentum "particles," with masses Δ and $E_1(0)$ respectively. The particle with mass $E_1(0)$ transforms as an O(N) singlet, while the states with ℓ mass-Δ particles are in the ℓth symmetric traceless tensor representation of O(N). We now argue that $H_{\text{eff},k=0}$ is precisely the $N=\infty$ limit of the Fock vacuum Hamiltonian in the ϵ-expansion.

We saw in Section 2.4 that the solutions to the Fock vacuum Hamiltonian satisfy the equation

$$\frac{1}{2}\left(-\frac{1}{\rho^{N-1}}\frac{\partial}{\partial r}\rho^{N-1}\frac{\partial}{\partial \rho} - \frac{\ell\,(\ell+N-2)}{\rho^{N-1}} + r\rho^2 + 2\rho^4\right) R_{n,\ell}(\rho) = E_{n,\ell} R_{n,\ell}(\rho) \tag{A.79}$$

Recall that this describes states in the ℓth symmetric traceless tensor representation of O(N). We now use the large-N expansion in quantum mechanics. The idea is that the centrifugal term acts as an effective mass at large-N, resulting in a harmonic well at the stationary point of the effective radial potential provided it is well-behaved. For a review of this expansion, see Ref. [145], which gives explicit formulae for the spectrum to leading order in $1/N$. At $N=\infty$ we find the spectrum

$$E_{n,\ell} = \mathcal{E}_0 + \Delta\ell + E_0 n \tag{A.80}$$

where $\mathcal{E}_0$ and Δ agree exactly with their expressions calculated in the large-N expression Eq. (A.78) to order $\epsilon^{4/3}$. Furthermore, while we cannot compare E_0 directly with the first

zero of $\Pi(0,\omega)$, we have evaluated it numerically for small values of ϵ and found very good agreement. Finally, the irreducible representations of the states under the O(N) symmetry agree exactly.

We mention that the $1/N$ expansion in quantum mechanics is an easy way to obtain $1/N$ corrections to the Fock vacuum Hamiltonian compared to the field-theoretic methods in Appendix A.6. One may also attempt to calculate the spectrum for the $k > 0$ effective Hamiltonians using the large-N expansion, which has been successfully applied to non-isotropic Hamiltonians in atomic and molecular physics [145].

Appendix B

Appendix to Chapter 5

B.1 Green's function and large N mass gap on the cylinder

In Section 5.3.2, we used the Green's function for a massive scalar on the infinite cylinder. This is given by

$$G_1(x,x;m^2) = \frac{1}{L}\sum_{k_y}\int \frac{d^2p}{(2\pi)^2}\frac{1}{p^2+k_y^2+m^2} \tag{B.1}$$

where we allow a twist in the finite direction

$$k_y = \frac{2\pi n_y + \varphi_y}{L}, \qquad n_y \in \mathbb{Z} \tag{B.2}$$

We evaluate this expression using Zeta function regularization. We first introduce an extra parameter ν, and consider the expression

$$G_1(x,x;m^2) = \frac{1}{L}\sum_{k_y}\int \frac{d^2p}{(2\pi)^2}\frac{1}{\left(p^2+k_y^2+m^2\right)^{\nu}} \tag{B.3}$$

This expression is convergent for $\nu > 3/2$. We evaluate this expression where it is convergent, and then analytically continue it to $\nu \to 1$. After evaluating the integrals, we obtain

$$G_1(x,x;m^2) = \frac{1}{8\pi^2 L\,(\nu-1)} \sum_{k_y} \frac{1}{\left(k_y^2+m^2\right)^{\nu-1}} \tag{B.4}$$

The remaining sum needs to be evaluated as a function of ν, which requires the use of generalized Zeta functions. General formulae for sums of this type can be found in Reference [146], and after evaluating this sum and taking $\nu \to 1$, we find

$$G_1(x,x;m^2) = -\frac{1}{4\pi L} \log\left[2\left(\cosh mL - \cos\varphi_y\right)\right] \tag{B.5}$$

We note that the original integral, Eq. (B.1), has a linear UV divergence which has been set to zero by our cutoff method. In other regularization methods, one generically expects an extra term proportional to the UV cutoff, $G_1(x,x;m^2) \propto 1/\delta$, which contributes to the area law in Eq. (5.31).

We also find the mass gap for the Wilson-Fisher fixed point at large-N. The gap equation is

$$G_1(x,x;m_1^2) = \frac{1}{g_c} \tag{B.6}$$

However, in Zeta regularization we have

$$\frac{1}{g_c} = \int \frac{d^3p}{(2\pi)^2} \frac{1}{p^2} = 0 \tag{B.7}$$

Then using Eq. (B.5), we find the energy gap on the cylinder

$$m_1 = \frac{1}{L}\operatorname{arccosh}\left(\frac{1}{2} + \cos\varphi_y\right) \tag{B.8}$$

as quoted in the main text.

B.2 Entanglement entropy of the Gross-Neveu model at large N

We discuss the Gross-Neveu model [24] in the large N limit. The calculation of the entanglement entropy is very similar to the critical O(N) model, and we find a mapping to the free fermion entanglement analogous to the mapping derived in Section 5.2.

The critical model is defined by the Euclidean Lagrangian

$$\mathcal{L}_n = -\bar{\psi}_\alpha \left(\not{\partial}_n + \sigma\right) \psi_\alpha + \frac{N}{2g_c^2}\sigma^2 \tag{B.9}$$

where the repeated index α is summed over, running from 1 to N. Here, $\sigma(x)$ is a Hubbard-Stratonovich field used to decouple the quartic interaction term $(\bar{\psi}_\alpha\psi_\alpha)^2$. We now follow the steps in Eq. (5.10) to obtain the partition function using the saddle point method.

$$\log \mathcal{Z}_n = N \ \mathrm{Tr} \log\left(\not{\partial}_n + \langle\sigma\rangle_n\right) - \frac{N}{2g_c^2}\int d^3x_n \ \langle\sigma\rangle_n^2 + \mathcal{O}(1/N) \tag{B.10}$$

The saddle point configuration of σ is determined by the Gross-Neveu gap equation

$$\begin{aligned} \mathrm{Tr}\ G_n^F(x,x;\langle\sigma\rangle_n) =& \frac{\langle\sigma\rangle_n}{g_c^2} \\ \left(\not{\partial}_n + \langle\sigma(x)\rangle_n\right) G_n^F(x,x';\langle\sigma\rangle_n) =& \delta^3(x-x') \end{aligned} \tag{B.11}$$

Here, the trace is over spinor indices and we have left the identity matrix in spinor space implicit. The critical coupling is

$$\frac{1}{g_c^2} = (\mathrm{Tr}\ \mathbb{I}) \int \frac{d^3p}{(2\pi)^3}\frac{1}{p^2} \tag{B.12}$$

Following our procedure for the O(N) model, we write the saddle point configuration as

$$\langle \sigma(x) \rangle_n \approx m_1 + (n-1)\, f(x) \tag{B.13}$$

to leading order in $(n-1)$, for an unknown function $f(x)$. Then by a similar reasoning to the calculations in Section 5.2, we find

$$-\log \frac{\mathcal{Z}_n}{\mathcal{Z}_1^n} = -N \Big[\mathrm{Tr} \log \left(\not{\partial}_n + m_1 \right) - n \mathrm{Tr} \log \left(\not{\partial}_1 + m_1 \right) \Big] \tag{B.14}$$

This is the n-sheeted partition function for N free Dirac fermions with mass m_1, where m_1 is the mass gap of the Gross-Neveu model on the one-sheeted physical spacetime, $\mathrm{Tr}\, G_1^F(x, x; m_1) = m_1/g_c^2$.

Just as for the O(N) Wilson-Fisher fixed point, we can verify our result for the special case where region A is a disk embedded in the infinite plane. The disk's universal entanglement entropy in the Gross-Neveu CFT was found to be that of N free massless Dirac fermions [98], $\gamma_{\mathrm{disk}} = N \gamma_{\mathrm{disk}}^{\mathrm{free}} + \mathcal{O}(N^0)$. This is exactly our result since $m_1 = 0$ for this geometry.

Appendix C

Appendix to Chapter 6

C.1 Spin traces

Here we tabulate spin traces. We give expressions in terms of the index $\mathcal{C}_S$ of the spin-S representation of $SU(2)$,

$$\mathcal{C}_S = \frac{1}{3}(2S+1)S(S+1) \tag{C.1}$$

This is defined as the constant appearing in the bilinear trace

$$\mathrm{Tr}\left(\hat{S}_\alpha \hat{S}_\beta\right) = \mathcal{C}_S \delta_{\alpha\beta} \tag{C.2}$$

Below we give the relevant traces, where we distinguish $\sigma' = 1, 2$ from the $z = 3$ direction. These traces give zero if one replaces one of the two σ' indices with z.

At one-loop, we need the following traces:

$$\begin{aligned}
\mathrm{Tr}\left(\hat{S}_{\alpha'}\hat{S}_{\sigma'}\hat{S}_{\sigma'}\hat{S}_{\beta'}\right) &= \left[\frac{4}{5}S(S+1)-\frac{1}{10}\right]\mathcal{C}_S\delta_{\alpha'\beta'} = \mathcal{S}_1'\mathcal{C}_S\delta_{\alpha'\beta'} \\
\mathrm{Tr}\left(\hat{S}_{z}\hat{S}_{\sigma'}\hat{S}_{\sigma'}\hat{S}_{z}\right) &= \left[\frac{2}{5}S(S+1)+\frac{1}{5}\right]\mathcal{C}_S = \mathcal{S}_1^z\mathcal{C}_S \\
\mathrm{Tr}\left(\hat{S}_{\alpha'}\hat{S}_{\sigma'}\hat{S}_{\beta'}\hat{S}_{\sigma'}\right) &= \left[\frac{4}{5}S(S+1)-\frac{3}{5}\right]\mathcal{C}_S\delta_{\alpha'\beta'} = \mathcal{S}_2'\mathcal{C}_S\delta_{\alpha'\beta'} \\
\mathrm{Tr}\left(\hat{S}_{z}\hat{S}_{\sigma'}\hat{S}_{z}\hat{S}_{\sigma'}\right) &= \left[\frac{2}{5}S(S+1)-\frac{4}{5}\right]\mathcal{C}_S = \mathcal{S}_2^z\mathcal{C}_S
\end{aligned} \tag{C.3}$$

At two-loop:

$$\begin{aligned}
\mathrm{Tr}\left(\hat{S}_{\alpha'}\hat{S}_{\sigma'}\hat{S}_{\sigma'}\hat{S}_{\eta'}\hat{S}_{\eta'}\hat{S}_{\beta'}\right) &= \frac{\mathcal{C}_S}{70}\left[48\ S^2(S+1)^2-6S(S+1)-5\right]\delta_{\alpha'\beta'} = \mathcal{S}_3'\mathcal{C}_S\delta_{\alpha'\beta'} \\
\mathrm{Tr}\left(\hat{S}_{z}\hat{S}_{\sigma'}\hat{S}_{\sigma'}\hat{S}_{\eta'}\hat{S}_{\eta'}\hat{S}_{z}\right) &= \frac{\mathcal{C}_S}{35}\left[8\ S^2(S+1)^2-S(S+1)+5\right] = \mathcal{S}_3^z\mathcal{C}_S \\
\mathrm{Tr}\left(\hat{S}_{\alpha'}\hat{S}_{\sigma'}\hat{S}_{\sigma'}\hat{S}_{\eta'}\hat{S}_{\beta'}\hat{S}_{\eta'}\right) &= \frac{\mathcal{C}_S}{70}\left[48\ S^2(S+1)^2-48S(S+1)+9\right]\delta_{\alpha'\beta'} = \mathcal{S}_4'\mathcal{C}_S\delta_{\alpha'\beta'} \\
\mathrm{Tr}\left(\hat{S}_{z}\hat{S}_{\sigma'}\hat{S}_{\sigma'}\hat{S}_{\eta'}\hat{S}_{z}\hat{S}_{\eta'}\right) &= \frac{\mathcal{C}_S}{35}\left[8\ S^2(S+1)^2-15S(S+1)-2\right] = \mathcal{S}_4^z\mathcal{C}_S \\
\mathrm{Tr}\left(\hat{S}_{\alpha'}\hat{S}_{\sigma'}\hat{S}_{\sigma'}\hat{S}_{\beta'}\hat{S}_{\eta'}\hat{S}_{\eta'}\right) &= \frac{\mathcal{C}_S}{35}\left[24\ S^2(S+1)^2-17S(S+1)+8\right]\delta_{\alpha'\beta'} = \mathcal{S}_5'\mathcal{C}_S\delta_{\alpha'\beta'} \\
\mathrm{Tr}\left(\hat{S}_{z}\hat{S}_{\sigma'}\hat{S}_{\sigma'}\hat{S}_{z}\hat{S}_{\eta'}\hat{S}_{\eta'}\right) &= \frac{\mathcal{C}_S}{35}\left[8\ S^2(S+1)^2-S(S+1)+5\right] = \mathcal{S}_5^z\mathcal{C}_S \\
\mathrm{Tr}\left(\hat{S}_{\alpha'}\hat{S}_{\sigma'}\hat{S}_{\eta'}\hat{S}_{\eta'}\hat{S}_{\sigma'}\hat{S}_{\beta'}\right) &= \frac{\mathcal{C}_S}{35}\left[24\ S^2(S+1)^2-17S(S+1)+8\right]\delta_{\alpha'\beta'} = \mathcal{S}_6'\mathcal{C}_S\delta_{\alpha'\beta'} \\
\mathrm{Tr}\left(\hat{S}_{z}\hat{S}_{\sigma'}\hat{S}_{\eta'}\hat{S}_{\eta'}\hat{S}_{\sigma'}\hat{S}_{z}\right) &= \frac{\mathcal{C}_S}{35}\left[8\ S^2(S+1)^2+27S(S+1)-16\right] = \mathcal{S}_6^z\mathcal{C}_S \\
\mathrm{Tr}\left(\hat{S}_{\alpha'}\hat{S}_{\sigma'}\hat{S}_{\eta'}\hat{S}_{\beta'}\hat{S}_{\eta'}\hat{S}_{\sigma'}\right) &= \frac{\mathcal{C}_S}{35}\left[24\ S^2(S+1)^2-38S(S+1)+15\right]\delta_{\alpha'\beta'} = \mathcal{S}_7'\mathcal{C}_S\delta_{\alpha'\beta'} \\
\mathrm{Tr}\left(\hat{S}_{z}\hat{S}_{\sigma'}\hat{S}_{\eta'}\hat{S}_{z}\hat{S}_{\eta'}\hat{S}_{\sigma'}\right) &= \frac{\mathcal{C}_S}{35}\left[8\ S^2(S+1)^2-29S(S+1)+26\right] = \mathcal{S}_7^z\mathcal{C}_S \\
\mathrm{Tr}\left(\hat{S}_{\alpha'}\hat{S}_{\sigma'}\hat{S}_{\eta'}\hat{S}_{\sigma'}\hat{S}_{\eta'}\hat{S}_{\beta'}\right) &= \frac{\mathcal{C}_S}{70}\left[48\ S^2(S+1)^2-48S(S+1)+9\right]\delta_{\alpha'\beta'} = \mathcal{S}_8'\mathcal{C}_S\delta_{\alpha'\beta'} \\
\mathrm{Tr}\left(\hat{S}_{z}\hat{S}_{\sigma'}\hat{S}_{\eta'}\hat{S}_{\sigma'}\hat{S}_{\eta'}\hat{S}_{z}\right) &= \frac{\mathcal{C}_S}{35}\left[8\ S^2(S+1)^2+6S(S+1)-9\right] = \mathcal{S}_8^z\mathcal{C}_S \\
\mathrm{Tr}\left(\hat{S}_{\alpha'}\hat{S}_{\sigma'}\hat{S}_{\eta'}\hat{S}_{\sigma'}\hat{S}_{\beta'}\hat{S}_{\eta'}\right) &= \frac{\mathcal{C}_S}{35}\left[24\ S^2(S+1)^2-38S(S+1)+15\right]\delta_{\alpha'\beta'} = \mathcal{S}_9'\mathcal{C}_S\delta_{\alpha'\beta'} \\
\mathrm{Tr}\left(\hat{S}_{z}\hat{S}_{\sigma'}\hat{S}_{\eta'}\hat{S}_{\sigma'}\hat{S}_{z}\hat{S}_{\eta'}\right) &= \frac{\mathcal{C}_S}{35}\left[8\ S^2(S+1)^2-22S(S+1)+12\right] = \mathcal{S}_9^z\mathcal{C}_S \\
\mathrm{Tr}\left(\hat{S}_{\alpha'}\hat{S}_{\sigma'}\hat{S}_{\eta'}\hat{S}_{\beta'}\hat{S}_{\sigma'}\hat{S}_{\eta'}\right) &= \frac{\mathcal{C}_S}{35}\left[24\ S^2(S+1)^2-45S(S+1)+29\right]\delta_{\alpha'\beta'} = \mathcal{S}_{10}'\mathcal{C}_S\delta_{\alpha'\beta'}
\end{aligned}$$

$$\mathrm{Tr}\left(\hat{S}_z\hat{S}_{\sigma'}\hat{S}_{\eta'}\hat{S}_z\hat{S}_{\sigma'}\hat{S}_{\eta'}\right) = \frac{\mathcal{C}_S}{35}\left[8\ S^2(S+1)^2 - 50S(S+1) + 33\right] = \mathcal{S}^z_{10}\mathcal{C}_S \tag{C.4}$$

C.2 Details of the two-loop calculation

In this appendix we detail some of the intermediate steps in the calculation of the two-loop contribution to the spin-spin correlation function quoted in Eqns. (6.37)-(6.38).

The relevant diagrams are pictured in Figures C.2.1 and C.2.2. Here, we have grouped the diagrams into three groups (a), (b), and (c). This is because, like the one-loop calculation in the main text, the three diagrams contributing to the denominator can be rewritten so that they are the sum of the diagrams in the numerator. Then we only need to compute the 15 diagrams which follow from the integrals pictured in Figure C.2.1, while keeping track of the difference in spin traces between the numerator and denominator. In the $O(3)$ symmetric case considered in Reference [136], this resulted in large cancellations and only 7 diagrams need to be computed. In contrast, there are no cancellations here, and all 15 diagrams need to calculated.

We label the loop integrals which follow from Figure C.2.1 as $\mathcal{I}_i$ for $i = 1, 2, ..., 15$, where we label the integrals from left-to-right and top-to-bottom according to the figure. In terms

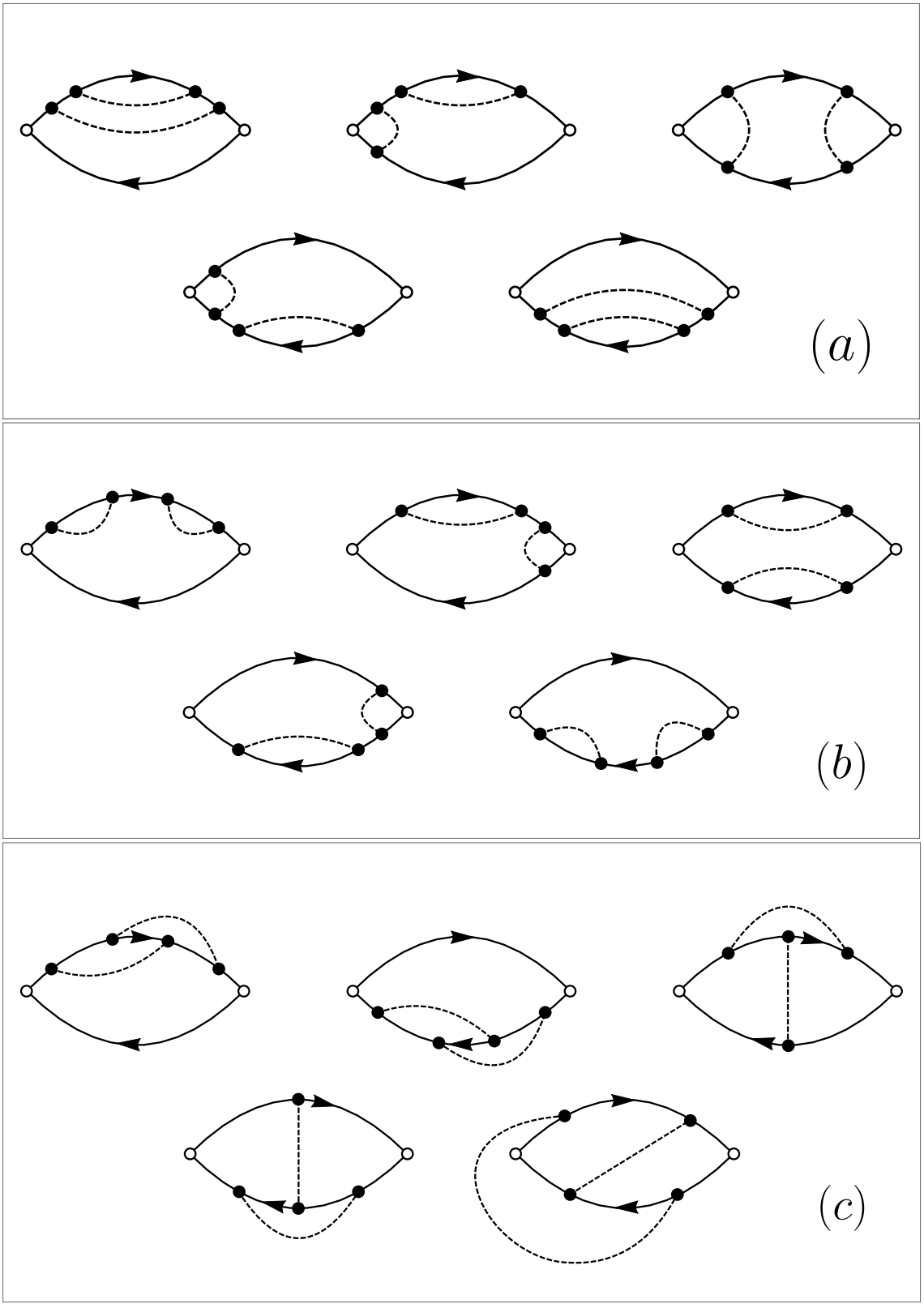

Figure C.2.1: The diagrams contributing to the numerator of the two-point function at two-loop.

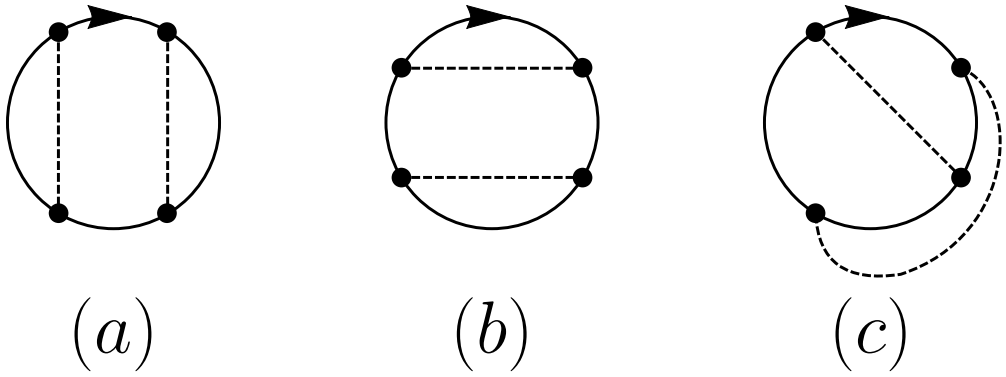

Figure C.2.2: The diagrams contributing to the denominator of the two-point function at two-loop.

of these integrals, the two-loop contribution to $\mathcal{G}$ is

$$\begin{aligned}
\mathcal{G}^{(\text{two-loop})} &= \frac{S(S+1)}{3}\gamma_0^4\Bigg\{\left[\mathcal{S}_6 - \frac{2S(S+1)}{3}\mathcal{S}_1'\right]\mathcal{I}_1 + \left[\mathcal{S}_4 - \frac{2S(S+1)}{3}\mathcal{S}_1'\right]\mathcal{I}_2 \\
&+ \left[\mathcal{S}_7 - \frac{2S(S+1)}{3}\mathcal{S}_1'\right]\mathcal{I}_3 + \left[\mathcal{S}_4 - \frac{2S(S+1)}{3}\mathcal{S}_1'\right]\mathcal{I}_4 \\
&+ \left[\mathcal{S}_6 - \frac{2S(S+1)}{3}\mathcal{S}_1'\right]\mathcal{I}_5 + \left[\mathcal{S}_3 - \frac{2S(S+1)}{3}\mathcal{S}_1'\right]\mathcal{I}_6 \\
&+ \left[\mathcal{S}_4 - \frac{2S(S+1)}{3}\mathcal{S}_1'\right]\mathcal{I}_7 + \left[\mathcal{S}_5 - \frac{2S(S+1)}{3}\mathcal{S}_1'\right]\mathcal{I}_8 \\
&+ \left[\mathcal{S}_4 - \frac{2S(S+1)}{3}\mathcal{S}_1'\right]\mathcal{I}_9 + \left[\mathcal{S}_3 - \frac{2S(S+1)}{3}\mathcal{S}_1'\right]\mathcal{I}_{10} \\
&+ \left[\mathcal{S}_8 - \frac{2S(S+1)}{3}\mathcal{S}_2'\right]\mathcal{I}_{11} + \left[\mathcal{S}_8 - \frac{2S(S+1)}{3}\mathcal{S}_2'\right]\mathcal{I}_{12} \\
&+ \left[\mathcal{S}_9 - \frac{2S(S+1)}{3}\mathcal{S}_2'\right]\mathcal{I}_{13} + \left[\mathcal{S}_9 - \frac{2S(S+1)}{3}\mathcal{S}_2'\right]\mathcal{I}_{14} \\
&+ \left[\mathcal{S}_{10} - \frac{2S(S+1)}{3}\mathcal{S}_2'\right]\mathcal{I}_{15}\Bigg\}
\end{aligned} \tag{C.5}$$

Within each bracket, the first spin sum is either $\mathcal{S}'$ or $\mathcal{S}^z$ depending on whether one wants the two point correlator $\mathcal{G}'$ or $\mathcal{G}^z$. We note that the denominator Z also contains an order γ_0^4 term from expanding the one-loop contribution to second order, but this contribution vanishes in dimensional regularization.

We now evaluate the 15 integrals above. Below, we will give the $T > 0$ integrals for each integral which follow from the diagrams in Fig. C.2.1, and then state the evaluation of the

divergent piece of the $T = 0$ limit. We take this limit according to the prescription described below Eq. 6.29 in the main text.

$$\begin{aligned} \mathcal{I}_1 &= \int_0^\tau d\tau_1 \int_{\tau_1}^\tau d\tau_2 \int_{\tau_1}^{\tau_2} d\tau_3 \int_{\tau_3}^{\tau_2} d\tau_4 D(\tau_1-\tau_2)D(\tau_3-\tau_4) \\ &\overset{\beta\to\infty}{\Longrightarrow} \left(\tilde{S}_{d+1}\tau^\epsilon\right)^2 \left(\frac{1}{2\epsilon^2}+\frac{3}{2\epsilon}+\cdots\right) \end{aligned} \tag{C.6}$$

$$\begin{aligned} \mathcal{I}_2 &= \int_0^\tau d\tau_1 \int_{\tau}^\beta d\tau_2 \int_{\tau_1}^{\tau} d\tau_3 \int_{\tau_3}^{\tau} d\tau_4 D(\tau_1-\tau_2)D(\tau_3-\tau_4) \\ &\overset{\beta\to\infty}{\Longrightarrow} \left(\tilde{S}_{d+1}\tau^\epsilon\right)^2 \left(-\frac{3}{2\epsilon^2}-\frac{3}{\epsilon}+\cdots\right) \end{aligned} \tag{C.7}$$

$$\begin{aligned} \mathcal{I}_3 &= \int_0^\tau d\tau_1 \int_{\tau}^\beta d\tau_2 \int_{\tau_1}^{\tau} d\tau_3 \int_{\tau}^{\tau_2} d\tau_4 D(\tau_1-\tau_2)D(\tau_3-\tau_4) \\ &\overset{\beta\to\infty}{\Longrightarrow} \left(\tilde{S}_{d+1}\tau^\epsilon\right)^2 \left(\frac{2}{\epsilon^2}+\frac{3}{\epsilon}+\cdots\right) \end{aligned} \tag{C.8}$$

$$\begin{aligned} \mathcal{I}_4 &= \int_0^\tau d\tau_1 \int_{\tau}^\beta d\tau_2 \int_{\tau}^{\tau_2} d\tau_3 \int_{\tau}^{\tau_3} d\tau_4 D(\tau_1-\tau_2)D(\tau_3-\tau_4) \\ &\overset{\beta\to\infty}{\Longrightarrow} \left(\tilde{S}_{d+1}\tau^\epsilon\right)^2 \left(-\frac{3}{2\epsilon^2}-\frac{3}{\epsilon}+\cdots\right) \end{aligned} \tag{C.9}$$

$$\begin{aligned} \mathcal{I}_5 &= \int_{\tau}^\beta d\tau_1 \int_{\tau}^{\tau_1} d\tau_2 \int_{\tau_2}^{\tau_1} d\tau_3 \int_{\tau_2}^{\tau_3} d\tau_4 D(\tau_1-\tau_2)D(\tau_3-\tau_4) \\ &\overset{\beta\to\infty}{\Longrightarrow} \left(\tilde{S}_{d+1}\tau^\epsilon\right)^2 \left(\frac{1}{2\epsilon^2}+\frac{3}{2\epsilon}+\cdots\right) \end{aligned} \tag{C.10}$$

$$\begin{aligned}\mathcal{I}_6 &= \int_0^\tau d\tau_1 \int_{\tau_1}^\tau d\tau_2 \int_{\tau_2}^\tau d\tau_3 \int_{\tau_3}^\tau d\tau_4 D(\tau_1-\tau_2)D(\tau_3-\tau_4) \\ &\overset{\beta\to\infty}{\Longrightarrow} \left(\tilde{S}_{d+1}\tau^\epsilon\right)^2 \left(\frac{1}{\epsilon^2}+\frac{2}{\epsilon}+\cdots\right) \end{aligned} \tag{C.11}$$

$$\begin{aligned}\mathcal{I}_7 &= \int_0^\tau d\tau_1 \int_{\tau_1}^\tau d\tau_2 \int_{\tau_2}^\tau d\tau_3 \int_{\tau}^\beta d\tau_4 D(\tau_1-\tau_2)D(\tau_3-\tau_4) \\ &\overset{\beta\to\infty}{\Longrightarrow} \left(\tilde{S}_{d+1}\tau^\epsilon\right)^2 \left(-\frac{3}{2\epsilon^2}-\frac{3}{\epsilon}+\cdots\right) \end{aligned} \tag{C.12}$$

$$\begin{aligned}\mathcal{I}_8 &= \int_0^\tau d\tau_1 \int_{\tau_1}^\tau d\tau_2 \int_{\tau}^\beta d\tau_3 \int_{\tau_3}^\beta d\tau_4 D(\tau_1-\tau_2)D(\tau_3-\tau_4) \\ &\overset{\beta\to\infty}{\Longrightarrow} \left(\tilde{S}_{d+1}\tau^\epsilon\right)^2 \left(\frac{1}{\epsilon^2}+\frac{2}{\epsilon}+\cdots\right) \end{aligned} \tag{C.13}$$

$$\begin{aligned}\mathcal{I}_9 &= \int_0^\tau d\tau_1 \int_{\tau}^\beta d\tau_2 \int_{\tau_2}^\beta d\tau_3 \int_{\tau_3}^\beta d\tau_4 D(\tau_1-\tau_2)D(\tau_3-\tau_4) \\ &\overset{\beta\to\infty}{\Longrightarrow} \left(\tilde{S}_{d+1}\tau^\epsilon\right)^2 \left(-\frac{3}{2\epsilon^2}-\frac{3}{\epsilon}+\cdots\right) \end{aligned} \tag{C.14}$$

$$\begin{aligned}\mathcal{I}_{10} &= \int_{\tau}^\beta d\tau_1 \int_{\tau_1}^\beta d\tau_2 \int_{\tau_2}^\beta d\tau_3 \int_{\tau_3}^\beta d\tau_4 D(\tau_1-\tau_2)D(\tau_3-\tau_4) \\ &\overset{\beta\to\infty}{\Longrightarrow} \left(\tilde{S}_{d+1}\tau^\epsilon\right)^2 \left(\frac{1}{\epsilon^2}+\frac{2}{\epsilon}+\cdots\right) \end{aligned} \tag{C.15}$$

$$\begin{aligned}\mathcal{I}_{11} &= \int_0^\tau d\tau_1 \int_{\tau_1}^\tau d\tau_2 \int_{\tau_1}^{\tau_2} d\tau_3 \int_{\tau_2}^\tau d\tau_4 D(\tau_1-\tau_2)D(\tau_3-\tau_4) \\ &\overset{\beta\to\infty}{\Longrightarrow} \left(\tilde{S}_{d+1}\tau^\epsilon\right)^2 \left(-\frac{1}{\epsilon^2}-\frac{5}{2\epsilon}\right) \end{aligned} \tag{C.16}$$

$$\begin{aligned}\mathcal{I}_{12} &= \int_{\tau}^{\beta} d\tau_1 \int_{\tau}^{\tau_1} d\tau_2 \int_{\tau_2}^{\tau_1} d\tau_3 \int_{\tau}^{\tau_2} d\tau_4 D(\tau_1-\tau_2)D(\tau_3-\tau_4) \\ &\overset{\beta\to\infty}{\Longrightarrow} \left(\tilde{S}_{d+1}\tau^{\epsilon}\right)^2 \left(-\frac{1}{\epsilon^2}-\frac{5}{2\epsilon}\right) \end{aligned} \tag{C.17}$$

$$\begin{aligned}\mathcal{I}_{13} &= \int_{0}^{\tau} d\tau_1 \int_{\tau}^{\beta} d\tau_2 \int_{\tau}^{\tau_2} d\tau_3 \int_{\tau_2}^{\beta} d\tau_4 D(\tau_1-\tau_2)D(\tau_3-\tau_4) \\ &\overset{\beta\to\infty}{\Longrightarrow} \left(\tilde{S}_{d+1}\tau^{\epsilon}\right)^2 \left(\frac{1}{\epsilon^2}+\frac{2}{\epsilon}+\cdots\right) \end{aligned} \tag{C.18}$$

$$\begin{aligned}\mathcal{I}_{14} &= \int_{0}^{\tau} d\tau_1 \int_{\tau}^{\beta} d\tau_2 \int_{0}^{\tau_1} d\tau_3 \int_{\tau_1}^{\tau} d\tau_4 D(\tau_1-\tau_2)D(\tau_3-\tau_4) \\ &\overset{\beta\to\infty}{\Longrightarrow} \left(\tilde{S}_{d+1}\tau^{\epsilon}\right)^2 \left(\frac{1}{\epsilon^2}+\frac{2}{\epsilon}+\cdots\right) \end{aligned} \tag{C.19}$$

$$\begin{aligned}\mathcal{I}_{15} &= \int_{0}^{\tau} d\tau_1 \int_{\tau}^{\beta} d\tau_2 \int_{0}^{\tau_1} d\tau_3 \int_{\tau}^{\tau_2} d\tau_4 D(\tau_1-\tau_2)D(\tau_3-\tau_4) \\ &\overset{\beta\to\infty}{\Longrightarrow} \left(\tilde{S}_{d+1}\tau^{\epsilon}\right)^2 \left(\frac{1}{\epsilon}+\cdots\right) \end{aligned} \tag{C.20}$$

Plugging these values into Eq. (C.5) and simplifying gives the full two-loop expression used in Eq. (6.38) in the main text.

References

[1] A. Pelissetto and E. Vicari, Physics Reports **368**, 549 (2002).

[2] L. Landau and E. Lifshitz, *Statistical Physics*, Vol. 5 (Elsevier Science, 2013).

[3] K. G. Wilson and J. Kogut, Physics Reports **12**, 75 (1974).

[4] K. G. Wilson and M. E. Fisher, Phys. Rev. Lett. **28**, 240 (1972).

[5] P. D. Francesco, P. Mathieu, and D. Sénéchal, *Conformal Field Theory*, Graduate Texts in Contemporary Physics (Springer, New York, 1997).

[6] S. El-Showk, M. F. Paulos, D. Poland, S. Rychkov, D. Simmons-Duffin, and A. Vichi, Phys. Rev. D **86**, 025022 (2012), arXiv:1403.4545 .

[7] S. El-Showk, M. F. Paulos, D. Poland, S. Rychkov, D. Simmons-Duffin, and A. Vichi, J. Stat. Phys. **157**, 869 (2014), arXiv:1403.4545v2 .

[8] P. C. Hohenberg and B. I. Halperin, Rev. Mod. Phys. **49**, 435 (1977).

[9] S. Sachdev, *Quantum Phase Transitions*, 2nd ed. (Cambridge University Press, Cambridge, UK, 2011).

[10] J. L. Cardy, Journal of Physics A: Mathematical and General **18**, L757 (1985).

[11] H. Casini and M. Huerta, Phys. Rev. D **85**, 125016 (2012), arXiv:1202.5650 [hep-th] .

[12] M. Greiner, O. Mandel, T. Esslinger, T. W. Hänsch, and I. Bloch, Nature **415**, 39 (2002).

[13] J. L. Cardy, Journal of Physics A: Mathematical and General **17**, L385 (1984).

[14] F. Kos, D. Poland, and D. Simmons-Duffin, J. High Energ. Phys. **2014**, 91 (2014), arXiv:1307.6856 .

[15] F. Kos, D. Poland, and D. Simmons-Duffin, J. High Energ. Phys. **2014**, 109 (2014), arXiv:1406.4858 .

[16] F. Kos, D. Poland, D. Simmons-Duffin, and A. Vichi, J. High Energ. Phys. **2016**, 36 (2016), arXiv:1603.04436 .

[17] A. Feiguin, S. Trebst, A. W. W. Ludwig, M. Troyer, A. Kitaev, Z. Wang, and M. H. Freedman, Phys. Rev. Lett. **98**, 160409 (2007).

[18] H. Suwa and S. Todo, Phys. Rev. Lett. **115**, 080601 (2015), arXiv:1402.0847 .

[19] F. C. Alcaraz and H. J. Herrmann, J. Phys. A. Math. Gen. **20**, 5735 (1987).

[20] M. Weigel and W. Janke, Europhys. Lett. **51**, 578 (2000), arXiv:0008292 [cond-mat] .

[21] Y. Deng and H. W. J. Blöte, Phys. Rev. Lett. **88**, 190602 (2002).

[22] R. C. Brower, G. T. Fleming, and H. Neuberger, Phys. Lett. B **721**, 299 (2013), arXiv:1212.6190v1 .

[23] R. C. Brower, G. Fleming, A. Gasbarro, T. Raben, C.-I. Tan, and E. Weinberg, In proceedings "The 33rd International Symposium on Lattice Field Theory (Lattice 2015)" **PoS(LATTICE 2015)296** (2016), arXiv:1601.01367 .

[24] J. Zinn-Justin, *Quantum Field Theory and Critical Phenomena*, International series of monographs on physics (Clarendon Press, 2002).

[25] M. Lüscher, Physics Letters B **118**, 391 (1982).

[26] E. Brezin and J. Zinn-Justin, Nuclear Physics B **257**, 867 (1985).

[27] J. Rudnick, H. Guo, and D. Jasnow, Journal of Statistical Physics **41**, 353 (1985).

[28] M. Lüscher, Nuclear Physics B **219**, 233 (1983).

[29] C. Bloch, Nuclear Physics **6**, 329 (1958).

[30] L. Skála, J. Cízek, and J. Zamastil, Journal of Physics A: Mathematical and General **32**, 5715 (1999).

[31] E. Stein and G. Weiss, *Introduction to Fourier Analysis on Euclidean Spaces*, Mathematical Series (Princeton University Press, 1971).

[32] C. K. Au and Y. Aharonov, Phys. Rev. A **20**, 2245 (1979).

[33] Y. Aharonov and C. K. Au, Phys. Rev. Lett. **42**, 1582 (1979).

[34] M. Schuler, S. Whitsitt, L.-P. Henry, S. Sachdev, and A. M. Läuchli, Phys. Rev. Lett. **117**, 210401 (2016).

[35] Z. Zhang, K. Wierschem, I. Yap, Y. Kato, C. D. Batista, and P. Sengupta, Phys. Rev. B **87**, 174405 (2013).

[36] E. M. Stoudenmire, P. Gustainis, R. Johal, S. Wessel, and R. G. Melko, Phys. Rev. B **90**, 235106 (2014), arXiv:1401.3504 .

[37] J. Helmes and S. Wessel, Phys. Rev. B **92**, 125120 (2015), arXiv:1411.7773v1 .

[38] S. Whitsitt, M. Schuler, L.-P. Henry, A. M. Läuchli, and S. Sachdev, Phys. Rev. B **96**, 035142 (2017).

[39] A. W. Sandvik and D. J. Scalapino, Phys. Rev. Lett. **72**, 2777 (1994).

[40] L. Wang, K. S. D. Beach, and A. W. Sandvik, Phys. Rev. B **73**, 014431 (2006), arXiv:0509747 [cond-mat] .

[41] M. Lohöfer, T. Coletta, D. G. Joshi, F. F. Assaad, M. Vojta, S. Wessel, and F. Mila, Phys. Rev. B **92**, 245137 (2015), arXiv:1508.07816 .

[42] Y. Nishiyama, Eur. Phys. J. B **89**, 31 (2016), arXiv:1601.04772 .

[43] S. Wenzel and W. Janke, Phys. Rev. B **79**, 014410 (2009), arXiv:0808.1418 .

[44] M. Matsumoto, C. Yasuda, S. Todo, and H. Takayama, Phys. Rev. B **65**, 014407 (2001).

[45] M. Hasenbusch and E. Vicari, Phys. Rev. B **84**, 125136 (2011).

[46] A. Polyakov, *Gauge fields and Strings* (Harwood Academic, New York, 1987).

[47] D. Podolsky and S. Sachdev, Phys. Rev. B **86**, 054508 (2012), arXiv:1205.2700 [cond-mat.quant-gas] .

[48] P. W. Anderson, Phys. Rev. **86**, 694 (1952).

[49] M. Gross, E. Sánchez-Velasco, and E. D. Siggia, Phys. Rev. B **40**, 11328 (1989).

[50] B. Bernu, C. Lhuillier, and L. Pierre, Phys. Rev. Lett. **69**, 2590 (1992).

[51] B. Bernu, P. Lecheminant, C. Lhuillier, and L. Pierre, Phys. Rev. B **50**, 10048 (1994), cond-mat/9407028 .

[52] P. Azaria, B. Delamotte, and D. Mouhanna, Phys. Rev. Lett. **70**, 2483 (1993).

[53] S. R. White and A. L. Chernyshev, Physical Review Letters **99**, 127004 (2007), arXiv:0705.2746 [cond-mat.str-el] .

[54] X. G. Wen, International Journal of Modern Physics B **04**, 239 (1990), https://www.worldscientific.com/doi/pdf/10.1142/S0217979290000139 .

[55] X. Wen, *Quantum Field Theory of Many-Body Systems: From the Origin of Sound to an Origin of Light and Electrons*, Oxford Graduate Texts (OUP Oxford, 2004).

[56] T. Senthil, A. Vishwanath, L. Balents, S. Sachdev, and M. P. A. Fisher, Science **303**, 1490 (2004), http://science.sciencemag.org/content/303/5663/1490.full.pdf .

[57] T. Senthil, L. Balents, S. Sachdev, A. Vishwanath, and M. P. A. Fisher, Phys. Rev. B **70**, 144407 (2004).

[58] N. Read and B. Chakraborty, Phys. Rev. B **40**, 7133 (1989).

[59] N. Read and S. Sachdev, Phys. Rev. Lett. **66**, 1773 (1991).

[60] X. G. Wen, Phys. Rev. B **44**, 2664 (1991).

[61] T. Hansson, V. Oganesyan, and S. Sondhi, Annals of Physics **313**, 497 (2004).

[62] F. J. Wegner, Journal of Mathematical Physics **12**, 2259 (1971), https://doi.org/10.1063/1.1665530 .

[63] E. Fradkin and S. H. Shenker, Phys. Rev. D **19**, 3682 (1979).

[64] T. Senthil and M. P. A. Fisher, Phys. Rev. B **62**, 7850 (2000), cond-mat/9910224 .

[65] S. Sachdev, Phys. Rev. B **45**, 12377 (1992).

[66] R. A. Jalabert and S. Sachdev, Phys. Rev. B **44**, 686 (1991).

[67] S. Sachdev and M. Vojta, J. Phys. Soc. Jpn **69**, Supp. B, 1 (1999), cond-mat/9910231 .

[68] R. Moessner and S. Sondhi, Phys. Rev. Lett. **86**, 1881 (2001).

[69] R. Moessner, S. L. Sondhi, and E. Fradkin, Phys. Rev. B **65**, 024504 (2001), cond-mat/0103396 .

[70] K. Hwang, Y. Huh, and Y. B. Kim, Phys. Rev. B **92**, 205131 (2015), arXiv:1507.04747 [cond-mat.str-el] .

[71] Y.-C. Wang, Y. Qi, S. Chen, and Z. Y. Meng, Phys. Rev. B **96**, 115160 (2017).

[72] A. A. Patel, D. Chowdhury, A. Allais, and S. Sachdev, Phys. Rev. B **93**, 165139 (2016), arXiv:1602.05954 [cond-mat.str-el] .

[73] A. V. Chubukov, T. Senthil, and S. Sachdev, Phys. Rev. Lett. **72**, 2089 (1994), cond-mat/9311045 .

[74] A. V. Chubukov, S. Sachdev, and T. Senthil, Nuclear Physics B **426**, 601 (1994), cond-mat/9402006 .

[75] S. V. Isakov, R. G. Melko, and M. B. Hastings, Science **335**, 193 (2012), http://science.sciencemag.org/content/335/6065/193.full.pdf .

[76] B. Swingle and T. Senthil, Phys. Rev. B **86**, 155131 (2012), arXiv:1109.3185 [cond-mat.str-el] .

[77] A. Y. Kitaev, Annals of Physics **303**, 2 (2003), quant-ph/9707021 .

[78] S. Trebst, P. Werner, M. Troyer, K. Shtengel, and C. Nayak, Phys. Rev. Lett. **98**, 070602 (2007).

[79] I. S. Tupitsyn, A. Kitaev, N. V. Prokof'ev, and P. C. E. Stamp, Physical Review B **82**, 085114 (2010), arXiv:arXiv:0804.3175v1 .

[80] J. Vidal, S. Dusuel, and K. P. Schmidt, Physical Review B **79**, 033109 (2009).

[81] F. Wu, Y. Deng, and N. Prokof'ev, Physical Review B **85**, 195104 (2012).

[82] Z. Zhu and S. R. White, Phys. Rev. B **92**, 041105 (2015), arXiv:1502.04831 [cond-mat.str-el] .

[83] W.-J. Hu, S.-S. Gong, W. Zhu, and D. N. Sheng, Phys. Rev. B **92**, 140403 (2015), arXiv:1504.00654 [cond-mat.str-el] .

[84] M. B. Hastings, Phys. Rev. B **69**, 104431 (2004), cond-mat/0305505 .

[85] S. V. Isakov, T. Senthil, and Y. B. Kim, Phys. Rev. B **72**, 174417 (2005).

[86] P. Calabrese and J. Cardy, J. Stat. Mech. **6**, 06002 (2004), hep-th/0405152 .

[87] S. Ryu and T. Takayanagi, Phys. Rev. Lett. **96**, 181602 (2006), arXiv:hep-th/0603001 [hep-th] .

[88] A. Kitaev and J. Preskill, Physical Review Letters **96**, 110404 (2006), hep-th/0510092 .

[89] M. Levin and X.-G. Wen, Physical Review Letters **96**, 110405 (2006), cond-mat/0510613 .

[90] E. Fradkin and J. E. Moore, Physical Review Letters **97**, 050404 (2006), cond-mat/0605683 .

[91] S. Dong, E. Fradkin, R. G. Leigh, and S. Nowling, Journal of High Energy Physics **5**, 016 (2008), arXiv:0802.3231 [hep-th] .

[92] B. Hsu, M. Mulligan, E. Fradkin, and E.-A. Kim, Phys. Rev. B **79**, 115421 (2009), arXiv:0812.0203 [cond-mat.stat-mech] .

[93] M. A. Metlitski, C. A. Fuertes, and S. Sachdev, Phys. Rev. B **80**, 115122 (2009), arXiv:0904.4477 [cond-mat.stat-mech] .

[94] Y. Zhang, T. Grover, A. Turner, M. Oshikawa, and A. Vishwanath, Phys. Rev. B **85**, 235151 (2012), arXiv:1111.2342 [cond-mat.str-el] .

[95] R. C. Myers and A. Sinha, Phys. Rev. D **82**, 046006 (2010), arXiv:1006.1263 [hep-th] .

[96] R. C. Myers and A. Sinha, JHEP **01**, 125 (2011), arXiv:1011.5819 [hep-th] .

[97] D. L. Jafferis, I. R. Klebanov, S. S. Pufu, and B. R. Safdi, JHEP **06**, 102 (2011), arXiv:1103.1181 [hep-th] .

[98] I. R. Klebanov, S. S. Pufu, and B. R. Safdi, JHEP **10**, 038 (2011), arXiv:1105.4598 [hep-th] .

[99] I. R. Klebanov, S. S. Pufu, S. Sachdev, and B. R. Safdi, JHEP **05**, 036 (2012), arXiv:1112.5342 [hep-th] .

[100] T. Grover, Phys. Rev. Lett. **112**, 151601 (2014), arXiv:1211.1392 [hep-th] .

[101] N. Ogawa, T. Takayanagi, and T. Ugajin, JHEP **01**, 125 (2012), arXiv:1111.1023 [hep-th] .

[102] L. Huijse, S. Sachdev, and B. Swingle, Phys. Rev. B **85**, 035121 (2012), arXiv:1112.0573 [cond-mat.str-el] .

[103] S. Giombi and I. R. Klebanov, JHEP **03**, 117 (2015), arXiv:1409.1937 [hep-th] .

[104] L. Fei, S. Giombi, I. R. Klebanov, and G. Tarnopolsky, Journal of High Energy Physics **12**, 155 (2015), arXiv:1507.01960 [hep-th] .

[105] S. Giombi, I. R. Klebanov, and G. Tarnopolsky, J. Phys. A **49**, 135403 (2016), arXiv:1508.06354 [hep-th] .

[106] L. Fei, S. Giombi, I. R. Klebanov, and G. Tarnopolsky, Progr. Theor. Exp. Phys. **2016**, 12C105 (2016), 1607.05316 .

[107] G. Tarnopolsky, Phys. Rev. D **96**, 025017 (2017).

[108] C. Holzhey, F. Larsen, and F. Wilczek, Nuclear Physics B **424**, 443 (1994).

[109] H. Casini and M. Huerta, J. Phys. **A42**, 504007 (2009), arXiv:0905.2562 [hep-th] .

[110] T. Hirata and T. Takayanagi, JHEP **02**, 042 (2007), arXiv:hep-th/0608213 [hep-th] .

[111] P. Bueno, R. C. Myers, and W. Witczak-Krempa, Physical Review Letters **115**, 021602 (2015), arXiv:1505.04804 [hep-th] .

[112] H. Elvang and M. Hadjiantonis, Physics Letters B **749**, 383 (2015), arXiv:1506.06729 [hep-th] .

[113] N. Laflorencie, D. J. Luitz, and F. Alet, Phys. Rev. B **92**, 115126 (2015), arXiv:1506.03703 [cond-mat.str-el] .

[114] P. Bueno and W. Witczak-Krempa, Phys. Rev. B **93**, 045131 (2016), arXiv:1511.04077 [cond-mat.str-el] .

[115] J. Helmes, L. E. Hayward Sierens, A. Chandran, W. Witczak-Krempa, and R. G. Melko, Phys. Rev. B **94**, 125142 (2016), arXiv:1606.03096 [cond-mat.str-el] .

[116] P. Bueno and R. C. Myers, Journal of High Energy Physics **8**, 68 (2015), arXiv:1505.07842 [hep-th] .

[117] T. Faulkner, R. G. Leigh, and O. Parrikar, Journal of High Energy Physics **4**, 88 (2016), arXiv:1511.05179 [hep-th] .

[118] H. Osborn and A. Petkou, Annals of Physics **231**, 311 (1994), hep-th/9307010 .

[119] S. Sachdev, Physics Letters B **309**, 285 (1993), hep-th/9305131 .

[120] M. Oshikawa, ArXiv e-prints (2010), arXiv:1007.3739 [cond-mat.stat-mech] .

[121] B. Hsu and E. Fradkin, Journal of Statistical Mechanics: Theory and Experiment **9**, 09004 (2010), arXiv:1006.1361 [cond-mat.stat-mech] .

[122] X. Chen, W. Witczak-Krempa, T. Faulkner, and E. Fradkin, Journal of Statistical Mechanics: Theory and Experiment **2017**, 043104 (2017).

[123] X. Chen, G. Y. Cho, T. Faulkner, and E. Fradkin, Journal of Statistical Mechanics: Theory and Experiment **2**, 02010 (2015), arXiv:1412.3546 [cond-mat.str-el] .

[124] W. Witczak-Krempa, L. E. Hayward Sierens, and R. G. Melko, ArXiv e-prints (2016), arXiv:1603.02684 [cond-mat.str-el] .

[125] L. Chojnacki, C. Q. Cook, D. Dalidovich, L. E. Hayward Sierens, É. Lantagne-Hurtubise, R. G. Melko, and T. J. Vlaar, Phys. Rev. B **94**, 165136 (2016), arXiv:1607.05311 [cond-mat.str-el] .

[126] M. A. Metlitski and T. Grover, ArXiv e-prints (2011), arXiv:1112.5166 [cond-mat.str-el] .

[127] M. B. Hastings, I. González, A. B. Kallin, and R. G. Melko, Physical Review Letters **104**, 157201 (2010), arXiv:1001.2335 [cond-mat.str-el] .

[128] S. Inglis and R. G. Melko, New Journal of Physics **15**, 073048 (2013), arXiv:1305.1069 [cond-mat.str-el] .

[129] M. P. A. Fisher, P. B. Weichman, G. Grinstein, and D. S. Fisher, Phys. Rev. B **40**, 546 (1989).

[130] X. Zhang, C.-L. Hung, S.-K. Tung, and C. Chin, Science **335**, 1070 (2012), arXiv:1109.0344 [cond-mat.quant-gas] .

[131] M. Endres, T. Fukuhara, D. Pekker, M. Cheneau, P. Schauß, C. Gross, E. Demler, S. Kuhr, and I. Bloch, Nature **487**, 454 (2012), arXiv:1204.5183 [cond-mat.quant-gas] .

[132] Y. Huang, K. Chen, Y. Deng, and B. Svistunov, Phys. Rev. B **94**, 220502 (2016), arXiv:1608.02232 [cond-mat.quant-gas] .

[133] J. L. Smith and Q. Si, EPL (Europhysics Letters) **45**, 228 (1999).

[134] A. M. Sengupta, Phys. Rev. B **61**, 4041 (2000).

[135] S. Sachdev, C. Buragohain, and M. Vojta, Science **286**, 2479 (1999), arXiv:cond-mat/0004156 .

[136] M. Vojta, C. Buragohain, and S. Sachdev, Phys. Rev. B **61**, 15152 (2000), arXiv:cond-mat/9912020 .

[137] S. Sachdev, Physica C: Superconductivity **357**, 78 (2001), arXiv:cond-mat/0011233 .

[138] K. Chen, Y. Huang, Y. Deng, and B. Svistunov, to appear.

[139] B. Capogrosso-Sansone, Ş. G. Söyler, N. Prokof'ev, and B. Svistunov, Phys. Rev. A **77**, 015602 (2008), arXiv:0710.2703 [cond-mat.other] .

[140] Ş. G. Söyler, M. Kiselev, N. V. Prokof'ev, and B. V. Svistunov, Phys. Rev. Lett. **107**, 185301 (2011), arXiv:1107.5437 [cond-mat.other] .

[141] G. Zaránd and E. Demler, Phys. Rev. B **66**, 024427 (2002).

[142] S. Sachdev, Phys. Rev. B **55**, 142 (1997), arXiv:cond-mat/9606083 .

[143] D. J. Klein, Journal of Chemical Physics **61**, 786 (1974).

[144] M. Abramowitz and I. Stegun, *Handbook of Mathematical Functions: With Formulas, Graphs, and Mathematical Tables*, Applied mathematics series (Dover Publications, 1964).

[145] A. Chatterjee, Physics Reports **186**, 249 (1990).

[146] E. Elizalde, *Ten Physical Applications of Spectral Zeta Functions*, Lecture Notes in Physics (Springer Berlin Heidelberg, 2012).